OFFICIAL JOURNAL OF THE SCIENTIFIC SOCIETY OF ANATOMISTS, HISTOLOGISTS, EMBRYOLOGISTS AND TOPOGRAPHIC ANATOMISTS OF UKRAINE

DOI: 10.31393
ISSN 1818-1295
eISSN 2616-6194

ВІСНИК МОРФОЛОГІЇ
REPORTS OF MORPHOLOGY

Vol. 28, №4, 2022

Scientific peer-reviewed journal in the fields of normal and pathological anatomy, histology, cytology and embryology, topographical anatomy and operative surgery, biomedical anthropology, ecology, molecular biology, biology of development

Published since 1993
Periodicity: 4 times a year

Vinnytsya · 2022

ВІСНИК МОРФОЛОГІЇ - REPORTS OF MORPHOLOGY

Founded by the "Scientific Society of Anatomists, Histologists, Embryologists, and Topographic Anatomists of Ukraine" and National Pyrogov Memorial Medical University, Vinnytsya in 1993

Certificate of state registration КВ №9310 from 02.11.2004

Professional scientific publication of Ukraine in the field of medical sciences in specialties 221, 222, 228, 229
According to the list of professional scientific publications of Ukraine, approved by the order of the Ministry of Education and Science of Ukraine No. 1188 of 24.09.2020
Professional scientific publication of Ukraine in the field of biological sciences in specialty 091
According to the list of professional scientific publications of Ukraine, approved by the order of the Ministry of Education and Science of Ukraine No. 1471 of 26.11.2020

Approved by the Academic Council of National Pyrogov Memorial Medical University, Vinnytsya, protocol №4 from 24.11.2022.

Indexation: CrossRef, Index Copernicus, Google Schoolar Metrics, National Library of Ukraine Vernadsky

Address editors and publisher:
Pyrogov Str. 56,
Vinnytsya, Ukraine - 21018
Tel.: +38 (0432) 553959
E-mail: nila@vnmu.edu.ua

Computer page-proofs - Klopotovska L.O.
Translator - Gunas V.I.
Technical support - Levenchuk S.S.
Scientific editing - editorship

The site of the magazine - https://morphology-journal.com

CONTENT

DOI: 10.31393/morphology-journal-2022-28(4)-01 Reports of Morphology, Vol. 28, №4, Pages 5-10

ISSN 1818-1295 eISSN 2616-6194

REPORTS OF MORPHOLOGY

Official Journal of the Scientific Society of Anatomists, Histologists, Embryologists and Topographic Anatomists of Ukraine

journal homepage: https://morphology-journal.com

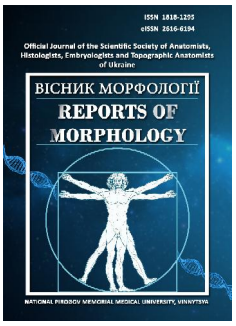

Ultrastructural reorganization of the constituent components of the rat periodontium under conditions of chronic opioid exposure

Fik V. B.[1], Podoliyk M. V.[1], Matkivska R. M.[2]

[1]Danylo Halytsky Lviv National Medical University, Lviv, Ukraine
[2]O.O. Bogomolets National Medical University, Kyiv, Ukraine

ARTICLE INFO

Received: 21 June 2022
Accepted: 20 July 2022

UDC:
616.311.2+616.314.17):615.212.7]-019-076.4

CORRESPONDING AUTHOR
e-mail: fikvolodymyr@ukr.net
Fik V. B.

CONFLICT OF INTEREST
The authors have no conflicts of interest to declare.

FUNDING
Not applicable.

Opioid addiction has acquired the characteristics of an epidemic in recent years and is a serious problem in modern medicine. In users of narcotic substances, a significant prevalence of diseases of the oral cavity and periodontal tissues is noted in comparison with the general population. The aim of the work was to investigate the ultrastructural organization of the periodontal tissues of rats at the end of the fourteenth week of the experimental opioid effect. The animals were administered intramuscularly, daily, once, the opioid analgesic nalbuphine (pharmacotherapeutic group: analgesics, opioids, morphinan derivatives) in increasing doses for 14 weeks: 1-2 weeks - 0.212 mg/kg, 3-4 weeks - 0.225 mg/kg, 5-6 weeks - 0.252 mg/kg, 7-8 weeks - 0.260 mg/kg, 9-10 weeks - 0.283 mg/kg; 11-12 - 0.300 mg/kg, 13-14 weeks - 0.450 mg/kg. At the end of the fourteenth week of opioid exposure, ultrastructural changes in the epithelium of the mucous membrane of the gums, periodontium, and hemomicrovessels with the development of decompensation and pronounced dystrophic-destructive changes were established. With the long-term effect of an opioid analgesic, signs of karyorrhexis, segregation of nucleoli, spongiosis, apoptosis, violation of the integrity of intercellular contacts, as well as vacuole-like formations, which were a manifestation of focal necrosis of epitheliocytes, were revealed. The development of necrotic changes was caused by significant damage and destruction of organelles, as well as fragmentation or lysis of bundles of tonofilaments. The intercellular spaces were mostly expanded and uneven, which was caused by edematous phenomena. Fragmentation and destruction of periodontal collagen fibers, destructive changes in fibrocytes and fibroblasts were found in the periodontium. The translucency of the amorphous component of the intercellular substance of the connective tissue was determined. The ultrastructural reorganization of the cellular components of the periodontium was caused by vascular disorders of a systemic nature, which were manifested by the phenomena of dilatation, hemoptysis, sludge phenomenon, dystrophic changes in the endotheliocytes of hemocapillaries and venules, and the progression of sclerotic changes, which significantly disturbed the trophism of the periodontal tissues of rats.

Key words: *opioid influence, rats, periodontium, ultrastructural study.*

Introduction

Opioid addiction has acquired the characteristics of an epidemic in recent years and is a serious problem in modern medicine [6, 18, 19]. Chronic use of narcotic substances leads to addiction, when there is a need for higher doses, after all, the constant and long-term use of opioids in 23 % of people leads to the development of opioid addiction [1, 19]. In view of this, experimental models for the purpose of studying the action of opioids, namely, the study of their analgesic potential, side effects, behavioral reactions, as well as their effects on various organs and systems, are of increasing interest recently [7, 8, 12, 17].

It should be noted that among users of narcotic substances, a significant prevalence of diseases of the oral cavity is noted, in comparison with the general population [9, 11, 20]. Taking into account the fact that the constituent components of the periodontium react quite distinctly to the action of various factors and homeostasis disturbances, the study of pathological changes in the oral cavity of addicted persons is relevant [21, 23]. The researchers note that comprehensive knowledge about

the condition of the organs and tissues of the oral cavity in opioid-dependent persons can ensure the effectiveness of diagnostic and therapeutic measures [5, 10, 22].

Analysis of modern scientific data shows that the problem of the pathogenesis of inflammatory and dystrophic periodontal diseases remains unsolved [4, 14, 15]. The reflection of the pathomorphological picture in the periodontal tissues is a rather complex process, and changes occur after a certain period of time with the involvement of various mechanisms of pathogenesis [2, 3, 13, 16]. In this regard, the study of pathomorphological changes at the ultrastructural level in the organs of the oral cavity, periodontal tissues, which develop against the background of the long-term effect of opioid agents, is undoubtedly an urgent problem today.

The aim of the study was to find out the peculiarities of the submicroscopic organization of the tissues of the periodontal complex at the end of the fourteenth week of the experimental action of the opioid analgesic nalbuphine.

Materials and methods

The study was conducted on 17 white outbred male rats of reproductive age, body weight 160 - 270 g. In the experiment, the animals were divided into two groups. The I group - control rats (5), which were injected with physiological solution during the experiment. In the II group of animals (12), the opioid analgesic nalbuphine (pharmacotherapeutic group: analgesics, opioids, morphine derivatives) was administered intramuscularly, daily, once, at the same time interval (10-11 a.m.) in increasing doses for 14 weeks: 1-2 weeks - 0.212 mg/kg, 3-4 weeks - 0.225 mg/kg, 5-6 weeks - 0.252 mg/kg, 7-8 weeks - 0.260 mg/kg, 9-10 weeks - 0.283 mg/kg; 11-12 - 0.300 mg/kg, 13-14 weeks - 0.450 mg/kg [11].

All animals were kept in a vivarium and work on keeping, care, labeling and all the other manipulations were carried out in compliance with the provisions of the European Convention for the Protection of Vertebrate Animals used for experimental and other scientific purposes (Strasbourg, 1985). The Commission on Bioethics of Danylo Halytskyi Lviv National Medical University has stated that the study meets ethical requirements in accordance with the order of the Ministry of Health of Ukraine No. 231 of 01.11.2000 (Protocol No. 10 of 24.05.2021).

For electron microscopic examination, pieces of periodontal soft tissue in the area of the gingival margin of the jaws were used, which were immediately immersed in a large drop of 2.5 % glutaraldehyde solution diluted in 0.1 M phosphate buffer (pH 7.36) with sucrose. Pieces were cut from the strips, tissue blocks were transferred to tubes with a fixing solution of the same composition. Subsequently, tissue blocks were fixed with a 2 % solution of osmium tetroxide in 0.1 M phosphate buffer (pH 7.36) with the addition of sucrose. For dehydration and preparation for impregnation with water-insoluble resins, fabric blocks washed from the remains of fixatives were passed through alcohols of increasing concentration. Fabric blocks were immersed in epon-araldite by passing through solutions of increasing resin concentration. Ultrathin sections were prepared on a УМТП-3М ultramicrotome using glass knives. For the study, sections of silver or gently lemon color were selected and contrasted in a 2 % solution of uranyl acetate, and then lead citrate. Studying and photographing the material was carried out with the help of an electronic microscope ПЕМ-100-01 (Ukraine) at magnifications of 1500x - 20000x on the microscope screen.

Results

Electron microscopic examination of rats of the I (control) group revealed layer-by-layer arrangement of gingival epithelium cells, clear and even contours of nuclei, and a low density of organelles in the cytoplasm were established. Ordered bundles of collagen fibers, intercellular substance and cells of the fibroblastic series are visualized in the periodontium. In the hemomicrovessels, a clear organization of endothelial cells, intercellular contacts, and small perivascular spaces containing constituent components of connective tissue has been established.

At the ultrastructural level, after 14 weeks of opioid exposure, significant changes were found in the studied periodontal components of laboratory animals. In the epitheliocytes of the basal layer of the free part of the gums, uneven contours of the nuclei are determined, the karyolemma forms rather deep intussusceptions, and karyorrhexis phenomena are observed in some places. The perinuclear space is of uneven width, in some places significantly expanded. Nucleoli are not detected in the electron light karyoplasm. In some areas, the contours of the plasmalemma are vaguely traced. Violation of the integrity of intercellular contacts, their significant reduction in individual areas was revealed. In places, intercellular contacts are visualized in the form of osmiophilic clusters. The intercellular spaces are mostly expanded and uneven, which is caused by edematous phenomena due to excessive fluid accumulation. In the karyolemma of the spinous layer of cells of the epithelium of the free part of the gums, deep intussusceptions were found, in the karyoplasm there are segregated components of nucleoli (Fig. 1). Vacuole-like formations are observed in structureless illuminated areas of the cytoplasm, which is a sign of the development of partial focal cell necrosis. Organelles in the cytoplasm are mostly damaged, destroyed cristae and a lighted matrix are found in swollen mitochondria. Bundles of tonofilaments have vague contours, mostly thickened. Electron-dense inclusions of keratohyalin of various sizes are visualized in the cytoplasm of the granular layer of epitheliocytes of the free part of the gums.

The contours of the nuclei of the epithelium of the gingival sulcus are uneven, the karyolemma forms multiple intussusceptions. Nucleoli are not detected in the illuminated karyoplasm. Organelles in the cytoplasm of epitheliocytes of the basal layer are destructively changed. In most of the

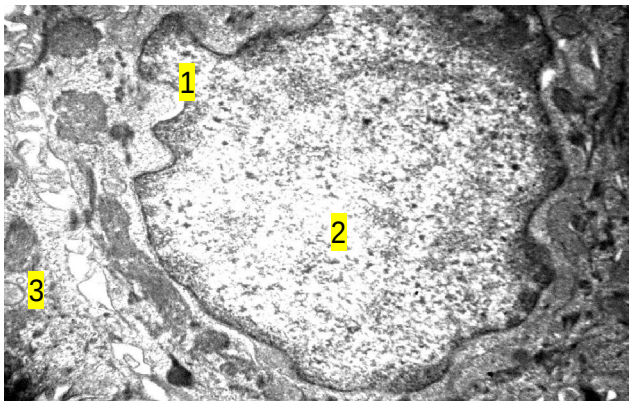

Fig. 1. Ultrastructural changes in the epithelium of the free part of the gingiva of a rat under conditions of 14-week opioid exposure. Intussusceptions of the karyolemma of the epitheliocyte of the spinous layer (1), segregation of the nucleolus (2), vacuole-like formations (3). x9000.

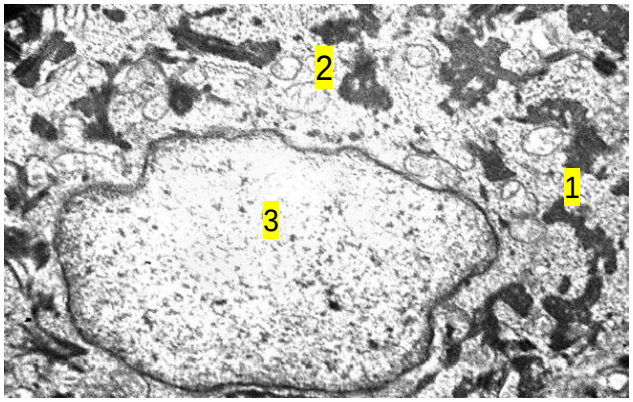

Fig. 2. Ultrastructural changes in the epithelium of the gingival sulcus of the rat under conditions of 14-week opioid exposure. Structureless osmiophilic inclusions in the cytoplasm of the epitheliocyte of the basal layer (1), vacuolization of mitochondria (2), clarification of the karyoplasm (3). x12000.

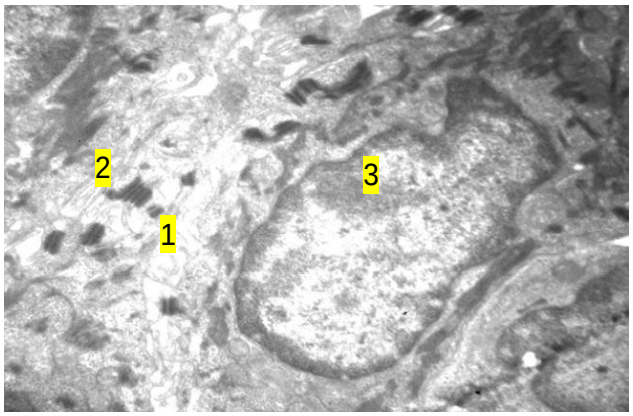

Fig. 3. Ultrastructural changes in the epithelium of the attached part of the rat's gingiva under conditions of 14-week opioid exposure. Necrotic areas of the cytoplasm of the epitheliocyte of the spinous layer (1), osmiophilic inclusions (2), heterochromatin cells in the karyoplasm (3). x12000.

mitochondria, lightening of their matrix and damaged cristae were found, vacuolization of mitochondria was observed in some places (Fig. 2). Destructive changes of tonofilaments are determined, where signs of their fragmentation are revealed, in some places they are lysed. In significant areas, intercellular contacts are not clearly visualized, most are reduced, which indicates the phenomenon of acantholysis. Intercellular spaces are mostly uneven and significantly expanded. In the cytoplasm of cells of the spinous layer, osmiophilic inclusions are observed, which is caused by increased keratinization of the epithelial plate in the area of the gingival sulcus of white rats.

In the epithelial cells of the attached part of the gums, apoptotic phenomena are observed, as well as structureless, illuminated areas of the cytoplasm, lysosomes, and osmiophilic inclusions (Fig. 3). The development of necrotic changes is caused by significant damage and destruction of organelles, as well as fragmentation or lysis of bundles of tonofilaments. Small pyknotic nuclei with uneven contours and heterochromatin in the karyoplasm are found in some of the epitheliocytes of the attached part of the gums. The karyolemma is mainly osmiophilic, the phenomena of karyorrhexis, in some places - karyolysis, as well as signs of destruction of karyoplasm are observed. Violation of intercellular contacts, their indistinctness and uneven expansion of intercellular spaces were revealed.

Ultrastructural studies demonstrated pronounced changes in periodontal components. Disruption of the orderly arrangement of collagen fibers and destructive changes, in particular, their fragmentation, destruction of fibers in places, were found in the bundles. The illumination of the amorphous component of the intercellular substance of the connective tissue is determined (Fig. 4).

Submicroscopic organization of fibroblasts and fibrocytes changes significantly, macrophages are activated. In fibroblasts, altered nuclei and damaged organelles in the cytoplasm are identified. Signs of karyopyknosis in fibrocytes, karyorrhexis phenomena in places. There is an expansion of the perinuclear space, indistinct contours of

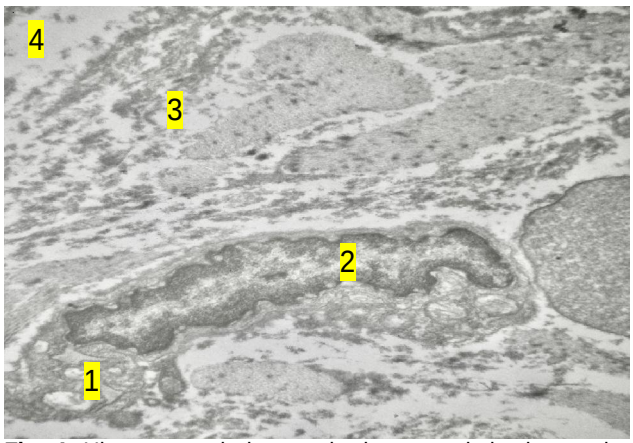

Fig. 4. Ultrastructural changes in the rat periodontium under conditions of 14-week opioid exposure. Vacuole-like formations in the cytoplasm of a fibrocyte (1), karyopyknosis (2), fragmented collagen fibers (3), swollen connective tissue (4). x12000.

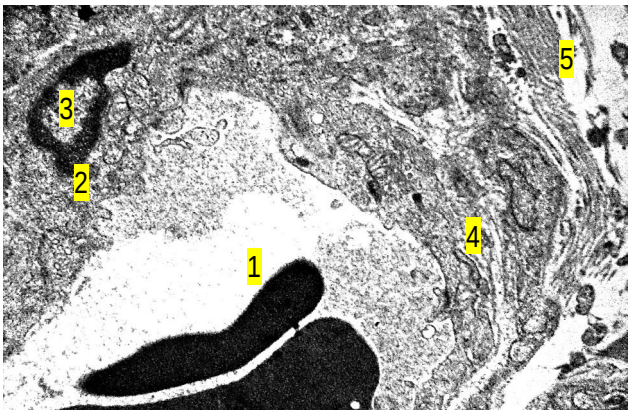

Fig. 5. Ultrastructural changes in the hemocapillary of the mucous membrane of the gingiva of the rat under conditions of 14-week opioid exposure. Hemocapillary lumen with formed blood elements (1), endotheliocyte cytoplasm (2), karyopyknosis (3), swelling of the basement membrane (4), swelling and delamination of collagen fibers in the perivascular space (5). x12000.

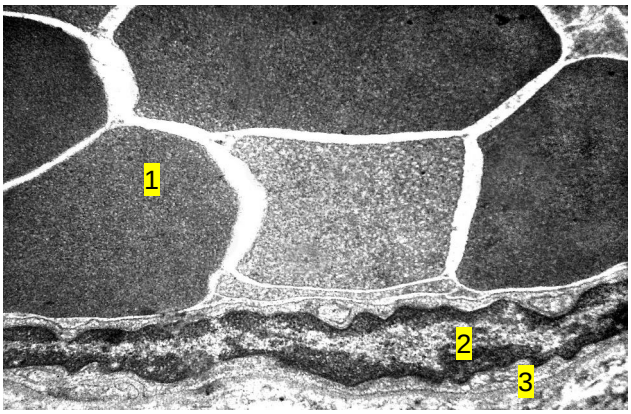

Fig. 6. Ultrastructural changes of the venules of the gingival mucosa of the rat under conditions of 14-week opioid exposure. Formed blood elements in the venule lumen (1), destruction of the endotheliocyte nucleus (2), basement membrane (3). x9000.

the karyolemma, where deep intussusceptions are revealed. Heterochromatin is determined on a significant area of osmiophilic karyoplasm. In the cytoplasm, organelles are mostly destructively changed, lysosomes, vacuole-like formations, expanded and fragmented tubules of the granular endoplasmic reticulum, and unevenly thickened cisterns of the Golgi complex are observed. Swollen mitochondria with destroyed cristae and lightened matrix were found (see Fig. 4).

Submicroscopically, significant changes were found in the links of the hemomicrocirculatory channel of the mucous membrane of the gums. In the wide lumens of the hemocapillaries, the formed elements of the blood, mostly erythrocytes, are determined. The phenomenon of "sludge phenomenon" is observed. Endotheliocyte nuclei are destructively altered, with signs of karyopyknosis and karyorrhexis. Numerous deep intussusceptions of the karyolemma and dense accumulations of heterochromatin in the karyoplasm were revealed. Destroyed organelles and few pinocytotic vesicles can be found in the cytoplasm. In some areas, vacuole-like structures are visualized. The basal membrane is vaguely contoured, in some places it is significantly thickened. Perivascular spaces are expanded, where thickened bundles of collagen fibers are determined, which is caused by the development and progression of sclerotic changes (Fig. 5).

In the venules, the signs of dilatation, hemoptysis and "sludge phenomenon" predominate. n the lumen of the venules, erythrocytes are identified, places where platelets accumulate. In the nuclei of endotheliocytes, osmiophilic karyoplasm with accumulation of heterochromatin, karyopyknosis and uneven contours of karyolemma are visualized (Fig. 6). The perinuclear space is expanded. Brightened areas, electron-dense inclusions, vacuoles, as well as damaged organelles and vacuolated mitochondria are observed in the cytoplasm, which is a sign of cytolysis. The adluminal surface of endotheliocytes is focally exfoliated in some areas and protrudes into the lumen of venules. The basal membrane thickens significantly, its contours are indistinct in places. Collagen fibers were found in significantly expanded perivascular spaces.

Discussion

The results obtained by us of the electron microscopic study of the constituent components of the periodontium against the background of chronic opioid exposure are compared with the data of the ultrastructural study in patients with periodontopathies. In particular, with generalized periodontitis, researchers submicroscopically detected destroyed contacts between epitheliocytes and signs of spongiosis in the layers of the gingival epithelium, the formation of which was caused by the penetration of serous fluid into the intercellular spaces, which had a significant volume [2, 13, 16]. The destruction of mitochondrial cristae and vacuolization of their matrix, the phenomena of apoptosis, cell nuclei acquired an irregular shape and lost nucleoli and chromatin were also noted [3]. In individual cells of the basal layer of the gingival epithelium, the researchers identified foci of destruction of the cell membrane [2, 16].

In our studies, we also observed fragmented or lysed bundles of tonofilaments, significant damage and destruction of organelles, phenomena of karyorrhexis and vacuole-like formations in illuminated areas of the cytoplasm, which is a sign of the development of partial focal necrosis. According to the researchers, in patients with generalized periodontitis, the lumen of hemocapillaries was filled with erythrocytes and platelets. The basal membrane is loose, in the cytoplasm of endotheliocytes, areas of lightening, mitochondria with disorganized cristae were determined. Nuclei of irregularly shaped endotheliocytes with karyolemma intussusception, destructive nucleoli were present, which indicated damage to the hemomicrocirculatory channel of the periodontium, causing ischemia of the gingival mucosa [3].

In patients with generalized periodontitis with accompanying cardiovascular pathology, obturation of the lumen of vessels of the gingival mucosa, desquamation of the endothelium, apoptosis of endotheliocytes, and obturation of blood vessels with formed blood elements were noted, which indicated the development of local endothelial dysfunction [13]. The given data in patients with periodontitis are compared with the results obtained by us of the study of microvessels under the experimental action of opioid, where submicroscopically in the lumen of the hemocapillaries of animals, the phenomenon of "sludge phenomenon", destructively changed nuclei of endotheliocytes, with signs of karyopyknosis, and damaged organelles and vacuole-like structures were found in the cytoplasm, which indicated the progression of hypoxia.

Conclusions

1. At the end of the fourteenth week of opioid exposure, ultrastructural changes in the epithelium of the mucous membrane of the gums, periodontium, and hemomicrovessels with the development of decompensation and pronounced dystrophic-destructive changes were established.

2. With the long-term effect of an opioid analgesic, signs of karyorrhexis, segregation of nucleoli, spongiosis, acantholysis, apoptosis, as well as vacuole-like formations, which are a manifestation of focal necrosis of epitheliocytes, were revealed. Fragmentation and destruction of periodontal collagen fibers, destructive changes in fibrocytes and fibroblasts were found in the periodontium.

3. Ultrastructural reorganization of the cellular components of the periodontium is caused by vascular disorders of a systemic nature, which are manifested by the phenomena of dilatation, hemoptysis, sludge phenomenon, dystrophic changes in the endotheliocytes of hemocapillaries and venules, and the progression of sclerotic changes, which significantly disrupts the trophism of rat periodontal tissues.

References

[1] Algera, M.H., Olofsen, E., Moss, L., Dobbins, R.L., Niesters, M., van Velzen, M., … Dahan, A. (2021). Tolerance to Opioid-Induced Respiratory Depression in Chronic High-Dose Opioid Users: A Model-Based Comparison with Opioid-Na?ve Individuals. *Clin Pharmacol Ther.*, 109(3), 637-645. doi: 10.1002/cpt.2027

[2] Babai, O. M. (2016). Методика та досвід оцінки ефективності лікування пацієнтів з генералізованим пародонтитом за даними ультраструктурного аналізу епітелію ясен [Methodology and experience of evaluating the effectiveness of treatment of patients with generalized periodontitis based on ultrastructural analysis of the gingival epithelium]. *Український журнал екстремальної медицини ім. Г.О. Можаєва - Ukrainian Journal of Extreme Medicine named after G.O. Mozaeva,* 17(2), 5-10.

[3] Buchkovska, A. Yu., Nakonechna, O. V., Petryshyn, O. A., & Strus, Kh. I. (2018). Ультраструктурне дослідження слизової оболонки ясен при генералізованому пародонтиті [Ultrastructural study of the gingival mucosa in generalized periodontitis]. *Світ медицини та біології - World of Medicine and Biology,* 4(66), 145-148. doi: 10.26724/2079-8334-2018-4-66-145-148

[4] Dahlen, G., Fejerskov, O., & Mangi, F. (2020). Current concepts and an alternative perspective on periodontal disease. *MC Oral Health,* 20(1), 1-9. doi: 10.1186/s12903-020-01221-4

[5] Dana, R., Azarpazhooh, A., Laghapour, N., Suda, K.J., Okunseri, C. (2018). Role of dentists in prescribing opioid analgesics and antibiotics: an overview. *Dent Clin. North Am.,* 62, 279-294. doi: 10.1016/j.cden.2017.11.007

[6] Erim, D., Obadan-Udoh, E., & Agaku, I. (2021). Cost savings from averted prescription opioidattributable dental diseases in the United States between 2013 and 2019. *Popul. Med.,* 3, 1-13. doi: https://doi.org/10.18332/popmed/136488

[7] Ferreira, R. C. M., Almeida-Santos, A. F., Duarte, I. D. G., & Aguiar, D. C. (2017). Peripheral antinociception induced by aripiprazole is mediated by the opioid system. *BioMed. Research International,* 2017, 8109205. doi: 10.1155/2017/8109205

[8] Fik, V.B., Paltov, E.V., & Kryvko, Y.Y. (2018). Morphofunctional peculiarities of the periodontal tissue under conditions of simulated eight-week opioid effect. Deutscher Wissenschaftscherold. *German Science Herald*, (1), 14-17. doi: 10.19221/201814

[9] Fitkalo, O.S., Ohonovskyi, R.Z., Pohranychna, K.R., Nahirnyi, Y.P., & Netlyukh, A.V. (2021). Clinical features of toxic jaw bone osteomyelitis in drug addicts. *Wiadomoscie Lekarskie,* 74(2), 263-267. doi: 10.36740/WLek202102116

[10] Hartnett, K.P., Jackson, K.A., Felsen, C., McDonald, R., Bardossy, A.C., Gokhale, R.H. … Dumyati, G. (2019). Bacterial and Fungal Infections in Persons Who Inject Drugs - Western New York, 2017. *Morbidity and Mortality Weekly Report,* 68(26), 583-586. doi: 10.15585/mmwr.mm6826a2

[11] Hegazi, F., Alhazmi, H., Abdullah, A., Alamer, N., Nelson, J., Aldosari, M. ... Vardavas, C. (2021). Prevalence of Oral Conditions Among Methamphetamine Users: NHANES 2009-2014. *J. Public Health Dent.,* 81(1), 21-28. doi: 10.1111/jphd.12389

[12] Jirkof, P. (2017). Side effects of pain and analgesia in animal experimentation. *Laboratory Animal,* 46(4), 123-128. doi: 10.1038/laban.1216

[13] Kopchak, O. V., Biloklytska, G. F., Stechenko, L. O., & Kryvosheeva, O. I. (2017). Ультраструктурна організація тканин ясен хворих на генералізований пародонтит при кардіоваскулярній патології [Ultrastructural organization of gingival tissues in patients with generalized periodontitis with cardiovascular pathology]. *Світ медицини та біології - World of Medicine and Biology,* 59(1), 121-126.

[14] Manji, F., Dahlen, G., & Fejerskov, O. (2018). Caries and periodontitis: contesting the conventional wisdom on their aetiology. *Caries Reports,* 52(6), 548-564. doi: 10.1159/000488948

[15] Martinez-Garcia, M., & Hernandez-Lemus, E. (2021). Periodontal Inflammation and Systemic Diseases: An Overview. F*ront Physiol.,* 12:709438. doi: 10.3389/fphys.2021.709438

[16] Matviykiv, T. I. (2017). Ультраструктурні зміни епітелію ясен хворих на генералізований пародонтит в динаміці терапії [Ultrastructural changes of the gingival epithelium of patients with generalized periodontitis in the dynamics of therapy]. *Хірургія Донбасу - Surgery of Donbass,* 6(2), 40-44.

[17] Paltov, E. V., Kovalyshyn, O. A., Fik, V. B., Kryvko, Y. Ya.,

Podoliuk, M. V., & Holeyko, M. V. (2019). Pathomorphological changes in rats retinal layers at the end of the twelfth week of experimental opioid influence. *International Academy Journal Web of Scholar,* 4(34), 19-22. doi: 10.31435/rsglobal_wos/30042019/6444

[18] Pergolizzi, J. V. Jr., Raffa, R. B., & Rosenblatt, M. H. (2020). Opioid withdrawal symptoms, a consequence of chronic opioid use and opioid use disorder: Current understanding and approaches to management. *J. Clin. Pharm.* Ther., 45(5), 892-903. doi: 10.1111/jcpt.13114

[19] Taqi, M. M., Faisal, M., & Zaman, H. (2019). OPRM1 A118G Polymorphisms and Its Role in Opioid Addiction: Implication on Severity and Treatment Approaches. *Pharmacogenomics and Personalized Medicine,* (12), 361-368. doi: 10.2147/PGPM.S198654

[20] Valadas, L. A. R., Fernandes, M. L., Silva, M. I. G., Cito, M. do C. de O., Oliveira I.C.M., Dias, M. L. … Sousa, F. C. F. (2020). Oral Manifestations of Drug Abuse: A Review of Literature. *Journal of Young Pharmacists,* 12(1), 11-14. doi: 10.5530/jyp.2020.12.3

[22] Zhao-Fleming, H., Hand, A., Zhang, K., Polak, R., Northcut, A., Jacob, D. ... Rumbaugh, K. P. (2018). Effect of non-steroidal anti-inflammatory drugs on post-surgical complications against the backdrop of the opioid crisis. *Burns Trauma,* 6(1), 25. doi: 10.1186/s41038-018-0128-x

[23] Zubachyk, V. M., & Fedun, I. R. (2017). Біохімічні показники ротової рідини у наркозалежних хворих на хронічний генералізований пародонтит [Biochemical indicators of oral fluid in drug-dependent patients with chronic generalized periodontitis]. *Клінічна стоматологія - Clinical Dentistry,* (2), 9-14. doi: 10.11603/2311-9624.2017.2.7741

УЛЬТРАСТРУКТУРНА РЕОРГАНІЗАЦІЯ СКЛАДОВИХ КОМПОНЕНТІВ ПАРОДОНТА ЩУРІВ ЗА УМОВ ХРОНІЧНОГО ОПІОЇДНОГО ВПЛИВУ

Фік В. Б., Подолюк М. В., Матківська Р. М.

Опіоїдна залежність за останні роки набула ознак епідемії та становить серйозну проблему у сучасній медицині. У споживачів наркотичних речовин відмічають значну поширеність захворювань ротової порожнини, тканин пародонта в порівнянні із загальною популяцією населення. Метою роботи було дослідити ультраструктурну організацію тканин пародонта щурів наприкінці чотирнадцятого тижня експериментальної дії опіоїда. Тваринам вводили внутрішньом'язово, щоденно, одноразово опіоїдний анальгетик налбуфін (фармакотерапевтична група: анальгетики, опіоїди, похідні морфінану) у зростаючих дозах упродовж 14 тижнів: 1-2 тижні - 0,212 мг/кг, 3-4 тижні - 0,225 мг/кг, 5-6 тижні - 0,252 мг/кг, 7-8 тижні - 0,260 мг/кг, 9-10 тижні - 0,283 мг/кг; 11-12 - 0,300 мг/кг, 13-14 тижні - 0,450 мг/кг. Наприкінці чотирнадцятого тижня опіоїдного впливу встановлено ультраструктурні зміни епітелію слизової оболонки ясен, періодонта та гемомікросудин з розвитком декомпенсації та виражених дистрофічно-деструктивних змін. При довготривалій дії опіоїдного анальгетика було виявлено ознаки каріорексису, сегрегації ядерець, спонгіозу, апоптозу, порушення цілісності міжклітинних контактів, а також вакуолеподібні утворення, що було проявом фокального некрозу епітеліоцитів. Розвиток некротичних змін зумовлювався значним ушкодженням і руйнуванням органел, а також фрагментацією чи лізисом пучків тонофіламентів. Міжклітинні простори переважно були розширеними та нерівномірними, що зумовлювалося набряковими явищами. У періодонті було виявлено фрагментацію та руйнування колагенових волокон періодонта, деструктивні зміни фіброцитів і фібробластів. Визначали просвітлення аморфного компоненту міжклітинної речовини сполучної тканини. Ультраструктурна реорганізація клітинних компонентів пародонта зумовлювалася судинними розладами системного характеру, які проявлялися явищами дилатації, повнокров'я, сладж-феномену, дистрофічними змінами ендотеліоцитів гемокапілярів і венул та прогресуванням склеротичних змін, що суттєво порушувало трофіку тканин пародонта щурів.

Ключові слова: *опіоїдний вплив, щури, пародонт, ультраструктурне дослідження.*

DOI: 10.31393/morphology-journal-2022-28(4)-02 Reports of Morphology, Vol. 28, №4, Pages 11-17

ISSN 1818-1295 eISSN 2616-6194

REPORTS OF MORPHOLOGY

Official Journal of the Scientific Society of Anatomists, Histologists, Embryologists and Topographic Anatomists of Ukraine

journal homepage: https://morphology-journal.com

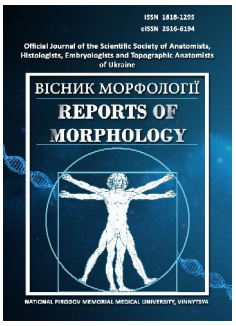

Brain morphometry and its relevance in cerebral small vessel disease

Moskovko S. P., Bartiuk R. S.
National Pirogov Memorial Medical University, Vinnytsya, Ukraine

ARTICLE INFO
Received: 25 June 2022
Accepted: 27 July 2022

UDC: 611.811.019:611.161

CORRESPONDING AUTHOR
e-mail: rambrs88@gmail.com
Bartiuk R. S.

CONFLICT OF INTEREST
The authors have no conflicts of interest to declare.

FUNDING
Not applicable.

Cerebral small vessel disease (CSVD) is a heterogeneous group of disorders which affect small perforating vessels of the brain. Clinically CSVD manifest with various constellations of symptoms, like cognitive, functional, affective as well as lacunar stroke or intracerebral hemorrhage. It is responsible for 25 % of all strokes and are the second contributor to dementia after Alzheimer's disease. The gold standard for CSVD diagnostic is neuroimaging. The main key features are white matter hyperintensity (WMH), lacunes, enlarged perivascular spaces (EPVS), brain atrophy. Brain atrophy have been recognized to play a synergistic role in both cerebrovascular and neurodegenerative disorders occurring in the aging brain. It reflects a final common pathway for pathological processes, which progress in time. CSVD progression results in gradual decrease of brain volume, which is seen as changes of ventricles size and cortical sulci span of the brain. But not much is known about its extent, correlates and consequences. The aim of the research is to investigate whether brain morphometric changes correlate with CSVD features. In this study, we included 129 CSVD patients and 165 non-CSVD controls, both with acute stroke. All participants underwent neuroimaging assessment with magnetic resonance imaging (MRI) and computed tomography (CT). We used both univariate and multivariate regression analysis, as well as correlation analysis to identify differences in brain morphometric parameters between groups. Multivariable regression analysis, adjusted for age and sex, revealed significant impact of Evans index (OR 1.09, 95 %; CI 1.01-1.16, p=0.018), the third ventricle index (OR 1.42, 95 %; CI 1.21-1.67, p<0.001), Schaltenbrand and N?rnberger index (OR 1.42, 95 %; CI 1.21-1.67, p<0.001), the fourth ventricle index (OR 1.31, 95 %; CI 1.13-1.51, p<0,001), bicaudate index (OR 1.19, 95 %; CI 1.10-1.30, p<0.001), cella media index (Schiersmann's index) (OR 0.55, 95 %; CI 0.42-0.72, p<0.001), Huckman number (OR 1.05, 95 %; CI 1.02-1.08, p<0.001), width of the longitudinal cerebral fissure in the anterior part of the frontal lobes (OR 1.46, 95 %; CI 1.22-1.75, p<0.001), width of the left insular cistern (OR 1.24, 95 %; CI 1.11-1.39, p<0.001), width of the right insular cistern (OR 1.31, 95 %; CI 1.17-1.46, p<0.001), width of the right and left insular cisterns in sum (OR 1.17, 95 %; CI 1.10-1.25, p<0.001), width of the cerebral fissure in the area of the skull vault (OR 1.49, 95 %; CI 1.21-1.84, p<0.001) on the CSVD presence. Width of the longitudinal cerebral fissure in the anterior part of the frontal lobes in CSVD was 6.13±1.56 mm vs 5.10±1.38 mm in non-CSVD, p<0.001 and width of the right and left insular cisterns in sum in CSVD was 16.98±4.60 mm vs 13.41±4.16 mm in non-CSVD, p<0.001. Width of the cerebral fissure in the area of the skull vault (parietal cortex) was also greater in CSVD patients: 5.04±1.85 mm vs 4.12±1.29 mm, p<0.001. Thus, all ventricular and cortical indices were increased in the group of patients with CSVD. Our results indicate that morphometric indicators of the brain are closely related to CSVD and can be useful for predicting the consequences of a stroke and ascertaining the decline of cognitive functions.

Key words: *brain morphometry, cerebral small vessel disease, Evans index.*

Introduction

Cerebral small vessel disease (CSVD) is a heterogeneous group of disorders which affect small perforating arteries, arterioles, capillaries, venules and veins (vessels of 5 mcm - 2 mm. in diameter) of the brain [5]. It affects brains parenchyma through chronic changes of perfusion, hypoxia, ischemia, blood-brain barrier

dysfunction, inflammation and endothelium abnormalities, which results in progressive changes of vessel walls such as hyalinosis (accumulation of plasma proteins in subendothelial space), hyperplastic arteriolosclerosis, segmental arteriolar desorganisation, microaneurisms formation, chronic vessel wall degeneration etc. [16]. These changes may affect both white and grey matter of the brain. As a consequence - gradual decrease of brain volume, which is seen as brain atrophy and changes of ventricles size and cortical sulci span of the brain. Clinically CSVD manifest with various constellations of symptoms, like cognitive, functional, affective as well as lacunar stroke or intracerebral hemorrhage. It is responsible for at least 20-25 % of all strokes and are the second contributor to dementia after Alzheimer's disease [15]. CSVD affects not only subcortical brain parenchyma, but also the cortex with cerebral microbleeds or microinfarcts etc. [9].

The key standard for CSVD diagnostic is neuroimaging. The main features are white matter hyperintensities (WMH), lacunes, enlarged perivascular spaces (EPVS), brain atrophy, recent lacunar infarcts, cerebral microbleeds, microinfarcts, superficial cortical siderosis [3]. Among these, brain atrophy have been recognized to play a synergistic role in both cerebrovascular and neurodegenerative disorders occurring in the aging brain. It reflects a final common pathway for pathological processes, which progress in time. But not much is known about its extent, correlates and consequences [14].

There are several types of brain atrophy, such as global cortical atrophy, deep atrophy, total atrophy, mediotemporal hippocampal atrophy, precuneus atrophy etc. [21], which helps better classified brain changes for diagnostics, treatments and prognostics purposes. Therefore, more precise and thorough measurement of the brain morphology can shed light on underlying pathology and give clues for better prevention strategies.

The aim of the research is to investigate whether brain morphometric changes correlate with CSVD features.

Material and methods

Subjects

It was a prospective cohort study based on specialized stroke department (Stroke Unit) № 22 of the Vinnytsia Regional Psychoneurological Hospital named after acad. O.I. Yushchenko. Committee on Bioethics of National Pirogov Memorial Medical University, Vinnytsya (Protocol № 6 from 3.10.2022) found that the studies do not contradict the basic bioethical standards of the Declaration of Helsinki, the Council of Europe Convention on Human Rights and Biomedicine (1977), the relevant WHO regulations and laws of Ukraine.

Between December 2016 and December 2019 294 patients with acute stroke were recruited (age: 61.94±10.11 years old; 115 females). 129 (44 %) stroke patients with CSVD (age: 65.78±8.28 years old; 46 females) and 165 (56 %) stroke patients without CSVD (age: 58.93±10.42 years old; 69 females). The inclusion criteria for CSVD patients included diagnosis of WMH of presumed vascular origin, lacunes of presumed vascular origin, EPVS based on current MRI consensus standards [18]. The total CSVD burden was assessed by amended CSVD score (0-3 scale, scores calculated based on the severity of WMH, lacunes, EPVS (we used CSVD score without atrophy) that was approved in variety of studies [12].

Image Acquisition

120 patients underwent Magnetic Resonance Imaging (MRI), 174 - Computed Tomography (CT). Some of the subjects were imaged only with either MRI or CT, some of them - both with MRI and CT. MRI was performed on a Philips Achieve 1.5 T. The brain scanning protocol consisted of a T1-weighted, T2-weighted, FRAIR and DWI sequences, slice thickness was 3.5-5 mm. CT was performed on a General Electric CT/e (Italy) with a tomographic section thickness of 3-7 mm.

Measurements of the brain morphometry

We calculated such brain parameters as Evans index, the third ventricle index, Schaltenbrand and Nürnberger index, the fourth ventricle index, the bicaudate index, ventricular index, the cella media index (also known as Schiersmann's index), the Huckman number [19]. We multiplied the indices by 100 for better representation. We also measured the width of the longitudinal cerebral fissure in the anterior part of the frontal lobes, the width of the right and left insular cisterns and their sum, the maximum width of the cerebral fissure in the area of the skull vault and the maximum width of the cerebellar fissure [4]. We assessed such CSVD featurea, as WMH, lacunes, EPVS. The severity of WMH was assessed using the Fazekas scale. The scale grades the severity from 0 to 3 [20]. A lacune typically is a lesion 3-20 mm in diameter that affects the subcortical white matter and the deep grey matter of the brain and brainstem. An enlarged PVS is a dilated space, <3 mm in diameter, with an ovoid, round, or linear shape, filled with CSF that surrounds perforating arterioles and venules, as they course from the subarachnoid space through the brain parenchyma [1]. Distinguishing among WMH, lacune, and enlarged PVS can occasionally be challenging by imaging. A marginally hyperintense rim seen with FLAIR is suggestive of a lacune instead of enlarged PVS. The typical anatomical location of enlarged PVS may be the best differentiating feature [21]. Total CSVD burden assessed by simple validate method, if there were one or more lacunes, one point was added, one point was added when the deep WMH Fazekas score reached 2 or periventricular WMH Fazekas score reached 3, if the number of EPVS at the basal ganglia or centrum semiovale level reached >10, one point was added [8].

Statistical analysis

We used univariable and multivariable regression analysis to establish the associations between morphometric data and CVSD features. Logistic regression was used in case of binomial, multinomial or ordinal dependent variable. Linear regression was used in case of

linear dependent variable. All multivariable analyses were adjusted for age and sex. Continuous variables were presented as mean ± standard deviations (SD). The results are shown as odds ratio (OR) and 95 % confidence intervals (CI) or as a beta-coefficient in case of linear regression. A p value <0.05 was considered statistically significant. Two groups comparison were performed by Student's t-test in Welch modification in normal distribution or Mann-Whitney U test if the variables were not normally distributed. Multiple group comparison were performed by ANOVA in normal distribution or Kruskal-Wallis test if the variables were not normally distributed. Categorical variables were presented as percentages and were compared with Pearson's chi square test or Fisher's exact test (if the number of observation were <5). Pearson or Spearman correlation were used to establish associations between two variables. Statistical analyses were performed by The jamovi project (2022). Jamovi (Version 2.2.5) [Computer Software]. Sydney, Australia and Microsoft Excel.

Results

Age of CSVD-patients was 65.76±8.28 years old, non-CSVD - 58.93±10.42 years old. Among 129 CSVD patients 83 (64.3 %) were males, 46 (35.7 %) - females. Among 165 non-CSVD patients 96 (58.2 %) were males, 69 (41.8 %) - females. 45 (34.9 %) CSVD patients had a previous stroke history, while 26 (15.7 %) non-CSVD reported about previous stroke. Hospitalization time for

Table 1. Brain morphometry depending on the CSVD presence.

Brain measurement	CSVD, 129	non-CSVD, 165	p
Evans index	28.12±4.23	26.40±3.47	<0.01
The third ventricle index	5.796±1.681	4.490±1.671	<0.01
Schaltenbrand and Nurnberger index	18.97±6.64	25.47±9.58	<0.01
The fourth ventricle index	12.85±2.24	12.18±1.41	<0.05
Bicaudate index	16.86±3.43	14.33±3.17	<0.01
Ventricular index	1.599±0.261	1.683±0.251	<0.01
Cella media index (Schiersmann's index)	4.719±1.030	5.538±1.193	<0.01
Huckman number	60.05±9.55	54.61±8.54	<0.01
Width of the longitudinal cerebral fissure in the anterior part of the frontal lobes, mm	6.130±1.560	5.097±1.377	<0.01
Width of the right insular cistern, mm	8.226±2.499	6.432±2.379	<0.01
Width of the left insular cistern, mm	8.705±2.553	6.982±2.397	<0.01
Width of the right and left insular cisterns in sum, mm	16.98±4.60	13.41±4.16	<0.01
Maximum width of the cerebral fissure in the area of the skull vault, mm	4.887±1.668	3.899±1.167	<0.01
Maximum width of the cerebellar fissure, mm	2.625±1.265	2.505±1.063	>0.05

Table 2. Brain morphometry depending on the lacunes presence.

Brain measurement	Presence of lacunes, 68	Lacunes-free, 225	p
Evans index	27.53±4.25	27.05±3.81	>0.05
The third ventricle index	5.937±1.779	4.802±1.721	<0.01
Schaltenbrand and Nurnberger index	18.80±7.20	23.78±9.21	<0.01
The fourth ventricle index	13.01±2.28	12.31±1.68	<0.05
Bicaudate index	16.56±3.41	15.10±3.49	<0.001
Ventricular index	1.626±0.283	1.653±0.251	>0.05
Cella media index (Schiersmann's index)	4.686±0.991	5.323±1.213	<0.01
Huckman number	59.18±9.80	56.33±9.19	0.014
Width of the longitudinal cerebral fissure in the anterior part of the frontal lobes, mm	6.181±1.638	5.367±1.468	<0.01
Width of the right insular cistern, mm	8.693±2.453	6.774±2.468	<0.01
Width of the left insular cistern, mm	9.044±2,504	7.352±2.517	<0.01
Width of the right and left insular cisterns in sum, mm	17.84±4.40	14.13±4.46	<0.01
Maximum width of the cerebral fissure in the area of the skull vault, mm	5.037±1.853	4.124±1.294	<0.01
Maximum width of the cerebellar fissure, mm	2.936±1.477	2.448±1.020	<0.01

Table 3. Brain morphometry depending on the WMH severity.

Brain measurement	WMH Fazekas 3, 106	WMH Fazekas 0-2, 188	p
Evans index	28.42±4.08	26.44±3.64	<0.01
The third ventricle index	5.946±1,.96	4.565±1.709	<0.01
Schaltenbrand and Nurnberger index	18.14±5.51	25.15±9.60	<0.01
The fourth ventricle index	12.92±2.23	12.22±1.54	<0.01
Bicaudate index	17.32±3.44	14.38±3.10	<0.001
Ventricular index	1.580±0.235	1.684±0.263	<0.01
Cella media index (Schiersmann's index)	4.596±0.984	5.508±1.179	<0.01
Huckman number	61.00±9.22	54.74±8.71	<0.01
Width of the longitudinal cerebral fissure in the anterior part of the frontal lobes, mm	6.284±1.549	5.137±1.384	<0.01
Width of the right insular cistern, mm	8.180±2.549	6.677±2.452	<0.01
Width of the left insular cistern, mm	8.829±2.633	7.123±2.387	<0.01
Width of the right and left insular cisterns in sum, mm	17.07±4.75	13.80±4.25	<0.01
Maximum width of the cerebral fissure in the area of the skull vault, mm	4.946±1.667	3.987±1.258	<0.01
Maximum width of the cerebellar fissure, mm	2.649±1.316	2.507±1.055	>0.05

Table 4. Correlation analysis of brain morphometrics and CSVD features.

Brain measurement	WMH	Total SCVD	Amount of lacunes	EPVS BG	EPVS CS
Evans index	0.34***	0.23***	0.06	0.14	0.07
The third ventricle index	0.48***	0.40***	0.28***	0.29**	0.18*
Schaltenbrand and Nurnberger index	-0.9***	-0.40***	-0,.8***	-0.29**	-0.18*
The fourth ventricle index	0.16**	0.21***	0.20***	0.24**	0.05
Bicaudate index	0.47*	0.37***	0.19**	0.26**	0.11
Ventricular index	-0.28***	-0.21***	-0.06	-0.12	0.02
Cella media index (Schiersmann's index)	-0.41***	-0.39***	-0.24***	-0.21**	-0.05
Huckman number	0.37***	0.31***	0.14*	0.20**	0.09
Width of the longitudinal cerebral fissure in the anterior part of the frontal lobes, mm	0.34***	0.35***	0.23***	0.26**	0.31***
Width of the right insular cistern, mm	0.34***	0.36***	0.33***	0.43***	0.23*
Width of the left insular cistern, mm	0.38***	0.35***	0.28***	0.35***	0.27*
Width of the right and left insular cisterns in sum, mm	0.41***	0.42***	0.35***	0.45***	0.29**
Maximum width of the cerebral fissure in the area of the skull vault, mm	0.36***	0.35***	0.25***	0.33***	0.50***
Maximum width of the cerebellar fissure, mm	0.12*	0.13*	0.22***	0.28**	0.24*

Note: *p<0.05; **p<0.01; ***p<0.001.

CSVD patients was 10.05±4.62 days, for non-CSVD - 8.94±3.72 days.

Brain morphometry measurements in accordance to CSVD, lacunes and WMH presence are shown in tables 1, 2, 3 respectively. Correlation analysis of brain morphometrics and CSVD features are shown in Table 4.

Multivariable regression analysis, adjusted for age and sex, revealed significant impact of Evans index (OR 1.09, 95 %; CI 1.01-1.16, p=0.018), the third ventricle index (OR 1.42, 95 %; CI 1.21-1.67, p<0.001), Schaltenbrand and Nürnberger index (OR 1.42, 95 %; CI 1.21-1.67, p<0.001), the fourth ventricle index (OR 1.31, 95 %; CI 1.13-1.51, p<0,001), bicaudate index (OR 1.19, 95 %; CI 1.10-1.30, p<0.001), cella media index (Schiersmann's index) (OR 0.55, 95 %; CI 0.42-0.72, p<0.001), Huckman number (OR 1.05, 95 %; CI 1.02-1.08, p<0.001), width of the longitudinal cerebral fissure in the anterior part of the frontal lobes (OR 1.46, 95 %; CI 1.22-1.75, p<0.001), width of the left insular cistern (OR 1.24, 95 %; CI 1.11-1.39, p<0.001), width of the right insular cistern (OR 1.31, 95 %; CI 1.17-1.46, p<0.001), width of the right and left insular cisterns in sum (OR 1.17, 95 %; CI 1.10-1.25, p<0.001), width of the cerebral fissure in the area of the skull vault (OR 1.49, 95 %; CI 1.21-1.84, p<0.001) on the CSVD presence.

Discussion

In this study we explored brain morphological alterations in a cohort of stroke patients with and without CSVD. We measured such indicators, as Evans index, the third ventricle index, Schaltenbrand and Nürnberger index, the fourth ventricle index, bicaudate index, ventricular index, cella media index (Schiersmann's index), Huckman number, width of the longitudinal cerebral fissure in the anterior part of the frontal lobes, width of the right and left insular cisterns and its sum, width of the cerebral fissure in the area of the skull vault, width of the cerebellar fissure. The results of the present research strongly support that brain atrophy is a key marker in CSVD.

Our study revealed that compared with the control group, the CSVD group showed significantly increased almost all deep indicators as well as cortical sulci span (except width of the cerebellar fissure). Lacunes and WMH separately also reflected similar results, however in lacunes group Evans index and ventricular index did not show significance. Explanation for it might be that WMH affects brain parenchyma more diffuse than lacunes. In the other words - CSVD and its features, like WMH and lacunes promote diminish of the brain volume, both white and grey matter. Our results showed that CSVD should be considered a whole-brain disease as deep and cortical morphometrics were both significantly altered. Decreasing of white matter volume may lead to loss of functional connectivity. It can disrupt white matter tracts or U-fibers that mediate cortical-cortical or cortical-subcortical connections [17]. Besides, some researches showed that local white matter lesions may influence the grey matter in remote areas [13]. So white and grey matter lesions complement each other [10].

According to our findings, width of the longitudinal cerebral fissure in the anterior part of the frontal lobes in CSVD was 6.13±1.56 mm vs 5.10±1.38 mm in non-CSVD, $p<0.001$ and width of the right and left insular cisterns in sum in CSVD was 16.98±4.60 mm vs 13.41±4.16 mm in non-CSVD, $p<0.001$. Width of the cerebral fissure in the area of the skull vault (parietal cortex) was also greater in CSVD patients: 5.04±1.85 mm vs 4.12±1.29 mm, $p<0.001$, which suggests diffusion cerebral cortex involvement during CSVD progression. The prefrontal and temporal cortex is a set of functionally connected regions that plays crucial roles in internal cognitive processing like working memory, attention and language, processing speed, autobiographical memory etc. [7] and its damage can cause cognitive deterioration. Early injury of temporal lobes in CSVD might be the reason of more serious cognitive decline [12], that's why measurement of width of the insular cisterns might be useful for patients selection for early cognitive decline prevention, like acetylcholinesterase inhibitors etc., whether it is neurodegeneration or vascular origin. It is necessarily to find out relationships between cortical and deep indices impact on cognitive functions as well as stroke outcome.

We also found out that EPVS CS mostly associated with width of the cerebral fissure in the area of the skull vault ($r=0.50$, $p<0.001$), but much less associated with ventricles size. It is known that beta-amyloid angiopathy mostly associated with EPVS at centrum semiovale [12]. Hence, predominantly cerebral fissures enlargement in the area of the skull vault might reflect beta-amyloid pathology of the brain.

For further investigations, measurements of ventricle size and cortical sulci span may be of interest, particularly for disentangling the effect of primary neurodegeneration from that of CSVD. It is also interesting, whether some particular index cause a specific neuro-cognitive, functional or affective change.

Conclusions

1. Brain morphometric indices is highly associated with CSVD and are key markers in it.

2. Different indices may reflect different underlying pathology, which can be useful for diagnostic and prognostic purposes.

3. Brain indices may be treated as a marker of CSVD progression. It might be useful for patients selection for early treatment or preventive strategies.

References

[1] Cannistraro, R. J., Badi, M., Eidelman, B. H., Dickson, D. W., Middlebrooks, E. H., & Meschia, J. F. (2019). CNS small vessel disease: A clinical review. *Neurology,* 92(24), 1146-1156. doi: 10.1212/WNL.0000000000007654

[2] Charidimou, A., Boulouis, G., Frosch, M. P., Baron, J. C., Pasi, M., Albucher, J. F., … & Greenberg, S. M. (2022). The Boston criteria version 2.0 for cerebral amyloid angiopathy: a multicentre, retrospective, MRI-neuropathology diagnostic accuracy study. *The Lancet. Neurology,* 21(8), 714-725. doi: 10.1016/S1474-4422(22)00208-3

[3] Chen, X., Wang, J., Shan, Y., Cai, W., Liu, S., Hu, M. … & Lu, Z. (2019). Cerebral small vessel disease: neuroimaging markers and clinical implication. *Journal of Neurology*, 266(10), 2347-2362. doi: 10.1007/s00415-018-9077-3

[4] Chrzan, R., Gleń, A., Bryll, A., & Urbanik, A. (2019). Computed Tomography Assessment of Brain Atrophy in Centenarians. *International Journal of Environmental Research and Public Health,* 16(19), 3659. doi: 10.3390/ijerph16193659

[5] Cuadrado-Godia, E., Dwivedi, P., Sharma, S., Ois Santiago, A., Roquer Gonzalez, J., Balcells, M., ... & Suri, J. S. (2018). Cerebral Small Vessel Disease: A Review Focusing on Pathophysiology, Biomarkers, and Machine Learning Strategies. *Journal of Stroke,* 20(3), 302-320. doi: 10.5853/jos.2017.02922

[6] De Guio, F., Duering, M., Fazekas, F., De Leeuw, F. E., Greenberg, S. M., Pantoni, L., … & Jouvent, E. (2020). Brain atrophy in cerebral small vessel diseases: Extent, consequences, technical limitations and perspectives: The HARNESS initiative. *Journal of Cerebral Blood Flow and Metabolism: official journal of the International Society of Cerebral Blood Flow and Metabolism,* 40(2), 231-245. doi: 10.1177/0271678X19888967

[7] Fan, F., Liao, X., Lei, T., Zhao, T., Xia, M., Men, W., ... & He, Y. (2021). Development of the default-mode network during

childhood and adolescence: A longitudinal resting-state fMRI study. *NeuroImage,* 226, 117581. doi: 10.1016/j.neuroimage.2020.117581

[8] Fan, Y., Shen, M., Huo, Y., Gao, X., Li, C., Zheng, R., & Zhang, J. (2021). Total Cerebral Small Vessel Disease Burden on MRI Correlates With Medial Temporal Lobe Atrophy and Cognitive Performance in Patients of a Memory Clinic. *Frontiers in Aging Neuroscience,* 13, 698035. doi: 10.3389/fnagi.2021.698035

[9] Gao, Y., Li, D., Lin, J., Thomas, A. M., Miao, J., Chen, D., … & Chu, C. (2022). Cerebral small vessel disease: Pathological mechanisms and potential therapeutic targets. *Frontiers in Aging Neuroscience,* 14, 961661. doi: 10.3389/fnagi.2022.961661

[10] Ghaznawi, R., Geerlings, M. I., Jaarsma-Coes, M. G., Zwartbol, M. H., Kuijf, H. J., van der Graaf, Y., … & de Bresser, J. (2019). The association between lacunes and white matter hyperintensity features on MRI: The SMART-MR study. *Journal of Cerebral Blood Flow and Metabolism: Official Journal of the International Society of Cerebral Blood Flow and Metabolism,* 39(12), 2486-2496. doi: 10.1177/0271678X18800463

[11] Klarenbeek, P., van Oostenbrugge, R. J., Rouhl, R. P., Knottnerus, I. L., & Staals, J. (2013). Ambulatory blood pressure in patients with lacunar stroke: association with total MRI burden of cerebral small vessel disease. *Stroke,* 44(11), 2995-2999. doi: 10.1161/STROKEAHA.113.002545

[12] Li, J., Wen, H., Wang, S., Che, Y., Zhang, N., & Guo, L. (2022). Altered Brain Morphometry in Cerebral Small Vessel Disease with Cerebral Microbleeds: An Investigation Combining Univariate and Multivariate Pattern Analyses. *Frontiers in Neurology,* 13, 819055. doi: 10.3389/fneur.2022.819055

[13] Litak, J., Mazurek, M., Kulesza, B., Szmygin, P., Litak, J., Kamieniak, P., & Grochowski, C. (2020). Cerebral Small Vessel Disease. *International Journal of Molecular Sciences,* 21(24), 9729. doi: 10.3390/ijms21249729

[14] Loos, C., Makin, S., Staals, J., Dennis, M. S., van Oostenbrugge, R. J., & Wardlaw, J. M. (2018). Long-Term Morphological Changes of Symptomatic Lacunar Infarcts and Surrounding White Matter on Structural Magnetic Resonance Imaging. *Stroke,* 49(5), 1183-1188. doi: 10.1161/STROKEAHA.117.020495

[15] Rost, N. S., & Etherton, M. (2020). Cerebral Small Vessel Disease. *Continuum* (Minneapolis, Minn.), 26(2), 332-352. doi: 10.1212/CON.0000000000000841

[16] Wang, Y., Yang, Y., Wang, T., Nie, S., Yin, H., & Liu, J. (2020). Correlation between White Matter Hyperintensities Related Gray Matter Volume and Cognition in Cerebral Small Vessel Disease. *Journal of Stroke and Cerebrovascular Diseases: the Official Journal of National Stroke Association,* 29(12), 105275. doi: 10.1016/j.jstrokecerebrovasdis.2020.105275

[17] Ward, A. M., Mormino, E. C., Huijbers, W., Schultz, A. P., Hedden, T., & Sperling, R. A. (2015). Relationships between default-mode network connectivity, medial temporal lobe structure, and age-related memory deficits. *Neurobiology of Aging,* 36(1), 265-272. doi: 10.1016/j.neurobiolaging.2014.06.028

[18] Wardlaw, J. M., Smith, E. E., Biessels, G. J., Cordonnier, C., Fazekas, F., Frayne, R., … & Greenberg, S. S. (2013). Tandards for Reporting Vascular changes on nEuroimaging (STRIVE v1) Neuroimaging standards for research into small vessel disease and its contribution to ageing and neurodegeneration. *The Lancet. Neurology,* 12(8), 822-838. doi: 10.1016/S1474-4422(13)70124-8

[19] Wilk, R., Kluczewska, E., Syc, B., & Bajor, G. (2011). Normative values for selected linear indices of the intracranial fluid spaces based on CT images of the head in children. *Polish Journal of Radiology,* 76(3), 16-25.

[20] Zeng, W., Chen, Y., Zhu, Z., Gao, S., Xia, J., Chen, X., … & Zhang, Z. (2020). Severity of white matter hyperintensities: Lesion patterns, cognition, and microstructural changes. *Journal of Cerebral Blood Flow and Metabolism: Official Journal of the International Society of Cerebral Blood Flow and Metabolism,* 40(12), 2454-2463. doi: 10.1177/0271678X19893600

[21] Zhu, H., Lu, H., Wang, F., Liu, S., Shi, Z., Gan, J., … & Ji, Y. (2022). Characteristics of Cortical Atrophy and White Matter Lesions Between Dementia with Lewy Bodies and Alzheimer's Disease: A Case-Control Study. *Frontiers in Neurology,* 12, 779344. doi: 10.3389/fneur.2021.779344

ЦЕРЕБРАЛЬНА МОРФОМЕТРІЯ ТА ЇЇ КЛІНІЧНЕ ЗНАЧЕННЯ ПРИ ЗАХВОРЮВАННІ МАЛИХ СУДИН МОЗКУ

Московко С. П., Бартюк Р. С.

Захворювання малих судин головного мозку (ЗМСМ) - це група гетерогенних розладів, що вражають дрібні перфорантні судини головного мозку. Клінічно ЗМСМ проявляється різними симптомами, такими як когнітивні, функціональні, афективні розлади, а також лакунарним інсультом або внутрішньомозковим крововиливом. ЗМСМ є причиною 25 % усіх інсультів та виступає другою причиною деменції після хвороби Альцгеймера. Золотим стандартом діагностики ЗМСМ є нейровізуалізація. Основними ключовими ознаками є гіперінтенсивність білої речовини (лейкоараіоз), лакуни, розширені периваскулярні простори, мозкова атрофія. Доведено, що атрофія мозку відіграє синергічну роль як у цереброваскулярних, так і в нейродегенеративних захворюваннях, що розвиваються у старіючому мозку. Вона відображає кінцевий загальний результат прогресування патологічних процесів, які розвиваються із часом. Прогресування ЗМСМ призводить до поступового зменшення об'єму мозку, що проявляється зміною розмірів шлуночків і борозн мозку. Але про його масштаби, кореляти та наслідки відомо небагато. Мета дослідження - з'ясувати, чи корелюють морфометричні зміни головного мозку з ознаками ЗМСМ. У дослідженні прийняли участь 129 пацієнтів зі ЗМСМ та 165 пацієнтів без ЗМСМ, у котрих розвинувся інсульт. Усі хворі пройшли нейровізуалізаційне обстеження за допомогою магнітно-резонансної та комп'ютерної томографії. Ми використали як однофакторний, так і багатофакторний регресійний аналіз, а також кореляційний аналіз із метою виявлення відмінностей у морфометричних параметрах мозку між групами. Багатофакторний регресійний аналіз, скоректований за віком і статтю, виявив достовірний вплив індексу Еванса (ВШ 1,09, 95%; ДІ 1,01-1,16, p=0,018), індексу третього шлуночка (ВШ 1,42, 95%; ДІ 1,21-1,67, p<0,001), індексу Шалтенбранда-Нюренбергера (ВШ 1,42, 95%; ДІ 1,21-1,67, p<0,001), індексу четвертого шлуночка (ВШ 1,31, 95%; ДІ 1,13-1,51, p<0,001), бікаудального індексу (ВШ 1,19, 95%; ДІ 1,10-1,30, p<0,001), індексу Шеєрсмана (ВШ 0,55, 95%; ДІ 0,42-0,72, p<0,001), числа Хакмана (ВШ 1,05, 95%; ДІ 1,02-1,08, p<0,001), ширини поздовжньої мозкової щілини в передній частині лобових часток (ВШ 1,46, 95%; ДІ 1,22-1,75, p<0,001), ширини лівої острівкової цистерни (ВШ 1,24, 95% ДІ 1,11-1,39, p<0,001), ширини правої острівкової цистерни (ВШ 1,31, 95% ДІ 1,17-1,46, p<0,001), ширини правої та лівої стрівкових цистерн у сумі (ВШ 1,17, 95%; ДІ 1,10-1,25, p<0,001), ширини мозкової щілини в ділянці склепіння черепа (ВШ 1,49, 95%; ДІ 1,21-1,84, p<0,001) на наявність ЗМСМ. Ширина поздовжньої мозкової щілини в передньому відділі лобових часток при ЗМСМ

становила 6,13±1,56 мм проти 5,10±1,38 мм у контрольній групі (p<0,001), сумарна ширина правої та лівої острівкових цистерн при ЗМСМ становила 16,98±4,60 мм проти 13,41±4,16 мм у групі контролю, p<0,001. Ширина мозкової щілини в ділянці склепіння черепа (тім'яної кори) також була більшою у хворих із ЗМСМ: 5,04±1,85 мм проти 4,12±1,29 мм, p<0,001. Таким чином, усі шлуночкові та кортикальні індекси були збільшеними в групі пацієнтів зі ЗМСМ. Дані результати вказують на те, що морфометричні показники головного мозку тісно пов'язані зі ЗМСМ і можуть бути корисними для прогнозування наслідків інсульту та констатації зниження когнітивних функцій.

Ключові слова: *морфометрія мозку, захворювання малих судин мозку, індекс Еванса.*

DOI: 10.31393/morphology-journal-2022-28(4)-03 Reports of Morphology, Vol. 28, №4, Pages 18-26

ISSN 1818-1295 eISSN 2616-6194

REPORTS OF MORPHOLOGY

Official Journal of the Scientific Society of Anatomists, Histologists, Embryologists and Topographic Anatomists of Ukraine

journal homepage: https://morphology-journal.com

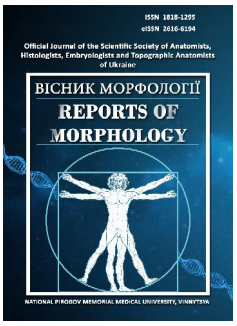

Neuron-glial relations of the posterior horns of the spinal cord of human fetuses

Prykhodko S. O., Shkolnikov V. S.
National Pirogov Memorial Medical University, Vinnytsya, Ukraine

ARTICLE INFO
Received: 27 June 2022
Accepted: 5 August 2022

UDC: 611.826:618.29

CORRESPONDING AUTHOR
e-mail: v.shkolnikov@gmail.com
Shkolnikov V. S.

CONFLICT OF INTEREST
The authors have no conflicts of interest to declare.

FUNDING
Not applicable.

Despite the relatively sufficient study of the structure and functioning of the nervous system, interest in the problem of neuron-glial relationships continues to grow steadily, as this parameter reflects the dynamics of the development of nervous tissue and can be used to assess the quality level of morphological changes. The purpose of the study: to establish the morphogenesis and neuron-glial relationships of the posterior horns of the human spinal cord in the fetal period of ontogenesis. This study was performed on the preparations of 104 human fetuses from 8-9 weeks to 39-40 weeks using anatomical, histological, immunohistochemical and morphometric methods. Statistical processing of the numerical data of the obtained results was carried out using the licensed software package "Statistica 6.1" of the StatSoft company using parametric and non-parametric methods. During the research, it was established that in the fetal period, the greater proliferative activity of the dorsal neuroepithelium is determined at 8-9 weeks: in the cervical segments - 10 % ($p<0.05$), in the thoracic, lumbar and sacral segments - 9 % ($p<0.05$). By 39-40 weeks, this indicator gradually becomes smaller: in the cervical and lumbar segments, 4 % of cells (2-3 cells reacted) ($p<0.05$) and in the thoracic and sacral segments - 3 % (1-2 cells reacted) ($p<0.05$). It was found that throughout the fetal period there is a tendency to a gradual decrease in the density of neurons and gliocytes. The glial index, on the contrary, up to 39-40 weeks increases, and at the time of birth it is equal to 2.1 in the cervical, thoracic and lumbar segments, and 2.0 in the sacral segments. It was found that at 11-12 weeks, radial glia fibers form mesh structures within the neuronal complexes, which coincides with the beginning of the formation of neuron-glial complexes of the posterior horns. At 17-18 weeks, the fibers of radial glia keep the radial direction only in the middle part of the posterior horns. At 34-35 weeks, vimentin expression was determined to be relatively moderate in the remnants of radial glia near the dorsal neuroepithelium and focal expression of vimentin around vessels within the posterior horns. Expression of vimentin in the neuroepithelium of fetuses of 39-40 weeks was absent. In this age period, the neuroepithelium is structured from ependymocytes and radial glia cells are absent, as there is a relatively strong expression of S-100 in the neuroepithelium. Relatively strong expression of synaptophysin occurred in the posterior horns of 8-9 week fetuses. This age period is the beginning of the establishment of synaptic connections.
Keywords: *human fetuses, spinal cord, posterior horns, neuron-glial relations, radial glia, neural stem cells.*

Introduction

Over the last decade, the study of the anatomy of the human fetus has grown in popularity among scientists around the world due to the development of modern imaging methods, as well as the technical complication of surgical interventions during the correction of malformations in the fetal period, which is required today [1].

It is known that the spinal cord is quite complex in terms of cytoarchitectonic and functional control system, and therefore plays a significant role in sensory-motor integration and in the implementation of control programs of the skeletal-muscular system [18]. In addition, over the past 2-3 years, the attention of scientists to the detailed study of the cellular composition of the posterior horns of

the spinal cord has significantly increased [16, 24]. This phenomenon is related to the fact that the rear horns perform a multifaceted functional load in the sensory integration of the entire body. Therefore, in understanding emerging pathological conditions [17, 28], a detailed study of the structuring and formation of the rear horns during ontogenesis, especially in the prenatal period, is important. Until now, there is no doubt about the presence of permanent neurogenesis of some areas of the brain due to colonies of neural stem cells (NSCs) [11, 20]. During the embryonic period of ontogenesis, NSCs of the cranial parts of the neural tube showed greater proliferative activity than neural cells of the caudal parts [21]. Thus, it is possible to predict that the above-mentioned processes are inherent in the spinal cord, which precede the formation of centers and cellular complexes, and this, in turn, requires further research and clarification.

According to Cedeno D. L. [10], the scientific world has an urgent problem of studying neuron-glial relations, since this parameter is a reflection of the dynamics of the development of the central nervous system and can be used to assess the quality level of morphological changes. As Stepanov A. S. noted [25], research in this direction is promising and certainly has practical significance.

Therefore, *the aim of this study* was to establish the morphogenesis and neuron-glial relationships of the posterior horns of the human spinal cord in the fetal period of ontogenesis.

Materials and methods

This study was performed on preparations of human fetuses aged from 8-9 weeks to 39-40 weeks of the fetal period with a total number of 104 objects. During the development of fetuses in the uterus, there were no pronounced harmful factors of the external and internal environment and those obtained during medical abortions, or stillbirths in relatively healthy women in the Regional Pathological Bureau and in the maternity hospitals of Vinnytsia. There was no pathology of central nervous system formations. As a result of the expert opinion of the commission on biomedical ethics of the National Pirogov Memorial Medical University, Vinnytsya (protocol of the meeting of the Bioethics Committee № 10 of December 6, 2018), the work was performed in compliance with the main provisions of the GCP (1996), the Council of Europe Convention on Human Rights and Biomedicine (1997) and research materials do not contradict the basic bioethical norms of the Helsinki Declaration on Ethical Principles of Scientific and Medical Research with Human Participation, adopted by the 59th General Assembly of the World Medical Association in 2008. Pursuant to the 2017 agreement on joint scientific and practical activities between the National Pirogov Memorial Medical University, Vinnytsya and VRPAB, pathological examination protocols were drawn up in accordance with form № 013-2/o approved by the order of the Ministry of Health of Ukraine dated August 14, 2004 № 417.

The preparations of the spinal cord were stained with hematoxylin and eosin, toluidine blue, and silver impregnation was carried out according to Bilzhovskyi.

Immunohistochemical technique: use of vimentin, CDX-2, Ki-67, S-100 and synaptophysin (diagnostic monoclonal antibodies of the company "DacoCytomation" (Denmark)). Vimentin and CDX-2 - to study the morphology of radial glia, Ki-67 - to evaluate the proliferative activity of neutral cells and synaptophysin - to study the development of synaptic connections and to evaluate the myelination of nerve fibers. The quality of protein expression was evaluated according to the scale of staining intensity: absent - absence of a positive reaction in cells; weak - up to 30 % cell reaction; average - 31-60 % and strong - 60 % and more [9].

Among the morphometric methods, histo- and karyometry were used. Histometry of the dorsal neuroepithelium and formations of the posterior horns of the spinal cord segments of human embryos and fetuses was performed using the PhotoM 1.21 software. Karyocytometry was performed using the software described above. Transverse and longitudinal dimensions were studied, and the area of cells and nuclei of radial glia, NSCs, neuroblasts and neurons of the marginal nucleus, gelatinous substance, nucleus of the posterior horn and thoracic nucleus was determined.

The method of determining the density of neurons and glial cells of the posterior horns of the human spinal cord in the prenatal period of ontogenesis was that five sections with an area of 0.01 mm2 were applied to each of five histological sections, after which cells were counted from the obtained data of 25 sections of the corresponding layer and determined the cell density. The glial index (GI) was calculated as the ratio of the number of gliocytes to the number of neurons, that is, the number of gliocytes per neuron. For clarity of comparison, the density of neurons was taken as one.

Statistical processing of the obtained morphometric parameters was carried out using the standard software package "Statistica 6.1" of StatSoft (owned by SRC National Pirogov Memorial Medical University, Vinnytsya, license № BXXR901E246022FA) using parametric and non-parametric criteria for evaluating the obtained results. Differences between samples were determined using the Mann-Whitney U-test and the Student's t-test, and average values for each characteristic and their standard deviations were determined.

Results

We found that the proliferative activity of neural stem cells in the dorsal part of the neuroepithelium of 8-9 weeks fetuses is relatively greatest in the cervical segments (Ki-67 expression was observed in 10 % of cells) ($p<0.01$), in the thoracic, lumbar and sacral segments the same proliferative activity, which was 9 % ($p<0.05$) (Fig. 1).

Vimentin expression remains relatively strong in the

neuroepithelium, within the most posterior horns, and within the posterior cords. Fibers of radial glia have a radial direction and in a fan-like manner penetrate the posterior horns and end in the posterior cords. Short fibers of radial glia are located in the posterior horns dorso-medially. It should be noted that in this age period, CDX-2 is also weakly expressed in radial glia fibers in the segments of the spinal cord. S-100 expression was absent in radial glia cells and neurons of the posterior horns. Synaptophysin expression was moderate within the posterior horns and synaptophysin expression was absent within the neuroepithelial layer. Thus, the process of establishing synaptic connections of neurons of the posterior horns continues.

The average value of the density of neurons and neuroblasts in the cervical segments of fetuses of 8-9 weeks was equal to 25.26±2.04 unit/0.01 mm^2 ($p<0.01$), in the thoracic segments - 19.32±1.81 unit/0.01 mm^2 ($p<0.05$), in the lumbar segments was 24.17±2.05 unit/0.01 mm^2 ($p<0.01$) and in the sacral segments - 17.88±1.64 unit/0.01 mm^2 ($p<0.01$). The density of glial cells of the posterior horns in the cervical segments was 42.80±2.19 unit/0.01 mm^2 ($p<0.05$), in the thoracic segments was equal 30.93±1.43 unit/0.01 mm^2 ($p<0.05$), in the lumbar segments - 38.66±1.50 unit/0.01 mm^2 ($p<0.05$) and in the sacral segments - 26.51±1.44 unit/0.01 mm^2 ($p<0.05$). Thus, the GI was 1.7, in the thoracic segments - 1.6, in the lumbar segments it was 1.6 and in the sacral segments - 1.5.

In weeks 9-10, the proliferative activity of NSCs of the dorsal neuroepithelium is relatively greatest in the cervical segments - 9 % of cells ($p<0.01$), in the thoracic segments - 8 % ($p<0.05$), in the lumbar - 9 % ($p<0.05$) and in sacrum - 8 % ($p<0.05$). Only the proliferation of glial cells was noted within the posterior horns. Vimentin expression remained relatively strong in the neuroepithelium, within the most posterior horns and within the posterior cords. In this age period, CDX-2 expression was absent in segments throughout the spinal cord.

The average value of the density of neurons and neuroblasts in the cervical segments of fetuses of 9-10 weeks was equal to 23.48±1.41 unit/0.01 mm^2 ($p<0.05$), in the thoracic segments - 21.55±1.30 unit/0.01 mm^2 ($p<0.05$), in the lumbar segments - 23.73±1.56 unit/0.01 mm2 ($p<0.01$) and in the sacral segments - 19.20±1.68 unit/0.01 mm^2 ($p<0.05$). Density of glial cells: in cervical segments - 42.12±2.39 unit/0.01 mm^2 ($p<0.05$), in the thoracic segments - 34.40±1.76 unit/0.01 mm^2 ($p<0.05$), in the lumbar segments - 41.84±2.04 unit/0.01 mm^2 ($p<0.05$), and in the sacral segments - 28.81±1.46 unit/0.01 mm^2 ($p<0.05$). The GI is 1.8 in the cervical segments, 1.6 in the thoracic segments, 1.7 in the lumbar segments, and 1.5 in the sacral segments.

We found that the proliferative activity of NSCs in the dorsal neuroepithelium of 11-12-weeks fetuses is relatively greatest in the cervical and lumbar segments, the expression of Ki-67 was observed in 7 % of cells (6-7 cells reacted) ($p<0.05$), in the thoracic and sacral segments - 6 % (5-6 cells reacted) ($p<0.05$). Moderate expression of vimentin was noted within the area of the posterior horns in all segments of the spinal cord. Within the neuron complexes, radial glia fibers form mesh structures (Fig. 2).

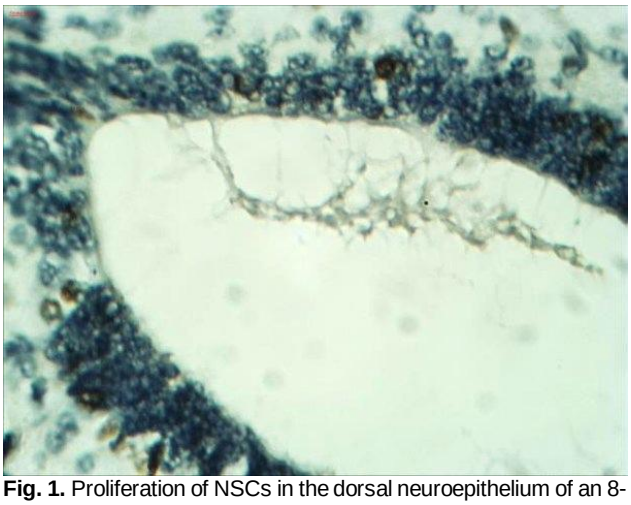

Fig. 1. Proliferation of NSCs in the dorsal neuroepithelium of an 8-9 weeks human fetus. Ki-67. x400.

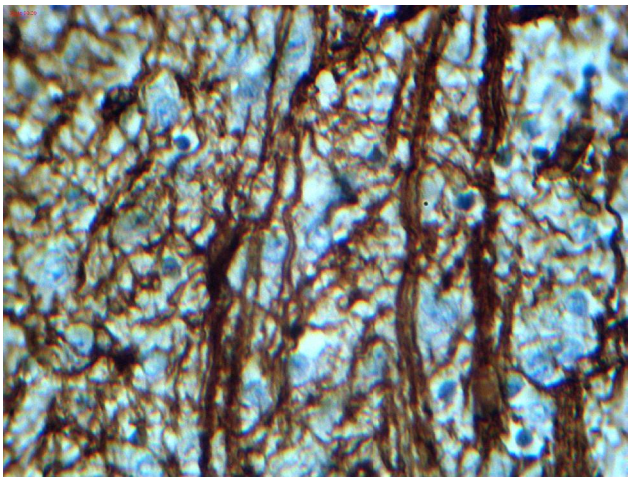

Fig. 2. The formation of reticular structures by radial glia fibers in the places of formation of neuron-glial complexes of the posterior horns of the spinal cord of fetuses of 11-12 weeks. Vimentin. x400.

Obviously, this phenomenon is related to the morphogenesis of the neuronal complexes themselves. Relatively strong expression of S-100 was observed in the posterior horns of the spinal cord. The expression of synaptophysin was relatively strong in the ventro-medial areas of the posterior horns, moderate in the thin bundle and other areas of the posterior horns, and weak in the wedge-shaped bundle. The expression of synaptophysin has not been established in the neuroepithelium itself.

The density index of neurons and neuroblasts in the posterior horns of fetuses of 11-12 weeks was obtained as follows: in the cervical segments - 22.33±1.39 unit/0.01 mm^2 ($p<0.01$), in the thoracic segments - 22.65±1.47 unit/0.01 mm^2 ($p<0.05$), in the lumbar segments - 23.12±

1.51 unit/0.01 mm^2 (p<0.01) and in the sacral segments - 21.89±1.74 unit/0.01 mm^2 (p<0.05). Density of glial cells: in cervical segments 41.61±2.15 unit/0.01 mm^2 (p<0.05), in the thoracic segments - 38.40±1.83 unit/0.01 mm^2 (p<0.05), in the lumbar segments - 41.64±1.97 unit/0.01 mm^2 (p<0.05) and in the sacral segments - 34.90±1.66 unit/0.01 mm^2 (p<0.05). Thus, GI in the cervical segments is 1.9, in the thoracic segments - 1.7, in the lumbar segments - 1.8, and in the sacral segments - 1.6.

In fetuses of 17-18 weeks, the proliferative activity of NSCs in the dorsal part of the neuroepithelium is relatively greatest in the cervical and lumbar segments, Ki-67 expression was observed in 5 % of cells (5-6 cells reacted) (p<0.05), in the thoracic and sacral segments - 4 % (4-5 cells reacted) (p<0.05). Long fibers of radial glia were observed only in the middle part of the posterior horns, and extended from the medial part of the base (starting from the dorsal neuroepithelium) to the dorso-lateral part. Relatively moderate expression of vimentin was noted in the posterior horns in all segments of the spinal cord. Relatively strong expression of S-100 in the posterior horns was noted at the base of the posterior horns and in the middle part. The expression of synaptophysin was relatively strong in the ventro-medial regions of the posterior horns, moderate in the thin bundle and the rest of the posterior horns.

The neuron density index in fetuses of 17-18 weeks in the cervical segments was equal 20.22±1.07 unit/0.01 mm^2 (p<0.05), in the thoracic segments - 20.43±1.14 unit/0.01 mm^2 (p<0.05), in the lumbar segments - 22.06±1.48 unit/0.01 mm^2 (p<0.05) and in the sacral segments - 22.61±1.52 unit/0.01 mm^2 (p<0.05). Density of glial cells: in cervical segments 38.36±1.70 unit/0.01 mm^2 (p<0.05), in the thoracic segments - 36.72±1.83 unit/0.01 mm^2 (p<0.05), in the lumbar segments - 40.39±1.75 unit/0.01 mm^2 (p<0.05) and in the sacral segments - 38.48±1.91 unit/0.01 mm^2 (p<0.01). Therefore, the GI was 1.9 in the cervical segments, 1.8 in the thoracic segments, 1.8 in the lumbar segments, and 1.7 in the sacral segments.

In weeks 20-21, we established that the proliferative activity of NSCs in the dorsal neuroepithelium of fetuses remains relatively greatest in the cervical and lumbar segments, where Ki-67 expression was observed in 5 % of cells (5-6 cells reacted) (p<0.01), in breast and sacral segments - 4 % (4-5 cells reacted) (p<0.05). The expression of vimentin in radial glia indicates the presence of short and long fibers of this formation. Moreover, the long fibers had an intermittent course in the middle part of the rear horns, and extended from the middle part of the base to the dorso-lateral part. Short fibers together with radial glia cell bodies form the neuroepithelium itself. In general, a relatively strong expression of vimentin was observed only in the neuroepithelium (radial glia cells), in the remaining areas of the posterior horns in all segments of the spinal cord, a relatively weak expression of vimentin was noted. Relatively strong expression of synaptophysin was noted in all areas of the posterior horns.

The density of neurons in the rear horns of fetuses of 20-21 weeks was as follows: in the cervical segments - 18.62±1.04 unit/0.01 mm^2 (p<0.01), in the thoracic segments - 20.21±1.15 unit/0.01 mm^2 (p<0.05), in the lumbar segments - 20.67±1.22 unit/0.01 mm^2 (p<0.01), and in the sacral segments - 21.90±1.41 unit/0.01 mm^2 (p<0.05). Density of glial cells: in cervical segments 37.24±1.75 unit/0.01 mm^2 (p<0.05), in the thoracic segments 36.33±1.92 unit/0.01 mm^2 (p<0.05), in the lumbar segments - 39.11±1.86 unit/0.01 mm^2 (p<0.01) and in the sacral segments - 39.44±1.79 unit/0.01 mm^2 (p<0.05). The glial index in the cervical segments was 2.0, in the thoracic segments - 1.8, in the lumbar segments - 1.9, and in the sacral segments - 1.8.

In fetuses of 25-26 weeks, the density of neurons of the posterior horns throughout the spinal cord in the cervical segments was equal to 17.80±0.91 unit/0.01 mm^2 (p<0.05), in the thoracic segments - 19.36±1.15 unit/0.01 mm^2 (p<0.05), in the lumbar segments 19.92±1.15 unit/0.01 mm^2 (p<0.05) and in the sacral segments - 21.37±1.40 unit/0.01 mm^2 (p<0.05). Density of glial cells: in cervical segments 35.12±1.62 unit/0.01 mm^2 (p<0.05), in the thoracic segments - 36.13±1.93 unit/0.01 mm^2 (p<0.01), in the lumbar segments - 38.06±1.87 unit/0.01 mm^2 (p<0.05) and in the sacral segments - 39.11±1.74 unit/0.01 mm^2 (p<0.05). Thus, the GI was 2.0 in the cervical segments, 1.9 in the thoracic segments, 1.9 in the lumbar segments, and 1.8 in the sacral segments.

We established that the density of neurons in the posterior horns of the spinal cord of fetuses of 29-30 weeks in the cervical segments was 17.29±0.85 unit/0.01 mm^2 (p<0.01), in the thoracic segments - 18.46±1.11 unit/0.01 mm^2 (p<0.05), in the lumbar segments - 18.54±1.02 unit/0.01 mm^2 (p<0.01) т and in the sacral segments 20.43±1.33 unit/0.01 mm^2 (p<0.05). Density of glial cells: in cervical segments - 34.30±1.65 unit/0.01 mm^2 (p<0.05), in the thoracic segments - 35.87±1.92 unit/0.01 mm^2 (p<0.05), in the lumbar segments - 36.77±1.61 unit/0.01 mm^2 (p<0.05) and in the sacral segments - 37.63±1.50 unit/0.01 mm^2 (p<0.05). GI in the cervical segments was 2.0, in the thoracic segments - 2.0, in the lumbar segments - 2.0, and in the sacral segments - 1.8.

It was established that the proliferative activity of NSCs in the dorsal neuroepithelium of fetuses at 34-35 weeks remains relatively greatest in the cervical and lumbar segments, expression of Ki-67 was observed in 5 % of cells (3-4 cells reacted) (p<0.01), in the thoracic and sacral segments - 4 % (2-3 cells reacted) (p<0.05). The expression of vimentin was determined to be relatively moderate in the remnants of radial glia near the dorsal neuroepithelium (area of the base of the posterior horns), and focal expression of vimentin was observed around the vessels within the boundaries of the posterior horns (Fig. 3).

The expression of S-100 was relatively strong in the base of the posterior horns and the middle part. It should

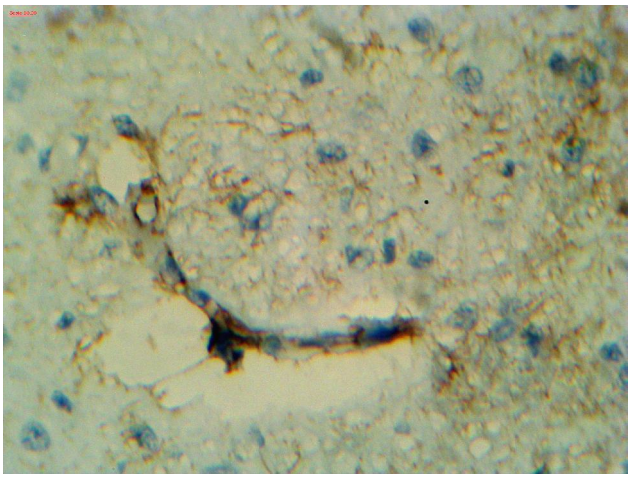

Fig. 3. Posterior horns of the spinal cord of a human fetus at 34-35 weeks. Focal expression of vimentin in remnants of radial glia near vessels. Vimentin. x400.

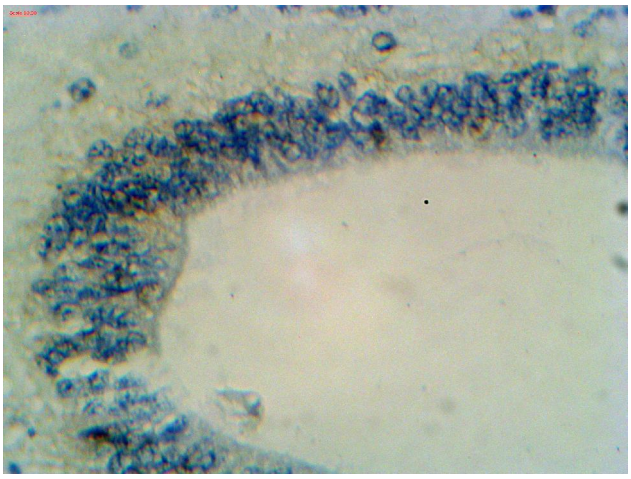

Fig. 4. Proliferation of NSCs in the dorsal neuroepithelium of a 39-40 weeks fetus. Ki-67. x400.

be noted that some neurons also expressed S-100. Relatively strong expression of synaptophysin was observed within the neck (proper nucleus) and head (gelatinous substance). Moderate expression of synaptophysin was at the apex of the posterior horns (posterior marginal nucleus).

The value of the density of neurons of the posterior horns in fetuses of 34-35 weeks in the cervical segments was 16.08±0.74 unit/0.01 mm^2 ($p<0.05$), in the thoracic segments - 17.25±1.05 unit/0.01 mm^2 ($p<0.05$), in the lumbar segments 17.54±0.91 unit/0.01 mm^2 ($p<0.05$) and in the sacral segments - 19.00±1.26 unit/0.01 mm^2 ($p<0.05$). Density of glial cells: in cervical segments 33.34±1.55 unit/0.01 mm^2 ($p<0,05$), in the thoracic segments 35.48±1.72 unit/0.01 mm^2 ($p<0.05$), in the lumbar segments - 35.66±1.49 unit/0.01 mm^2 ($p<0.05$) and in the sacral segments - 36.93±1.52 unit/0.01 mm^2 ($p<0.05$). Accordingly, the GI of the posterior horns in the cervical segments was 2.1, in the thoracic segments - 2.1, in the lumbar segments - 2.0, and in the sacral segments - 1.9.

The proliferative activity of NSCs of the dorsal neuroepithelium at 39-40 weeks remains relatively greatest in the cervical and lumbar segments, expression of Ki-67 was observed in 4 % of cells (2-3 cells reacted) ($p<0.05$), in the thoracic and sacral segments - 3 % (1-2 cells reacted) ($p<0.05$) (Fig. 4). The expression of vimentin in the posterior horns was relatively moderate in the remnants of radial glia around the neuroepithelium, and in the neuroepithelium itself, vimentin expression was absent and focal vimentin expression was observed around the vessels. The expression of S-100 protein in the posterior horns is relatively strong at the base of the posterior horns and in the middle part. It should be noted that some neurons also expressed S-100.

Expression of synaptophysin was noted in all areas of the posterior horns. Relatively strong expression of synaptophysin was observed within the neck (proper nucleus) and head (gelatinous substance). Moderate expression of synaptophysin was at the top of the posterior horns (posterior marginal nucleus).

The parameter of the density of neurons in the posterior horns during the spinal cord in fetuses of 39-40 weeks was as follows: in the cervical segments - 15.04±0.59 unit/0.01 mm^2 ($p<0.05$), in the thoracic segments - 16.44±0.83 unit/0.01 mm^2 ($p<0.05$), in the lumbar segments - 16.11±0.81 unit/0.01 mm^2 ($p<0.05$) and in the sacral segments - 17.74±1.03 unit/0.01 mm^2 ($p<0.05$). Density of glial cells: in cervical segments 31.72±1.46 unit/0.01 mm^2 ($p<0.05$), in the thoracic segments - 34.42±1.57 unit/0.01 mm^2 ($p<0.05$), in the lumbar segments - 33.84±1.38 unit/0.01 mm^2 ($p<0.05$) and in the sacral segments - 35.40±1.40 unit/0.01 mm^2 ($p<0.05$). Therefore, the GI was 2.1 in the cervical segments, 2.1 in the thoracic segments, 2.1 in the lumbar segments, and 2.0 in the sacral segments.

Thus, in the course of the study, we determined the density of neurons and glial cells of the posterior horns of human fetuses, as well as the glial index and proliferative activity of NSCs of the dorsal neuroepithelium.

Discussion

The parameter of the density of neurons and neuroblasts in the posterior horns during intrauterine development is quantitatively asynchronous. Thus, in the cervical and lumbar segments, this parameter increases to 8-9 weeks, in the thoracic segments - to 11-12 weeks, in the sacral segments - to 14-15 weeks. In the following, before birth, the density of neurons and neuroblasts in the posterior horns of all segments gradually becomes smaller.

In our previous studies, it was established that the proliferative activity of NSCs of the dorsal epithelium and the maximum density of neurons of the posterior horns occurs in the embryonic period, up to 8-9 weeks [26]. Comparing such indicators with the results of this study, we can conclude that from the beginning of the fertile period, the above-mentioned parameters before birth have a

Table 1. Quantitative composition of neuron-glial cells of the spinal cord of an adult according to Bahney J. and von Bartheld C. S. (2018).

Segments	Total number of cells, million	Neurons, %	Glia cells, %	Neuron-glial relation
Cervical	535.5±98.9	13.5	86.5	1:7
Thoracical	670.3±131.9	14.0	86.0	1:5
Lumbar	457.9±97.7	12.6	87.4	1:7

tendency to gradually decrease.

We have established that the parameter of the density of gliocytes in the posterior horns during intrauterine development is also quantitatively asynchronous. An increase in the density of glial cells in the cervical segments was observed up to 8-9 weeks [26], in the thoracic segments - up to 11-12 weeks, in the lumbar segments - up to 9-10 weeks, and in the sacral segments - up to 20-21 weeks. Before birth, the density of glial cells in the posterior horns of all segments gradually becomes smaller.

Before the beginning of the fetus period (8-9 weeks), the cervical segments have the maximum GI value of the posterior horns (GI - 1.7), the thoracic and lumbar segments have the GI value - 1.6, and the sacral segments have the minimum GI value - 1.5 [26]. By 29-30 weeks, the GI index in the cervical, thoracic and lumbar segments is the same and is 2.0. At 34-35 weeks, the value of GI in the rear horns of the lumbar segments, in contrast to the cervical and thoracic segments, becomes somewhat smaller, but before birth, the GI indicator becomes the same again in the above-mentioned segments (GI - 2.1). It should be noted that the GI value in the posterior horns of the sacral segments remains smaller throughout the fetal period and at the time of birth its value was 2.0.

S.V. Ryhlik [22] found that with increasing human age, there is a progressive decrease in the distribution density, number and size of nerve cells, a decrease in the amount of Nissl's substance, dystrophy and degeneration of neurons, accumulation of lipofuscin in them, a decrease in protein-synthesizing function, an increase in the number of gliocytes, reduction of the capillary network, polymorphism of endothelial cells. In her own research, M. A. Berezhnaya [6] also came to the conclusion that with age in the V layer in the upper frontal gyri of the human brain, a decrease in the number of neurons and capillaries was observed, but the number of glial cells increased, which is characterized by pronounced dynamics of changes in the glial index. The most pronounced changes for all parameters were noted between the age groups of 35-50 years and 51-75 years. According to O. Ya. Zhurakivska [29], the numerical density of glial cells also decreases with age. It should be noted that similar studies were concerned with the study of neuron-glial relations in the formations of the central nervous system of adults. However, the scientific conclusions regarding the decrease with age in the density of neural cells and the increase in the glial index are also confirmed by our research.

After long contradictory statements regarding the number of neurons and glial cells in the brain of humans and primates, scientists have recently reached a consensus [27]. However, the number of cellular components in relation to another component of the central nervous system, i.e. the spinal cord, remains uncertain [3, 13]. Thus, Burish M. J. [8] proposed the highest limit of the neuron-glial ratio, which is 1:40. Analyzing similar works by other authors and taking into account the above results from available literature sources, similar ratios in animals are on average 1:2 or 1:3 [7]. In general, most scientists adhere to the opinion that in such structures of the central nervous system as the cerebral cortex, cerebellum, brain stem, etc., a more consistent and gradual change in the neuron-glial ratio occurs, including in humans [12]. Therefore, we believe that the obtained data of the neuron-glia ratio in the spinal cord Burish M. J. [8] do not look expected.

In our opinion, more accurate results regarding the number of neurons and glial cells, as well as establishing the neuron-glial ratio in the spinal cord of an adult person and animals, were obtained by Bahney J. and von Bartheld C. S. [3]. The authors studied the spinal cord of three monkeys and three adults using the method of isotropic fractionation; there were no CNS diseases. Scientists determined the number of neurons and glial cells, as well as the neuron-glia ratio separately in the cervical, thoracic, and lumbar segments (Table 1).

Therefore, the ratio of glial cells and neurons was determined in human brain tissue [14], and not so long ago in the entire human spinal cord [3]. However, there is almost no purposeful description of the ratios of different populations of glial cells and neurons in the posterior horn of the segments of the human spinal cord, except for isolated reports. Thus, in their research Ruiz-Sauri A. [21] studied the relationship of glial cells to neurons in the posterior horns of the spinal cord of an adult and only in the thoracic segments (T8-T11). The authors emphasized the importance of understanding the anatomical and histological structure of the posterior horn in the above segments. The results of Ruiz-Sauri A. [21] showed that the number of neuron bodies in the gray matter of the segments is much smaller than the number of glial cells. The neuron-glia ratio in the gray matter was 1:12.

Therefore, the obtained results of our research coincide with the main provisions of the proposed concept of Herculano-Houzel S. [13], that as the brain matter increases, the following processes should occur: an obvious decrease in the number of neurons and their enlargement, an increase in the number of glial cells per neuron (since glial cells are engaged in providing the needs of neurons and do not actually increase in size), then the density of the distribution of neurons in the brain tissue should decrease. In addition, in our opinion, the growth of satellite glia indicates a high degree of functional activity of neurons, therefore the nature of structural and quantitative changes

of glia demonstrates high plasticity of nervous tissue.

The issue of discussion today is the study of the intensity of the proliferation processes of the dorsal neuroepithelium of the human spinal cord during the prenatal period [23] and their effect on the density of neural cells in the posterior horns [2, 14], as this is the basis for the formation of the NGC [5].

Again taking into account our previous works [26] and analyzing the results of this study, we concluded that the greatest proliferative activity of the dorsal neuroepithelium occurs during the embryonic period. Starting from the beginning of the fetal period and before birth, the proliferative activity of the dorsal neuroepithelium becomes less. After proliferation, NSCs of the dorsal neuroepithelium migrate into the mantle layer along radial glia fibers. The fibers of the radial glia of the posterior horns express vimentin relatively strongly and are characterized by a clear radial direction. With its short fibers, radial glia forms a "stripedness", which, in our opinion, enables NSCs to move not only radially, but also in other directions. T. J. Nowakowski and others [15] also describe the presence of intermittent fibers of radial glia already in the early stages of embryogenesis in brain formations. In addition, in this age period, radial glia fibers are part of the posterior roots of the spinal cord. This phenomenon can be explained by the fact that the neural cells of the dorsal neuroepithelium have the ability to migrate not only to the mantle layer, but also to the spinal nodes. Also, at 11-12 weeks. in the formations of the posterior horns, radial glia fibers form mesh structures, which is obviously connected with the beginning of the formation of neuron-glial complexes of the posterior horns. The final involution of radial glia in the posterior horns of the spinal cord of human fetuses begins at 34-35 weeks, i.e. these are the terms when neuron-glial complexes are already formed. The results we obtained correspond to the concept of Rakic P. [19] regarding the leading role of radial glia in the mechanisms of development of CNS structures, as well as in the formation of NGK. But, in general, we also support the opinion of Balazs A. [4] that the development of neurons of the posterior horn of the spinal cord is not completed before birth and in the prenatal period proceeds slowly and moderately. Although inhibitory and excitatory neurons appear in the early embryonic period.

Conclusions

1. In the fetal period, greater proliferative activity of the dorsal neuroepithelium is determined at 8-9 weeks: in the cervical segments - 10 % ($p<0.05$), in the thoracic, lumbar and sacral segments - 9 % ($p<0.05$). By 39-40 weeks, this indicator gradually becomes smaller: in the cervical and lumbar segments, 4 % of cells (2-3 cells reacted) ($p<0.05$) and in the thoracic and sacral segments - 3 % (1-2 cells reacted) ($p<0.05$).

2. Throughout the fetal period, there is a tendency towards a gradual decrease in the density of neurons and gliocytes. The glial index, on the contrary, up to 39-40 weeks. increases and at the time of birth was equal to 2.1 in cervical, thoracic and lumbar, and 2.0 in sacral.

3. At 11-12 weeks, radial glia fibers form mesh structures within the neuronal complexes, which coincides with the beginning of the formation of neuron-glial complexes of the posterior horns. At 17-18 weeks, the fibers of radial glia keep the radial direction only in the middle part of the posterior horns. At 34-35 weeks, vimentin expression was determined to be relatively moderate in the remnants of radial glia near the dorsal neuroepithelium and focal expression of vimentin around vessels within the posterior horns. Expression of vimentin in the neuroepithelium of fetuses of 39-40 weeks was absent. In this age period, the neuroepithelium is structured from ependymocytes and radial glia cells are absent, as there is a relatively strong expression of S-100 in the neuroepithelium. Relatively strong expression of synaptophysin occurred in the posterior horns of 8-9 weeks fetuses. This age period is the beginning of the establishment of synaptic connections.

References

[1] Arora, M. (2016). Fetal anatomy: morphometry of vertebral canal and spinal cord of cervical region in human fetuses. *Annals of International Medical and Dental Research,* 2(3), 128-131.

[2] Arulkandarajah, K. H., Osterstock, G., Lafont, A., Le Corronc, H., Escalas, N., Corsini, S. ... Mangin, J.-M. (2021). Neuroepithelial progenitors generate and propagate non-neuronal action potentials across the spinal cord. *Curr. Biol.,* 31(20), 4584-4595. doi: 10.1016/j.cub.2021.08.019

[3] Bahney, J., & von Bartheld, C. S. (2018). The cellular Composition and glia-neuron ratio in the spinal cord of a human and a non-human primate: comparison with other species and brain regions. *Anat. Rec.,* 301(4), 697-710. doi: 10.1002/ar.23728

[4] Balazs, A., Meszar, Z., Hegedüs, K., Kenyeres, A., Hegyi, Z., Docs, K., & Antal, M. (2017). Development of putative inhibitory neurons in the embryonic and postnatal mouse superficial spinal dorsal horn. *Brain Struct. Funct.,* 222(5), 2157-2171. doi: 10.1007/s00429-016-1331-9

[5] Bentivoglio, M., & Mazzarello, P. (1999). The history of radial glia. *Brain Res. Bull.,* 49(5), 305-315. doi: 10.1016/s0361-9230(99)00065-9

[6] Berezhnaya, M. A., Gargin, V. V., & Maslovskiy, S. Yu. (2013). Межполушарная ассиметрия нейроно-глиально-капиллярных взаимоотношений V слоя в верхних лобных извилинах головного мозга человека [Interhemispheric asymmetry of the neuron-glial-capillary interrelated layer V in the upper frontal gyri of the human brain]. *Вісник проблем біології і медицини - Bulettin of problems in biology and medicine,* 3(2), 274-277.

[7] Bjugn, R. (1993). The use of the optical dissector to estimate the number of neurons, glial and endothelial cells in the spinal cord of the mouse - with a comparative note on the rat spinal cord. *Brain Res.*, 627(1), 25-33. doi: 10.1016/0006-8993(93)90744-8

[8] Burish, M. J., Peebles, J. K., Baldwin, M. K., Tavares, L., Kaas, J. H., & Herculano-Houzel, S. (2010). Cellular scaling rules for primate spinal cords. *Brain Behav. Evol.,* 76, 45-59. doi:

10.1159/000319019
[9] Cassaro, M., Rugge, M., Tieppo, C., & Giacomelli, L. (2007). Indefinite for non-invasive neoplasia lesions pn gastric intestinal metaplasia: the immunophenotype. *J. Clin. Pathol.,* 60, 615-621. doi: 10.1136/jcp.2006.040386
[10] Cedeno, D. L., Smith, W. J., Kelley, C. A., & Vallejo, R. (2020). Spinal cord stimulation using differential target multiplexed programming modulates neural cell-specific transcriptomes in an animal model of neuropathic pain. *Mol. Pain,* 16, 1744806920964360. doi: 10.1177/1744806920964360
[11] Costa, V., Lugert, S., & Jagasia, R. (2015). Role of adult hypocampal neurogenesis in cognition in physiology and disease: pharmacological targets and biomarkers. *Handbook of Experimental Pharmacology,* 228, 99-155. doi: 10.1007/978-3-319-16522-6_4
[12] Herculano-Houzel, S. (2014). The glia/neuron ratio: how it varies uniformly across brain structures and species and what that means for brain physiology and evolution. *Glia,* 62, 1377-1391. doi: 10.1002/glia.22683
[13] Herculano-Houzel, S. (2017). Numbers of neurons as biological correlates of cognitive capability. *Curr. Opin. Behav. Sci.,* 16, 1-7. doi: 10.1016/j.cobeha.2017.02.004
[14] Kuzmicz-Kowalska, K, & Kicheva, A. (2021). Regulation of size and scale in vertebrate spinal cord development. *Rev. Dev. Biol.,* 10(3), e383. doi: 10.1002/wdev.383
[15] Nowakowski, T. J., Pollen, A. A., Sandoval-Espinosa, C., & Kriegstein, A. R. (2016). Transformation of the radial glia scaffold demarcates two stages of human cerebral cortex development. *Neuron,* 91(6), 1219-1227. doi: 10.1016/j.neuron.2016.09.005
[16] Ma, J. J., Zhang, T. Y., Diao, X. T., Yao, L., Li, Y. X., Suo, Z. W. … Liu, Y. N. (2021). BDNF modulated KCC2 ubiquitylation in spinal cord dorsal horn of mice. *Eur. J. Pharmacol.,* (5), 906. doi: 10.1016/j.ejphar.2021.174205
[17] Peirs, C., Williams, S. G., Zhao, X., Arokiaraj, C. M., Ferreira, D. W., Noh, M. C. … Seal, R. P. (2021). Mechanical allodynia circuitry in the dorsal horn is defined by the nature of the injury. *Neuron,* 109(1), 73-90. doi: 10.1016/j.neuron.2020.10.027
[18] Popele, R., & Bosco, G. (2003). Sophisticated spinal contributions to motor control. Trends Neurosci., 26(5), 269-276. doi: 10.1016/S0166-2236(03)00073-0
[19] Rakic, P. (2003). Elusive radial glial cells: historical and evolutionary perspective. *Glia,* 43, 19-32. doi: 10.1002/glia.10244
[20] Rueger, M., & Schroeter, M. (2015) In vivo imaging of endogenous neural stem cells in the adult brain. *World Journal Stem Cells,* 7(1), 75-83. doi: 10.4252/wjsc.v7.i1.75
[21] Ruiz-Sauri, A., Orduna-Valls, J. M., Blasco-Serra, A., Tornero-Tornero, C., Cedeno, D. L., Bejarano-Quisoboni, D. … Vallejo, R. (2019). Glia to neuron ratio in the posterior aspect of the human spinal cord at thoracic segments relevant to spinal cord stimulation. *J. Anat.,* 235(5), 997-1006. doi: 10.1111/joa.13061
[22] Ryhlik, S. V. (2014). Морфологічні особливості вентролатеральної групи ядер таламуса проміжного мозку людини [Morphological features of the ventrolateral group of nuclei of the thalamus of the human midbrain]. *Вісник проблем біології і медицини - Bulettin of Problems in Biology and Medicine,* 4(1), 285-289.
[23] Skarlatou, S., Herent, C., Toscano, E., Mendes, C. S., Bouvier, J., & Zampieri, N. (2020). Afadin Signaling at the Spinal Neuroepithelium Regulates Central Canal Formation and Gait Selection. *Cell. Rep.*, 31(10), 107741. doi: 10.1016/j.celrep.2020.107741
[24] Smith, T. M., Lee, D., Bradley, K., & McMahon, S. B. (2020). Methodology for quantifying excitability of identified projection neurons in thedorsal horn of the spinal cord, specifically to study spinal cord stimulation paradigms. *J. Neurosc. Methods,* 330, 108479. doi: 10.1016/j.jneumeth.2019.108479
[25] Stepanov, A. S., Akulinin, V. A., Mysik, A. V., Stepanov, S. S., & Avdeev, D. B. (2017). Neuro-glio-vascular complexes of the brain after acute ischemia. *General Reanimatology,* 13(6), 6-17. doi: 10.15360/1813-9779-2017-6-6-17
[26] Vernygorodskyi, S. V., Shkolnikov, V. S., & Prykhodko, S. O. (2021). The morphology and neuronal-glial correlations of the spinal cord posterior horns of human embryos. *International Medical Journal,* 3(3), 93-100. doi: 10.5455/im.41865
[27] Von Bartheld, C. S., Bahney, J., & Herculano-Houzel, S. (2016). The search for true numbers of neurons and glial cells in the human brain: a review of 150 years of cell counting. *J. Comp. Neurol.,* 524, 3865-3895. doi: 10.1002/cne.24040
[28] Zhou, W., Xie, Z., Li, C., Xing, Z., Xie, S., Li, M., & Yao, J. (2021). Driving effect of BDNF in the spinal dorsal horn on neuropathic pain. *Neuroscience Letters,* 756, 135965. doi: 10.1016/j.neulet.2021.135965
[29] Zhurakivska, O. Ya. (2014). Становлення нейрон-гліо-капілярних співвідношень у вентромедіальному ядрі гіпоталамуса в постнатальному періоді онтогенезу [Formation of neuron-glio-capillary ratios in the ventromedial nucleus of the hypothalamus in the postnatal period of ontogenesis]. *Науковий вісник міжнародного гуманітарного університету - Scientific Bulletin of the International Humanitarian University,* (7), 15-18.

НЕЙРОНО-ГЛІАЛЬНІ ВІДНОШЕННЯ ЗАДНІХ РОГІВ СПИННОГО МОЗКУ ПЛОДІВ ЛЮДИНИ

Приходько С. О., Школьніков В. С.

Не дивлячись на відносно достатнє вивчення будови та функціонування нервової системи, зацікавленість до проблеми нейроно-гліальних відношень продовжує неухильно зростати, оскільки даний параметр віддзеркалює динаміку розвитку нервової тканини та може бути використаний для оцінювання рівня якості морфологічних змін. Мета дослідження: встановити морфогенез та нейроно-гліальні взаємовідносини задніх рогів спинного мозку людини у плодовому періоді онтогенезу. Дане дослідження виконано на препаратах 104 плодів людини від 8-9 тижнів до 39-40 тижнів при використанні анатомічних, гістологічних, імуногістохімічних та морфометричних методик. Статистичну обробку числових даних отриманих результатів проводили за допомогою ліцензійного програмного пакету "Statistica 6.1" фірми StatSoft із застосуванням параметричних і непараметричних методів. У процесі дослідження встановлено, що у плодовому періоді більша проліферативна активність дорзального нейроепітелію визначається у 8-9 тижнів: у шийних сегментах - 10 % ($p<0,05$), у грудних, поперекових та крижових - 9 % ($p<0,05$). До 39-40 тижнів даний показник поступово повільно стає меншим: у шийних і поперекових сегментах 4 % клітин (прореагувало 2-3 клітини) ($p<0,05$) та у грудних і крижових сегментах - 3 % (прореагувало 1-2 клітини) ($p<0,05$). Виявлено, що увесь плодовий період триває тенденція до поступового зменшення щільності нейронів та гліоцитів. Гліальний індекс, навпаки, до 39-40 тиж. збільшується, і на момент народження дорівнює

у шийних, грудних та поперекових сегментах - 2,1, а у крижових - 2,0. З'ясовано, що у 11-12 тижнів у межах нейронних комплексів волокна радіальної глії формують сітчасті структури, що співпадає з початком формоутворення нейроно-гліальних комплексів задніх рогів. У 17-18 тижнів волокна радіальної глії зберігають радіальний напрямок лише у середній частині задніх рогів. У 34-35 тижнів експресія віментину визначалась відносно посередньою у залишках радіальної глії біля дорзального нейроепітелію та вогнищева експресія віментину навколо судин у межах задніх рогів. Експресія віментину у нейроепітелії плодів 39-40 тижнів була відсутня. У даному віковому періоді нейроепітелій структурований з епендимоцитів та відсутні клітин радіальної глії, оскільки є відносно сильна експресія S-100 у нейроепітелії. Відносно сильна експресія синаптофізину відбувалась у задніх рогах у плодів 8-9 тижня. Даний віковий період є початком встановлення синаптичних зв'язків.

Ключові слова: *плоди людини, спинний мозок, задні роги, нейроно-гліальні відношення, радіальна глія, нейральні стовбурові клітини.*

DOI: 10.31393/morphology-journal-2022-28(4)-04 Reports of Morphology, Vol. 28, №4, Pages 27-33

ISSN 1818-1295 eISSN 2616-6194

REPORTS OF MORPHOLOGY

Official Journal of the Scientific Society of Anatomists, Histologists, Embryologists and Topographic Anatomists of Ukraine

journal homepage: https://morphology-journal.com

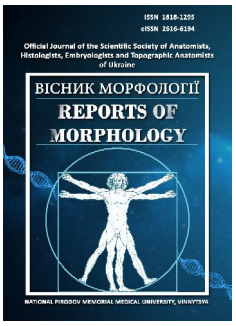

Craniometric parameters of the spatial position of the supraorbital, infraorbital and mental foramens depending on the facial index of the skull of a mature person

Onashko Yu. M.[1], Vovk O. Yu.[1], Dubina S. O.[2], Sosonna L. O.[1], Yakymenko R. O.[1]

[1] Kharkiv National Medical University, Kharkiv, Ukraine
[2] Donetsk National Medical University, Kropyvnytskyi, Ukraine

ARTICLE INFO
Received: 9 August 2022
Accepted: 12 September 2022

UDC: 611.716-053.85:611.714.6:611.716.4

CORRESPONDING AUTHOR
e-mail: ym.onashko@knmu.edu.ua
Onashko Yu. M.

CONFLICT OF INTEREST
The authors have no conflicts of interest to declare.

FUNDING
Not applicable.

Due to increase of various operative interventions in the facial region of a mature person, it is expedient to study in detail the spatial position of the foramens of the facial part of the skull. Knowing the exact position of the foramens will help doctors during operations and minimally invasive interventions to prevent damage to the vascular and nerve bundles that pass through these foramens. The purpose of our work is to determine the craniometric characteristics and spatial position of the supraorbital (SF), infraorbital (IF) and mental (MF) foramen, depending on the type of structure of the facial part of the skull. The study was performed on 52 bone specimens of skulls and 60 CT images of adults without damage to the bone structures of the front part of the skull. Statistical methods were used to analyze the obtained measurement results in our research, which was carried out with the help of the Microsoft Excel 2010© licensed program package and with the help of the "STATISTYCA" program. When determining the position of the foramens of the facial part of the skull, first of all, we determined the individual anatomical variability of the facial part of the skull, which has the following extreme types: europrosopics (broad-faced), mesoprosopics (medium-faced), leptoprosopics (long-faced). By dividing the skulls according to the facial index, we determined the width and height of SF, IF and MF, and it was found that their diameter does not depend on the extreme types of the facial part of the skull. With the help of corresponding program, the average, lateral and line between the zy-zy points were constructed on the CT images of the 3-D models of the skulls to determine the position of SF, IF, MF relative to these lines depending on the facial index. The average values obtained were analyzed and it was established that the distance from SF, IF and MF to the median and lateral lines has larger values in europrosopics, intermediate values have mesoprosopics, the smallest results were determined in leptoprosopics. The results of the study of the distances from the above-mentioned foramens to the zy-zy line indicate an increase in their values in leptoprosopics, as opposed to europrosopics. The data we obtained confirm the dependence of the spatial position of the foramens on the type of structure of the facial part of the skull. The obtained data will supplement the craniotopographical characteristics of SF, IF and MF, and also provide a basis for further research of their position depending on the facial index.

Keywords: *craniometry, infraorbital foramen, supraorbital foramen, mental foramen.*

Introduction

At this stage of the development of modern medicine, a variety of surgical interventions, including aesthetic plastic and medical ones, are increasingly performed in the area of the facial part of the skull. As you know, the above-mentioned area is rich in the passage of various nerve branches and vessels, therefore, knowledge of their exact position is extremely necessary for operations in this area. To date, a large number of scientists conduct research on the location of the supraorbital foramen (notch) (SF (SN)), infraorbital foramen (IF) and mental foramen (MF) in relation to the main craniological landmarks, depending on sex, race, and climatic conditions. The highlighted results show small but significant differences in the topography, shape and position of these foramens [2, 6, 14, 18]. Vascular-

nerve bundles pass through SF, IF, and MF, and therefore, when performing complex surgical interventions, as well as during local anesthesia, it is extremely important to know the exact position of these foramens, and accordingly, the exit of nerve branches and vessels [1, 9, 10, 15, 22]. Further development of plastic and maxillofacial surgery is impossible without an in-depth and systematic study of the range of individual anatomical variability of the facial skull as a whole, features of its shape, size, position, and relationships of its structures [11, 19, 20, 21]. Taking into account the types of skull structure, the studied craniometric parameters have pronounced individual differences, which confirms the existing range of variability of the profile anatomy of the facial skull [21]. Therefore, in our opinion, it is important to determine the variability of SF (SN), IF and MF depending on the range of individual anatomical variability.

Considering the above facts, *the aim of the study* is to establish the main craniotopographic parameters and spatial position of SF (SN), IF and MF of a mature person depending on the facial index.

Materials and methods

Craniometric studies were carried out on 52 bone specimens of skulls, with the help of commonly accepted tools: a craniocircumfer, a set of face rulers, ordinary rulers, angular, sliding and combined rulers, calipers and a protractor. Also, the study was conducted on 60 CT images using the Anatomage table (Fig. 1), located at the Department of Human Anatomy of the Kharkiv National Medical University. The DICOM program "Vidar Dicom Viewer 3.0" was used to view CT images (Fig. 2). Bone preparations of the skulls and CT images belonged to people of Caucasian race of mature age, without pathology of the bones of the facial part of the skull. The research material was taken on the basis of the Department of Human Anatomy of the Kharkiv National Medical University.

The Committee on Bioethics of the Kharkiv National Medical University (protocol No.7 dated 11.09.2018) found that the research was carried out with respect for human rights, in accordance with the legislation in force in Ukraine,

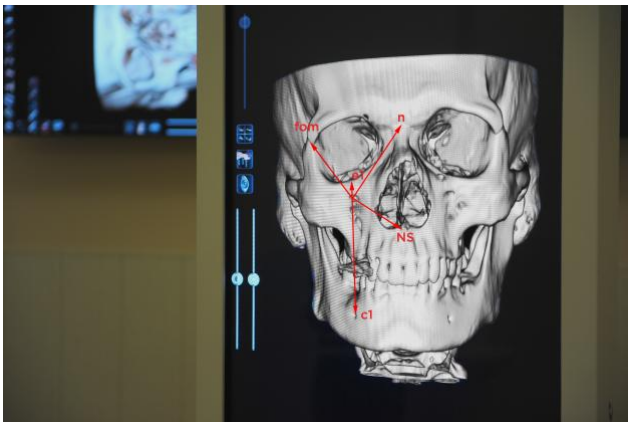

Fig. 1. "Anatomage table".

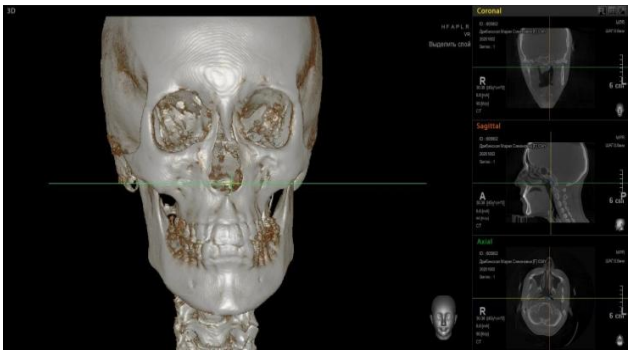

Fig. 2. Program DICOM "Vidar Dicom Viewer 3.0".

meets international ethical requirements and does not violate ethical norms in science and standards for conducting biomedical research.

Statistical methods were used to analyze the obtained measurement results in our research, which was carried out with the help of the Microsoft Excel 2010© licensed program package and with the help of the "STATISTYCA" program. The following were determined: minimum and maximum value; arithmetic mean ($\overline{X}$); mean square deviation (σ); mean error (m) [3, 7, 13].

Results

To determine the features of SF (SN) localization, we investigated the height and width of the foramens, their position relative to craniometric points depending on the facial index, and carried out a variational and statistical analysis.

Table 1 presents the results of measurements of supraorbital foramen on the right and left depending on the facial index.

According to the obtained data, the width of the supraorbital foramens among europrosopics on the right is $\overline{X}$ ±σ=4.307±1.129 mm, on the left - $\overline{X}$ ±σ=4.371±1.222 mm; in mesoprosopics, this indicator on the right is $\overline{X}$ ±σ=4.496±1.206 mm, on the left - $\overline{X}$ ±σ=4.546±1.227 mm; among leptoprosopics on the right is $\overline{X}$ ±σ=4.273±1.332 mm, on the left - $\overline{X}$ ±σ=4.623±1.157 mm.

When determining the SF height on both sides, we obtained the following indicators: in europrosopics on the right - $\overline{X}$ ±σ=1.987±0.425 mm, on the left is $\overline{X}$ ±σ=2.185±0.448 mm; among mesoprosopics, the average value of the foramen height is on the right $\overline{X}$ ±σ=2.118±0.698 mm, on the left - $\overline{X}$ ±σ=2.164±0.700 mm, and among leptoprosopics, the SF height on the right is $\overline{X}$ ±σ=2.551±0.541 mm, on the left - $\overline{X}$ ±σ=2.451±0.539 mm.

Analyzing the obtained data, it should be noted that the diameter of the SF does not depend on the facial index, but its increase is clearly observed on the left side compared to the right side among the above-mentioned types of facial skull.

With the help of the corresponding program, the median, lateral and line between the zy-zy points were constructed on the CT images of the 3-D models of the skulls to

Table 1. Statistical indicators of width and height SF.

Investigated signs	min	max	$\bar{x}$	σ	m
The width of the foramen on the right					
Europrosopic	2.2	6.5	4.307	1.129	0.213
Mesoprosopic	2.0	6.9	4.496	1.206	0.164
Leptoprosopic	1.0	7.1	4.273	1.332	0.243
The width of the foramen on the left					
Europrosopic	2.0	6.2	4.371	1.222	0.231
Mesoprosopic	1.8	7.0	4.546	1.227	0.167
Leptoprosopic	2.7	7.0	4.623	1.157	0.211
The height of the foramen on the right					
Europrosopic	1.5	2.5	1.987	0.425	0.150
Mesoprosopic	1.0	3.5	2.118	0.698	0.174
Leptoprosopic	1.5	3.3	2.551	0.541	0.156
The height of the foramen on the left					
Europrosopic	1.5	2.9	2.185	0.448	0.169
Mesoprosopic	1.0	3.1	2.164	0.700	0.187
Leptoprosopic	1.5	3.0	2.451	0.539	0.220

determine the position of the SF (SN) relative to these lines depending on the facial index.

The obtained results indicate an increase in the distances from the SF (SN) to the median and lateral lines on both sides in europrosopics (to the median line on the right - $\bar{x}$ ±σ=20.29±4.01 mm; on the left - $\bar{x}$ ±σ=20.14±1.70 mm; to the lateral line on the right - $\bar{x}$ ±σ=7.818±1.611 mm; on the left - $\bar{x}$ ±σ=6.554±2.033 mm), smaller values of these distances are noted in mesoprosopics (to the midline on the right - $\bar{x}$ ±σ=19.71±2.41 mm; on the left - $\bar{x}$ ±σ=19.67±2.10 mm; to the lateral line on the right - $\bar{x}$ ±σ=6.945±3.422 mm; on the left - $\bar{x}$ ±σ=5.842±2.637 mm) and the minimum above-mentioned distances are established in leptoprosopics (to the median line on the right - $\bar{x}$ ±σ=18.98±2.59 mm; on the left - $\bar{x}$ ±σ=18.70 ±1.18 mm; to the lateral line on the right - $\bar{x}$ ±σ=5.631±1.988 mm; on the left - $\bar{x}$ ±σ=5.362±2.694 mm) (Fig. 3).

The features of the distances from SF (SN) to the zy-zy line on both sides depending on the facial index are also established. According to the data we obtained, the maximum distance was determined in leptoprosopics (right - $\bar{x}$ ±σ=35.88±3.09 mm; left - $\bar{x}$ ±σ=35.55±4.20 mm), intermediate in mesoprosopics (right - $\bar{x}$ ±σ=35.75±3.55 mm; left - $\bar{x}$ ±σ=35.48±3.60 mm) and minimal in europrosopics (right - $\bar{x}$ ±σ=33.18±2.69 mm; left - $\bar{x}$ ±σ=32.94±2.60 mm). It is also possible to note an increase in distances in all types of facial skull on the right side compared to the left side.

When conducting research related to the position of the IF, first of all, we determined the diameter of this foramen on both sides. Variational and statistical indicators of the width and height of the IF depending on the type of facial structure are shown in Table 2.

In the course of determining the width of the foramen in a mature person with a wide type of facial structure, the average value on the right is $\bar{x}$ ±σ=3.896±0.896 mm, on the left - $\bar{x}$ ±σ=3.821±0.824 mm; in mesoprosopics, the foramen width on the right is $\bar{x}$ ±σ=3.664±0.789 mm, on the left - $\bar{x}$ ±σ=3.544±0.827 mm; in long-faced, it is $\bar{x}$ ±σ=3.834±1.332 mm on the right, $\bar{x}$ ±σ=3.820±1.157 mm on the left.

In parallel with the width of the IF, the height of this foramen was set: in wide-faced people, it does not exceed $\bar{x}$ ±σ=3.662±1.029 mm on the right, $\bar{x}$ ±σ=3.360±1.111 mm on the left; the average value of the height in mesoprosopics is on the right - $\bar{x}$ ±σ=3.371±0.721 mm, on the left - $\bar{x}$ ±σ=3.327±0.711 mm, in long-faced people the IF height is slightly lower than in broad-faced people on the right - $\bar{x}$ ±σ=3.517±0.834 mm and slightly higher on the left - $\bar{x}$ ±σ=3.468±0.793 mm.

Analyzing the obtained data, we did not establish the regularity of IF sizes depending on the type of facial structure.

To determine the individual anatomical variability of the IF, we additionally determined the distance to the median, lateral and zy-zy lines of an adult person.

The obtained latitudinal indicators indicate an increase in the distance from the IF to the median and lateral lines on both sides from leptoprosopics to europrosopics. Accordingly, in people with an elongated face type, the distance from the

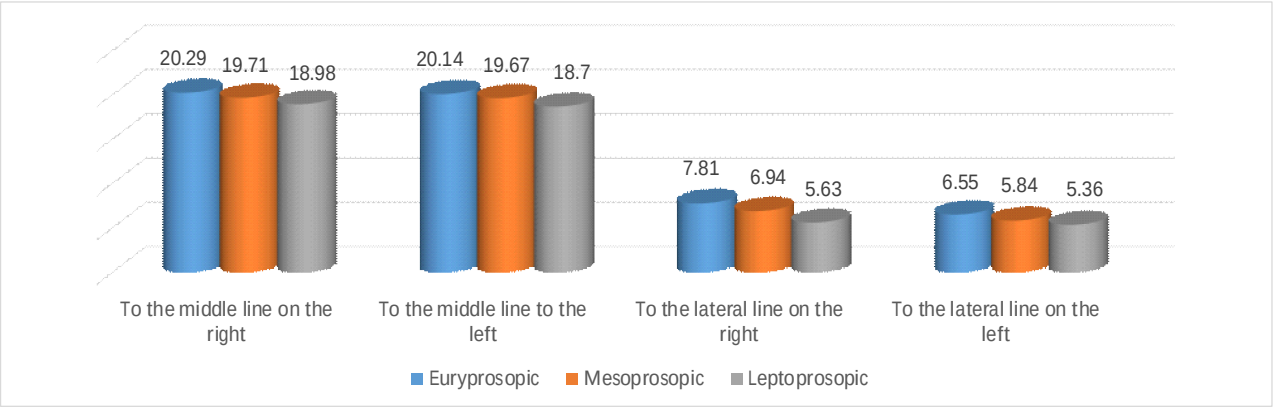

Fig. 3. The existing range of distances from SF (SN) to the median and lateral lines of a mature person depending on the facial index (mm).

Table 2. Statistical indicators of IF in a person of mature age.

Investigated signs	min	max	$\bar{X}$	σ	m
The width of the foramen on the right					
Europrosopic	2.4	6.2	3.896	0.896	0.172
Mesoprosopic	2.3	5.8	3.664	0.789	0.108
Leptoprosopic	2.4	5.8	3.834	0.960	0.178
The width of the foramen on the left					
Europrosopic	2.5	6.2	3.821	0.824	0.155
Mesoprosopic	2.2	5.6	3.544	0.827	0.112
Leptoprosopic	1.8	6.4	3.820	0.989	0.183
The height of the foramen on the right					
Europrosopic	2.0	6.2	3.662	1.029	0.198
Mesoprosopic	2.2	4.9	3.371	0.721	0.099
Leptoprosopic	1.5	5.5	3.517	0.834	0.154
The height of the foramen on the left					
Europrosopic	1.7	7.0	3.360	1.111	0.209
Mesoprosopic	1.8	5.0	3.327	0.711	0.096
Leptoprosopic	1.6	4.8	3.468	0.793	0.147

IF to the midline on the right is $\bar{X}$ ±σ=21.17±1.64 mm; on the left - $\bar{X}$ ±σ=21.06±1.56 mm; to the lateral line on the right - $\bar{X}$ ±σ=5.600±1.542 mm; on the left - $\bar{X}$ ±σ=5.350±1.690 mm. In mesoprosopics, the above-mentioned distances occupy an intermediate value: to the middle line on the right - $\bar{X}$ ±σ=22.20±3.46 mm; on the left - $\bar{X}$ ±σ=22.05±1.68 mm; to the lateral line on the right - $\bar{X}$ ±σ=5.933±2.110 mm; on the left - $\bar{X}$ ±σ=5.460±2.240 mm. The largest latitudinal indicators are established in europrosopics (broad-faced): the distance to the middle line on the right is $\bar{X}$ ±σ=22.70±2.38 mm; on the left - $\bar{X}$ ±σ=22.50±2.75 mm; to the lateral line on the right is $\bar{X}$ ±σ=6.436±1.580 mm; on the left - $\bar{X}$ ±σ=5.590±2.414 mm (Fig. 4).

In the course of determining the distances from the IF to the zy-zy line of a mature person in comparison with latitudinal distances, europrosopics prevailed (right - $\bar{X}$ ±σ=5.981±0.770 mm; left - $\bar{X}$ ±σ=5.809±1.676 mm), in mesoprosopics this indicator takes the intermediate value (right - $\bar{X}$ ±σ=6.090±3.664 mm; left - $\bar{X}$ ±σ=6.063±3.434 mm) and the smallest in leptoprosopics (right - $\bar{X}$ ±σ=7.062±4.442 mm; left - $\bar{X}$ ±σ=6.375±4.221 mm). The obtained above-mentioned data indicate the dependence of the location of the foramens on the extreme types of the structure of the facial part of the skull.

Similar to the study of SF (SN) and IF to characterize the position of the MF, first of all, we examined the width and height of the MF (Table 3).

It was found that the width of the MF on the right and left in europrosopics ranges from 2.0 mm to 4.2 mm on the right; on the left - from 2.3 mm to 4.8 mm. In mesoprosopics, this distance also has a significant range, which is on the right from 1.7 mm to 6.0 mm; on the left from 2.0 mm to 6.4 mm. The variability of the width of the foramen is also determined in leptoprosopics, which has a range from 1.9 mm to 4.5 mm on the right, from 2.0 mm to 5.0 mm on the left.

Similar variability was found when determining the height of the MF. In mature people with a europrosopic type of facial skull, the height varies on the right from 2.0 mm to 3.6 mm; on the left - from 1.5 mm to 3.6 mm. In mesoprosopics, the height range of the foramen is set on the right from 1.2 mm to 5.3 mm, on the left from 1.7 mm to 5.8 mm. The height of the MF in leptoprosopics has a minimum value of 1.5 mm, a maximum value of 4.2 mm (on the right), on the left varies from 1.9 mm to 4.1 mm.

The next stage of our study of the position of the MF depending on the facial index was to determine its position by establishing the distances to the median, lateral and zy-zy lines of a mature person.

According to the obtained data, there is a certain morphometric dependence of the above-mentioned distances on the type of structure of the facial part of the skull. Thus, in europrosopics, the distance from the MF to the median line on both sides has the largest values (right - $\bar{X}$ ±σ=21.27±1.16 mm; left - $\bar{X}$ ±σ=22.75±2.02 mm), similarly when establishing the distance from the MF to the lateral line (right - $\bar{X}$ ±σ=12.47±6.93 mm; on the left - $\bar{X}$ ±σ=10.26±5.14 mm). Significantly smaller values to the

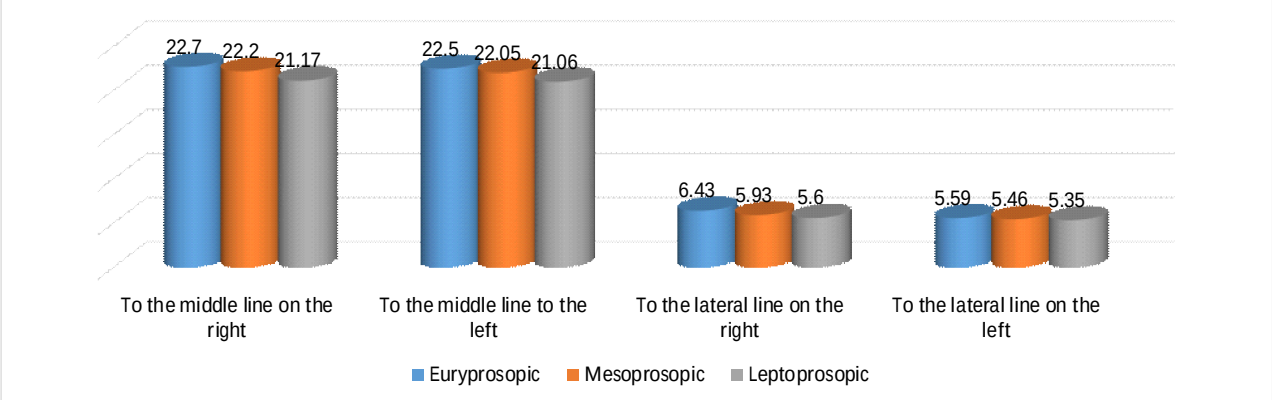

Fig. 4. The existing range of distances from the IF to the median and lateral lines of a mature person depending on the facial index (mm).

Table 3. Statistical indicators of the diameters of the MF of a mature person.

Investigated signs	min	max	$\bar{X}$	σ	m
The width of the foramen on the right					
Europrosopic	2.0	4.2	3.042	0.704	0.188
Mesoprosopic	1.7	6.0	3.311	0.842	0.140
Leptoprosopic	1.9	4.5	3.235	0.727	0.162
The width of the foramen on the left					
Europrosopic	2.3	4.8	3.564	0.666	0.178
Mesoprosopic	2.0	6.4	3.644	0.894	0.149
Leptoprosopic	2.0	5.0	3.540	0.795	0.177
The height of the foramen on the right					
Europrosopic	2.0	3.6	2.685	0.602	0.160
Mesoprosopic	1.2	5.3	2.669	0.833	0.138
Leptoprosopic	1.5	4.2	2.685	0.721	0.161
The height of the foramen on the left					
Europrosopic	1.5	3.6	2.485	0.632	0.168
Mesoprosopic	1.7	5.8	2.711	0.749	0.124
Leptoprosopic	1.9	4.1	2.850	0.722	0.161

median line were established in mesoprosopics (right - $\bar{X}$ ±σ=20.93±2.06 mm; left - $\bar{X}$ ±σ=22.41±2.26 mm), the same difference was found in the distance from the MF to the lateral line (right - $\bar{X}$ ±σ= 9.942±2.307 mm; on the left - $\bar{X}$ ±σ=7.924±2.059 mm). In comparison with the above-mentioned types of structure of the facial part of the skull, we found the minimum values in leptoprosopics both to the median line (right - $\bar{X}$ ±σ=20.31±1.31 mm; left - $\bar{X}$ ±σ=21.81±1.67 mm) and to the lateral line (on the right - $\bar{X}$ ±σ=8.912± 2.032 mm; on the left - $\bar{X}$ ±σ=7.193± 2.291 mm) (Fig. 5).

The peculiarity of the distances from the MF to the zy-zy line is the opposite regularity compared to the lateral and median lines, because the above-mentioned distance has maximum values precisely in leptoprosopics on both sides (right - $\bar{X}$ ±σ=71.80±6.75 mm; left - $\bar{X}$ ±σ=71.12±6.81 mm), several centimeters lower in mesoprosopics (right - $\bar{X}$ ±σ=68.71±3.62 mm; left - $\bar{X}$ ±σ=69.29±3.32 mm) and minimum values were set in europrosopics (right - $\bar{X}$ ±σ=66.15±3.78 mm; left - $\bar{X}$ ±σ=67.00±2.34 mm).

Discussion

The study of individual anatomical variability of the facial part of the skull and its structures is extremely important for the further use of this knowledge in clinical practice [21]. We analyzed the scientific works related to the study of the position of the foramens of the front part of the skull by domestic and foreign scientists. It should be noted that the variability of SF (SN), IF and MF depending on the facial index has not been sufficiently studied to date. Such scientists as Alper Sinanoglu, Kaan Orhan, etc. studied the width and height of SF, depending on sex, and they confirmed the increase of these indicators in men [18]. M. S. Chung and co-authors established the average values of distances from SF, IF and MF to the midline in people of Korean nationality [4]. Brian Cutright and others investigated the position of SF, IF and MF relative to surgical landmarks and the midline depending on sex, as a result of the obtained data, they established differences in the position of the above-mentioned foramens in men and women [5]. A study of the position of the SF, IF, and MF relative to the midline in Latin Americans was also conducted in comparison with the position of the above foramens in Europeans. As a result of the study, it was found that among all the studied ethnic groups, SF, IF, MF were at a distance of 25.32 mm, 29.57 mm, and 25.55 mm from the midline, respectively [8]. V. O. Kostiuk and O. M. Slobodian using modern anatomical methods studied the distances between SF, IF, MF and to standard landmarks in fetuses and newborns, due to which they established the average values of the above-mentioned parameters in different age periods [11]. There is a large number of experiments related to the determination of the position of the MF relative to various structures, namely differences in the position of this foramen among different population groups, regardless of sex, age, and extreme types of the head [13]. J. C. Prados-Frutos and others determined a large variability of the position of the PBO on CT images of

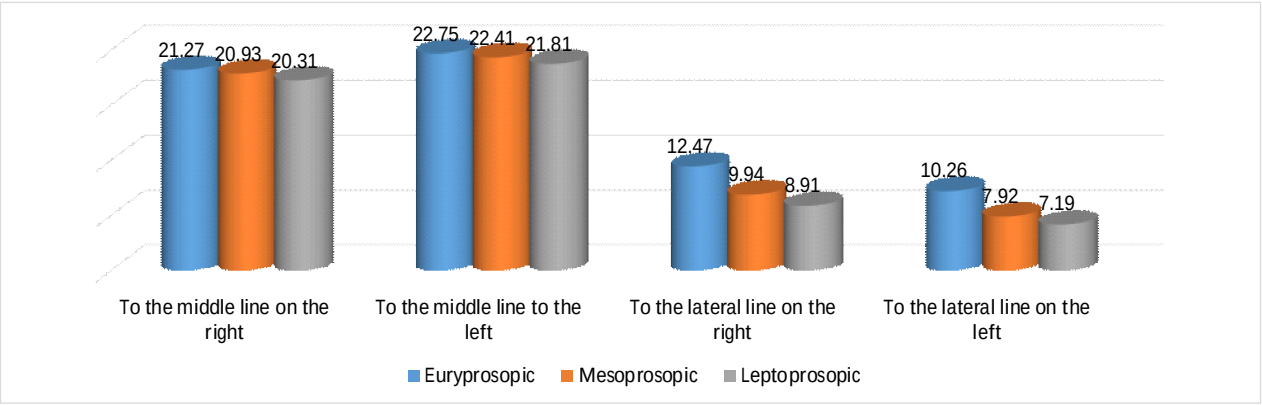

Fig. 5. The existing range of distances from the MF to the median and lateral lines of a mature person depending on the facial index (mm).

people aged 65 years and older [17]. D. Nanayakkara and others conducted a study to determine the shape, size, presence of additional foramina and the exact position of the IF in relation to the lower edge of the orbit, the craniological point of the nasion, the teeth of the upper jaw on specimens of the skulls of adults in the Sri Lankan population [14]. In a research paper by Zhang K. R. and co-authors, the aim of the study was to determine the position, size, and additional IF in the African American population and compare them with the Caucasian population. As a result of the obtained data, the aforementioned scientists established a significant difference in the specified parameters among different population groups [23]. We, for the first time, studied in detail and determined the range of individual variability of craniotomographic and craniometric features of the spatial position of the foramens of the front part of the skull, depending on the extreme types of facial structure.

To establish the variability of the position of SF, IF and MF, the width and height of these foramens on the right and left, the distance to the lateral, median lines and the zy-zy line were determined depending on the facial index.

It should be noted that the obtained width and height of the above-mentioned foramens do not depend on the facial index (europrosopics, mesoprosopics, leptoprosopics), but an increase in the diameter of the foramens on the left side compared to the right side is clearly observed among the above-mentioned types of facial skull. When determining the distance from the SF to the median and lateral lines on both sides, the maximum values were obtained in europrosopics, the average values of these distances were determined in mesoprosopics, and the minimum above-mentioned distances were set in leptoprosopics. The distance from SF to the zy-zy line is characterized, on the contrary, by increases in its values in leptoprosopics, slightly smaller values were established in mesoprosopics and minimal in europrosopics.

To determine the individual variability of the IF, latitudinal indicators were established, which were also determined relative to the distance from the given foramen to the lateral and midline. The obtained data indicate an increase in the above-mentioned distance on both sides in broad-faced (europrosopics), respectively, in long-faced (leptoprosopics) latitude indicators have the smallest values. In the course of determining the position of the IF relative to the zy-zy line of a mature person, it was established that their predominance is the opposite in long-faced people.

In our study, as well as when determining the position of the previous foramens, a morphometric dependence on the facial index of the distances from the MF to the median, lateral and zy-zy lines of a mature person was revealed. According to the obtained data, an increase in the distance from the MF to the midline on both sides in europrosopics was established. A few millimeters smaller values were obtained to the midline in mesoprosopics. The minimum values found in leptoprosopics are both to the midline and to the lateral line.

Analyzing the latitudinal and altitudinal indicators of the position of SF, IF, and MF, their dependence on the type of structure of the facial part of the skull was clearly traced.

Висновки

1. The width and height of SF, IF and MF do not depend on the face index.

2. The average distance from SF and IF to the lateral and midline is greater in europrosopics than in leptoprosopics.

3. The obtained results of distances from SF and IF to the zy-zy line have greater values in leptoprosopics than in europrosopics.

4. The research indicators of the distances from the MF to the lateral and median lines and the zy-zy line also indicate a morphometric dependence on the facial index. According to the obtained data, larger values of the distance from the MF to the median and lateral lines on both sides were established in europrosopics, and vice versa, when determining the distance from the MF to the zy-zy line, larger values of the indicators were noted in leptoprosopics.

References

[1] Atef, M., Abdallah, A. M., Shawky, M., Shaheen, M., Khiry, M., & Sholkamy, H. (2020). Two-stage distalization of the mental foramen to manage posterior mandibular vertical bone deficiency - a prospective observational study. *International Journal of Oral and Maxillofacial Surgery,* 49(12), 1622-1629. doi: 10.1016/j.ijom.2020.04.008

[2] Barbosa, D. A. F., Mesquita, L. R., Borges, M. M. C., de Mendonca, D. S., de Carvalho, F. S. R., Kurita, L. M., ... Costa, F. W. G. (2021). Mental foramen and anterior loop anatomic characteristics: a systematic review and meta-analysis of cross-sectional imaging studies. *Journal of Endodontics,* 47(12), 1829-1843. doi: 10.1016/j.joen.2021.08.006

[3] Bondarchuk, S. S., Godovannaya, I. G., & Perevozkin, V. P. (2009). *Основы практической биостатистики: учебное пособие для вузов [Fundamentals of Practical Biostatistics: Textbook for Universities].* Томск: Издательство ТГПУ - Tomsk: TSPU Publishing House.

[4] Chung, M. S., Kim, H. J., Kang, H. S., & Chung, I. H. (1995). Locational relationship of the supraorbital notch or foramen and infraorbital and mental foramina in Koreans. *Cells Tissues Organs,* 154(2), 162-166. doi: 10.1159/000147763

[5] Cutright, B., Quillopa, N., & Schubert, W. (2003). An anthropometric analysis of the key foramina for maxillofacial surgery. *Journal of Oral and Maxillofacial Surgery,* 61(3), 354-357. doi: 10.1053/joms.2003.50070

[6] Garg, R. K., Lee, K. S., Kohn, S. C., Baskaya, M. K., & Afifi, A. M. (2015). Can sonography distinguish a supraorbital notch from a foramen?. *Journal of Ultrasound in Medicine,* 34(11), 2089-2091. doi: 10.7863/ultra.14.12015

[7] Glantz, S. (2012). *Primer of Biostatistics.* New York: McGraw-Hill Medical Pub.

[8] Hester, K. M., Rahimi, O. B., Fry, C. L., & Nation, H. L. (2021). The

relative locations of the supraorbital, infraorbital, and mental foramina: A cadaveric study. *Journal of Anatomy,* 239(4), 782-787. doi: 10.1111/joa.13482

[9] Hufschmidt, K., Bronsard, N., Foissac, R., Baque, P., Balaguer, T., Chignon-Sicard, B. ... Camuzard, O. (2019). The infraorbital artery: clinical relevance in esthetic medicine and identification of danger zones of the midface. *Journal of Plastic, Reconstructive & Aesthetic Surgery,* 72(1), 131-136. doi: 10.1016/j.bjps.2018.09.010

[10] Kikuta, S., Iwanaga, J., Kusukawa, J., & Tubbs, R. S. (2020). The mental artery: anatomical study and literature review. *Journal of Anatomy,* 236(3), 564-569. doi: 10.1111/joa.13113

[11] Kostiuk, V. O., & Slobodian, O. M. (2021). Anatomical modeling of super-, sub-eye patch and chin foramens in fetuses and newborn. *World Science,* 8(69), 44-49. doi: 10.31435/rsglobal_ws/30082021/7657

[12] Kravchenko, N. S. (2011). *Методы обработки результатов и оценки погрешности в учебном лабораторном практикуме: учебное пособие [Methods for processing results and assessing errors in the educational laboratory workshop: a tutorial].* Томск: Издательство Томского политехнического университета - Tomsk: Tomsk Polytechnic University Publishing House.

[13] Laher, A. E., Wells, M., Motara, F., Kramer, E., Moolla, M., & Mahomed, Z. (2016). Finding the mental foramen. *Surgical and Radiologic Anatomy,* 38(4), 469-476. doi: 10.1007/s00276-015-1565-x

[14] Nanayakkara, D., Peiris, R., Mannapperuma, N., & Vadysinghe, A. (2016). Morphometric analysis of the infraorbital foramen: the clinical relevance. *Anatomy Research International,* 2016, 1-8. doi: 10.1155/2016/7917343

[15] Napier, A., De Jesus, O., & Taylor, A. (2021). *Supraorbital Nerve Block.* In: StatPearls [Internet]. StatPearls Publishing. PMID: 30725622

[16] Nardi, N. M., Alvarado, A. C., & Schaefer, T. J. (2018). *Infraorbital nerve block.* In: StatPearls. Treasure Island (FL): StatPearls Publishing. PMID: 29763056

[17] Prados-Frutos, J. C., Salinas-Goodier, C., Manchon, A., & Rojo, R. (2017). Anterior loop of the mental nerve, mental foramen and incisive nerve emergency: tridimensional assessment and surgical applications. *Surgical and Radiologic Anatomy,* 39(2), 169-175. doi: 10.1007/s00276-016-1690-1

[18] Sinanoglu, A., Orhan, K., Kursun, S., Inceoglu, B., & Oztas, B. (2016). Evaluation of optic canal and surrounding structures using cone beam computed tomography: considerations for maxillofacial surgery. *Journal of Craniofacial Surgery,* 27(5), 1327-1330. doi: 10.1097/SCS.0000000000002726

[19] Slobodian, O. M., Kostiuk, V. O., Lavriv, L. P., & Korchyns'ka, N. S. (2017). Сучасні відомості про топографо-анатомічні особливості над-, підочноямкового та підборідного отворів [Modern information about the topographical and anatomical features of the supraorbital, infraorbital and mental foramens]. *Biomedical and Biosocial Anthropology,* (29), 240-245.

[20] Vovk, Ju. N., Vovk, O. Ju., Ikramov, V. B., Shmargalev, A. A., Malahov, S. S. (2016). Практическое значение индивидуальной анатомической изменчивости для современной краниологии [Practical significance of individual anatomical variability for modern craniology]. *Клінічна анатомія та оперативна хірургія - Clinical Anatomy and Operative Surgery,* 15(1), 105-109.

[21] Vovk, Yu. M., & Vovk, O. Yu. (2019). *Індивідуальна анатомічна мінливість та її клініко-анатомічне значення [Individual anatomical variability and its clinical and anatomical significance].* Харків: ФОП Бровін О. В. - Kharkiv: FOP Brovin O.V.

[22] Ward, M., Majmundar, N., Mammis, A., & Paskhover, B. (2020). Endoscopic infraorbital microdissection for localized v2 trigeminal neuralgia. *Journal of Oral and Maxillofacial Surgery,* 78(3), 374-e1. doi: 10.1016/j.joms.2019.10.011

[23] Zhang, K. R., Blandford, A. D., Hwang, C. J., & Perry, J. D. (2019). Anatomic variations of the infraorbital foramen in Caucasian versus African American skulls. *Ophthalmic Plastic & Reconstructive Surgery,* 35(1), 25-28. doi: 10.1097/iop.0000000000001126

КРАНІОМЕТРИЧНІ ПАРАМЕТРИ ПРОСТОРОВОГО ПОЛОЖЕННЯ НАДОЧНОЯМКОВОГО, ПІДОЧНОЯМКОВОГО ТА ПІДБОРІДНОГО ОТВОРІВ В ЗАЛЕЖНОСТІ ВІД ЛИЦЕВОГО ІНДЕКСУ ЧЕРЕПУ ЛЮДИНИ ЗРІЛОГО ВІКУ

Онашко Ю. М., Вовк О. Ю., Дубина С. О., Сосонна Л. О., Якименко Р. О.

У зв'язку зі збільшенням різноманітних оперативних втручань в лицевій області людини зрілого віку, є доцільним детальне вивчення просторового положення отворів лицевого відділу черепа. Знання точного положення отворів допоможе лікарям під час операцій та малоінвазивних втручань запобігти пошкодження судинно-нервових пучків, які проходять через дані отвори. Метою нашої роботи є визначення краніометричних характеристик та просторового положення надочного (НОО), підочного (ПОО) та підборідного (ПБО) отворів в залежності від типу будови лицевого відділу черепа. Дослідження було виконане на 52 кісткових препаратах черепів та 60 КТ-знімках людей зрілого віку без пошкоджень кісткових структур лицевого відділу черепа. Для аналізу отриманих результатів вимірювань у нашому дослідженні були використані статистичні методи, що здійснювалися за допомогою ліцензованого пакету програм Microsoft Excel 2010© та за допомогою програми "STATISTYCA". При визначенні положення отворів лицевого відділу черепа, в першу чергу, ми визначали індивідуальну анатомічну мінливість лицевого відділу черепа, що має наступні крайні типи: еуріпрозопи (широколиці), мезопрозопи (середньоліці), лептопрозопи (довголиці). Розподіливши черепа за лицевим індексом, ми визначили ширину та висоту НОО, ПОО та ПБО та було з'ясовано, що їх діаметр не залежить від крайніх типів лицевого відділу черепа. Завдяки відповідній програмі на КТ-знімках 3-D моделях черепів були побудовані середня, латеральна та лінія між точками zy-zy для визначення положення НОО, ПОО, ПБО відносно даних ліній в залежності від лицевого індексу. Проаналізували отримані середні значення та встановили, що відстань від НОО, ПОО та ПБО до серединної та латеральної ліній має більші значення у еуріпрозопів, проміжні значення мають мезопрозопи, найменші результати були визначенні у лептопрозопів. Результати дослідження відстаней від вищезазначених отворів до лінії zy-zy свідчать про збільшення їх значень у лептопрозопів, на відміну від еуріпрозопів. Отримані нами дані підтверджують залежність просторового положення отворів від типу будови лицевого відділу черепа. Отримані дані доповнять краніотопографічну характеристику НОО, ПОО та ПБО, а також є основою для подальшого дослідження їх положення в залежності від лицевого індексу.

Ключові слова: *краніометрія, підочноямковий отвір, надочноямковий отвір, підборідний отвір.*

DOI: 10.31393/morphology-journal-2022-28(4)-05 Reports of Morphology, Vol. 28, №4, Pages 34-40

ISSN 1818-1295 eISSN 2616-6194

REPORTS OF MORPHOLOGY

Official Journal of the Scientific Society of Anatomists, Histologists, Embryologists and Topographic Anatomists of Ukraine

journal homepage: https://morphology-journal.com

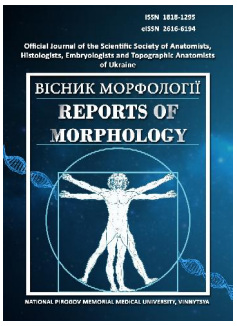

Changes in the structural organization of lymph nodes during short-term exposure to monosodium glutamate

Mateshuk-Vatseba L. R.[1], Holovatskyi A. S.[2], Harapko T. V.[2], Foros A. I.[2], Lytvak Yu. V.[2]

[1]Lviv National Medical University named Danylo Halytskyi, Lviv, Ukraine
[2]Uzhhorod National University, Uzhhorod, Ukraine

ARTICLE INFO

Received: 16 August 2022
Accepted: 19 September 2022

UDC: 611.018.53.428:611.08:616

CORRESPONDING AUTHOR

e-mail: garapkotv@gmail.com
Harapko T. V.

CONFLICT OF INTEREST

The authors have no conflicts of interest to declare.

FUNDING

Not applicable.

Monosodium glutamate is a common food additive that belongs to the group of flavor enhancers used in a wide range of food products. The potentially negative impact of monosodium glutamate on human health prompts us to question the safety of its widespread use. The article presents and analyzes the data of an experimental study conducted on 40 white male and female rats of reproductive age (2.5-3.5 months old) weighing 120-190 g. The purpose of the study is to study histological, morphometric, and ultrastructural changes in the lymph nodes of rats under conditions of short-term exposure to monosodium glutamate. An experimental group of animals (10 male rats, 10 female rats), which was on a standard vivarium diet, was given monosodium glutamate at a dose of 0.07 g/kg of rat body weight by pipette every day at the same time for four weeks, followed by free access to water and food. In animals of the intact group, the structure of mesenteric lymph nodes corresponded to the species norm. In the experimental group of animals, after four weeks of monosodium glutamate exposure, it was found that the paracortical area contained a g larger number of post-capillary venules with a high endothelium compared to the intact and control groups of animals. Changes in the vascular bed were established, in particular, the arteries both in the thickness of the organ and in its hilum contain a thickened wall, their lumen is full of blood. Veins are also full-blooded, dilated and deformed. Swelling of the parenchyma of nodes and signs of immune activity are observed. There is a significant decrease in the relative area of lymphoid nodules and the mantle zone, an increase in the relative area of the medullary substance of the node, corticomedullary index, germinal centers, paracortical area, and medullary cords. Part of lymphocytes of all populations with signs of apoptosis. The other part has an uneven karyolemma contour, the nucleolus is not visualized in all lymphocytes, the cytoplasm is clear and contains organelles. Mitochondria are hypertrophied with a light matrix. Therefore, even a short-term daily exposure to monosodium glutamate, namely four weeks, causes changes in the structural organization of mesenteric lymph nodes.

Keywords: *experiment, monosodium glutamate, lymphatic node, cortical substance, medullary substance, lymphocytes.*

Introduction

Monosodium glutamate (MSG) is a monosodium salt of glutamic acid, which is often found in nature and exists as a free substance glutamate, and as bound to other amino acids in protein [2, 6, 12]. It is a common food additive, belongs to the group of flavor enhancers used in a wide range of food industry products, for example, soups, sauces, puddings, chips, meat products and mixed seasonings [3, 11]. In addition to enhancing the taste of foods, MSG increases appetite, which causes an increase in the amount of food consumed, leading to a high-calorie diet [1]. Long-term use of monosodium glutamate causes a number of diseases and complications that are difficult to treat [14].

The potentially negative impact of monosodium glutamate on human health prompts us to question the safety of its widespread use [12]. It is known that monosodium glutamate has a negative effect on the structures of the central nervous system, causes insulin resistance, diabetes, hypertension, metabolic syndrome, etc. [17, 19]. Its listed negative effects are still

underestimated, and at the same time, people continue to consume increasing amounts of monosodium glutamate, not knowing about the possible consequences.

Therefore, studying the influence of additives, in particular monosodium glutamate, on the state of the body as a whole and the structure of tissues and organs directly is an urgent issue today, both medically and socially [14].

Lymphoid organs protect the body against exposure to various exo- and endoantigens. One of them are lymph nodes, which are also called "biological filters" [7, 9, 12, 13]. By "filtering" lymph through themselves, they are the first to react to antigens "settled" in them [8, 10]. That is why the functional capacity of these organs is undeniably extremely important for the stability and condition of the entire organism.

The purpose of the study: to study the histological, morphometric and ultrastructural changes of the lymph nodes of rats under conditions of short-term exposure to monosodium glutamate.

Materials and methods

The study was conducted on 40 white male and female rats of reproductive age (2.5-3.5 months old) weighing 120-190 g.

The structure of mesenteric lymph nodes under physiological conditions was studied in 10 animals of the intact group (5 male rats, 5 female rats). An experimental group of animals (10 male rats, 10 female rats), which was on a standard vivarium diet, was given monosodium glutamate at a dose of 0.07 g/kg rat body weight with a pipette every day at the same time for four weeks, with subsequent free access to water and food. A control group of animals (5 male rats, 5 female rats) fed a standard vivarium diet received saline solution (0.9 % NaCl solution) daily with a pipette for four weeks.

All experimental animals were kept in the vivarium of Danylo Halytsky Lviv National Medical University. The research was conducted in accordance with the provisions of the "European Convention on the Protection of Vertebrate Animals Used for Experimental and Other Scientific Purposes" (Strasbourg, 1986), Council of Europe Directives 86/609/EEC (1986), Law of Ukraine No. 3447-IV "On the Protection of Animals from cruelty", general ethical principles of experiments on animals, adopted by the First National Congress of Ukraine on Bioethics (2001).

Preparation of preparations of mesenteric lymph nodes for histological and electron microscopic examination was carried out according to generally accepted methods. Spleen pieces were fixed with a 1.5 % solution of osmium tetroxide in a 0.2 M solution of sodium cacodylate at pH 7.2 for 2-2.5 hours in the cold. Sections were made on an ultramicrotome UMTP-6M with a diamond knife (DIATOM), double contrast was performed according to Reynolds and uranyl acetate. Electron microscopic research was carried out using a TEM-100 transmission electron microscope. Photo documentation using a SONY-H9 digital camera. Semi-thin sections with a thickness of 1-2 μm were made on an LKB-3 ultramicrotome (Sweden). They were stained with methylene blue.

Morphometric studies were performed after four weeks of the experiment on histological preparations stained with hematoxylin and eosin, using VideoTest-5.0, KAARA Image Base, Stepanizer and Microsoft Excel programs on a personal computer. Statistical processing of digital data was performed with the help of the "Excel" software using the parametric method.

Results

As the research results obtained by us showed, the structure of the mesenteric lymph nodes in animals of the intact group corresponded to the species norm. The morphological structure of nodes in the group of control male and female rats corresponded to the norm for the given age of the animal, and no deviations from the norm were observed at the end of the research. Lymph nodes are surrounded by a connective tissue capsule, which gives cortical and medullary trabeculae to the thickness of the parenchyma of the organ. Vessels and nerves pass through the latter. There is a gate on the concave part of the node. The parenchyma is built from the cortex of the node, located on the periphery, and the more centrally located medulla. The cortex contains primary and secondary lymphoid nodules. The medulla, in turn, consists of medullar sinuses and medullar cords (Fig. 1).

The lymphoid component of the parenchyma of mesenteric lymph nodes is formed by lymphocytes, macrophages, and plasma cells. Lymphocytes are divided into small, medium and large. Reticular cells and tissue form a three-dimensional framework that is filled with lymphoid cells. Electron microscopy established that all cells have a typical structure. Small lymphocytes with a diameter

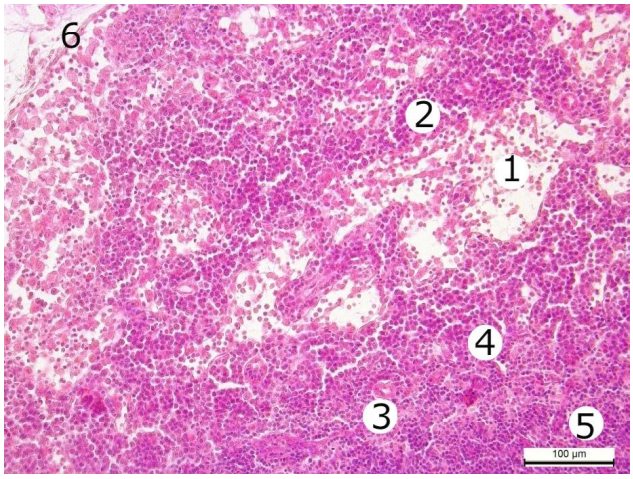

Fig. 1. A fragment of a mesenteric lymph node of an intact female white rat. Coloring with azan. Magnification: x200. Conventional signs: 1 - medullar intermediate lymphatic sinus; 2 - medullar cord; 3 - capillary venule; 4 - paracortical area; 5 - cortex; 6 - lymph node capsule.

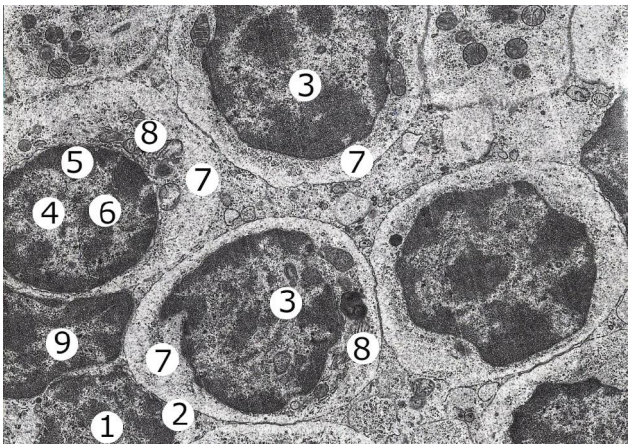

Fig. 2. Submicroscopic structure of the mesenteric lymph node cortex of a white female rat of the intact group. Electron micrograph. Magnification: x6000. Conditional signs: 1 - the nucleus of a small lymphocyte; 2 - cytoplasm of a small lymphocyte; 3 - the nucleus of an average lymphocyte, 4 - euchromatin in the nucleus of an average lymphocyte; 5 - heterochromatin; 6 - nucleolus; 7 - cytoplasm of an average lymphocyte; 8 - mitochondria; 9 - nucleus of a dendritic cell.

of 6-7 microns contain an oval large nucleus, which is surrounded by a thin rim of cytoplasm containing unchanged organelles (Fig. 2). Medium lymphocytes with a diameter of 7-9 μm have a rounded nucleus. Cytoplasm contains ribosomes, granular endoplasmic reticulum and mitochondria. Lymphoblasts with a diameter of about 10 μm are distinguished by the fact that their nucleus contains more euchromatin than heterochromatin, which makes them appear lighter.

After four weeks of daily exposure to monosodium glutamate, when studying the histological structure of mesenteric lymph nodes of male and female rats, it was found that the capsule of the organ thickens, which is associated with an increase in blood vessels in it, an increase in the proportion of adipose tissue, and the appearance of vacuole-like structures. An increase in the number of secondary lymphoid nodules in the nodule cortex was noted, which indicates the immune activity of this organ (Fig. 3). Germinal centers are clearly visualized, somewhat elongated in shape. The cortex and medulla layers are also moderately thickened.

The cortex sinuses and the marginal sinus are not expanded. The medullar sinuses are tortuous and narrowed. Medullar cords are thickened, contain densely located B-lymphocytes, plasma cells and macrophages (Figs. 3, 4). No differences in the histological structure of the mesenteric lymph nodes of male and female rats were found after four weeks of monosodium glutamate exposure. The paracortical area contains a greater number of post-capillary venules with a high endothelium compared to the intact and control groups of animals.

Changes in the vascular bed are observed, in particular, the arteries both in the thickness of the organ and in its gates contain a thickened wall, their lumen is full of blood. Veins are also full-blooded, dilated and deformed.

Using the morphometric method, it was established that the relative area of the mesenteric lymph node cortex after four weeks of the experiment decreases compared to the intact group of animals by only 1.95 % in male rats and by 4.21 % in female rats. The relative area of the node medulla increases by 3.06 % and 6.65%, respectively. The cortico-medullar index is 5.09 % ($p<0.05$) and 10.06 % ($p<0.001$) significantly less than the indicator of the intact group of animals (tables 1, 2).

The relative area of lymphoid nodules increases in comparison with the intact group of animals by 4.84 % in

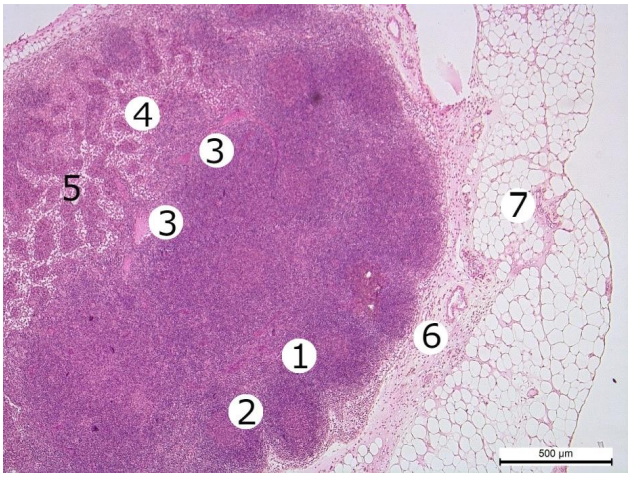

Fig. 3. A fragment of a mesenteric lymph node from a male white rat after four weeks of MSG exposure. Staining with hematoxylin and eosin. Magnification: x50. Conventional signs: 1 - secondary lymphoid nodule; 2 - cortical intermediate lymphatic sinus; 3 - post-capillary venules in the cotrex; 4 - thickened medullary cord; 5 - narrowed medullary sinus; 6 - thickened capsule; 7 - fatty tissue around the organ.

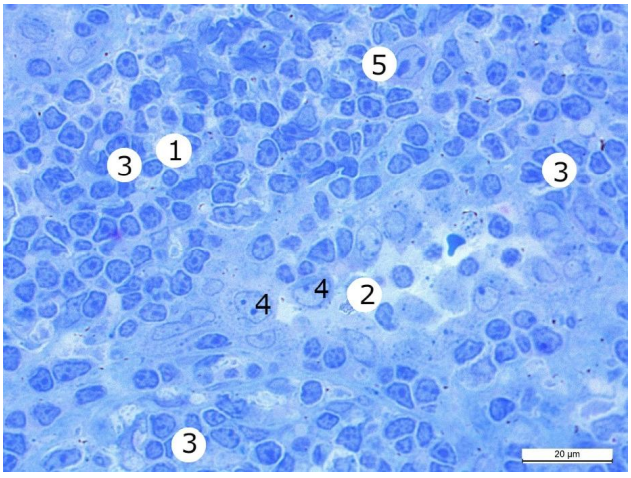

Fig. 4. A fragment of a mesenteric lymph node medulla of a female white rat after four weeks of monosodium glutamate exposure. Semi-thin cut. Staining with methylene blue. Magnification: x1000. Conventional signs: 1 - medullary cord; 2 - medullary sinus; 3 - small and medium lymphocytes; 4 - reticuloendotheliocytes; 5 - lymphoblast.

Table 1. Morphometric parameters of the structural components of the mesenteric lymph nodes of the studied male rats (M±m).

Parameter, units of measurement	Group of animals		p
	Intact	Experimental	
The relative area of the mesenteric lymph node cortex, %:	61.08±1.56	59.89±1.31	p>0.05
- lymphoid nodule	45.28±1.19	43.09±1.01	p<0.05
- germinal center	8.109±0.128	10.82±0.29	p<0.001
- mantle	37.17±0.97	32.27±0.94	p<0.001
- subcapsular sinus	4.389±0.219	4.519±0.161	p>0.05
- cortical sinus	4.031±0.159	4.131±0.122	p>0.05
- paracortical area	7.379±0.292	7.983±0.251	p<0.05
The relative area of the mesenteric lymph node medulla, %:	38.92±0.78	40.11±0.61	p>0.05
- medullary cord	18.71±1.01	21.33±0.76	p<0.05
- medullary sinus	20.41±1.15	18.78±0.69	p<0.05
Cortico-medullar index	1.571±0.112	1.491±0.11	p<0.05

Table 2. Morphometric parameters of the structural components of the mesenteric lymph nodes of the studied female rats (M±m).

Parameter, units of measurement	Group of animals		p
	Intact	Experimental	
The relative area of the mesenteric lymph node cortex, %:	61.23±1.70	58.65±1.43	p<0.05
- lymphoid nodule	45.37±1.22	42.2±1.21	p<0.05
- germinal center	8.152±0.109	10.69±0.24	p<0.001
- mantle	37.22±0.89	31.51±0.87	p<0.001
- subcapsular sinus	4.409±0.191	4.511±0.109	p>0.05
- cortical sinus	4.041±0.133	4.022±0.133	p>0.05
- paracortical area	7.412±0.269	7.923±0.332	p<0.05
The relative area of the mesenteric lymph node medulla, %:	38.77±0.76	41.35±0.63	p<0.05
- medullary cord	18.65±1.05	21.62±0.83	p<0.05
- medullary sinus	20.12±1.04	19.73±0.75	p>0.05
Cortico-medullar index	1.581±0.109	1.422±0.178	p<0.001

male rats and by 6.99 % (p<0.05) in female rats. The relative area of the germinal center increases by 33.42 % and 31.17 % (p<0.001). The mantle zone decreases by 13.18 % and 15.34 %, respectively (see Tables 1, 2).

The relative area of the marginal lymphatic sinus increases compared to the intact group of animals by 2.96 % in male rats and by 2.27 % in female rats. The relative area of cortical intermediate lymphatic sinuses increases in male rats by 2.48 % and decreases in female rats by 0.47 %. The relative area of the cortical area increases and is, respectively, 8.13 % and 6.88 % significantly more (p<0.05) than the indicator of the intact group of animals. The relative area of the medullar intermediate lymphatic sinuses decreases and is 7.99 % (p<0.05) and 1.94 % (p>0.05) less than the parameters of the intact group of animals. The relative area of medullar cords increases and is, respectively, 14.01 % and 15.92 % significantly more (p<0.05) than the parameters of the intact group of animals (see Tables 1, 2).

During the electron microscopic examination of the mesenteric lymph nodes of the experimental group of animals, it was found that the intercellular spaces are expanded, often containing vacuole-like structures. Part of lymphocytes of all populations with signs of apoptosis (Fig. 5). The other part has an uneven contour of the karyolemma, the nucleolus is not visualized in all

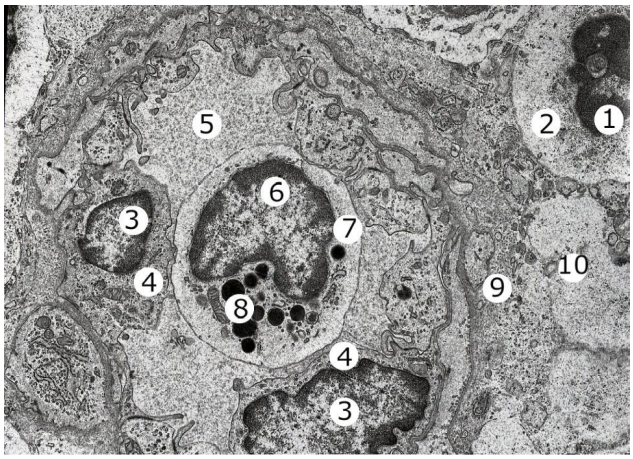

Fig. 5. Fragment of a mesenteric lymph node medulla of a white male rat after four weeks of exposure to monosodium glutamate. Electron micrograph. Magnification: x6000. Conventional signs: 1 - lymphocyte karyolysis; 2 - organelle-free cytoplasm of a lymphocyte; 3 - endotheliocyte nucleus, 4 - endotheliocyte cytoplasm, 5 - venule lumen; 6 - monocyte nucleus, 7 - monocyte cytoplasm, 8 - osmiophilic inclusions, 9 - swollen and thickened basement membrane, 10 - perivascular edema.

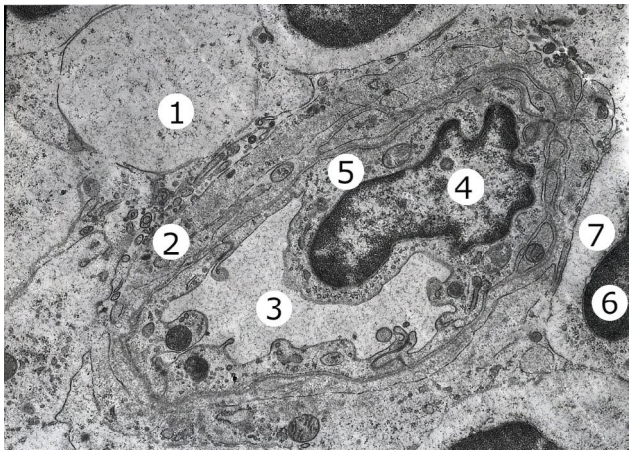

Fig. 6. Blood capillary in the cortex of a mesenteric lymph node of a white female rat after four weeks of MSG exposure. Electron micrograph. Magnification: x8000. Conventional signs: 1 - severe perivascular edema; 2 - stratified basement membrane; 3 - narrowed, deformed hemocapillary lumen; 4 - deformed, swollen endotheliocyte nucleus in the vessel wall; 5 - endotheliocyte cytoplasm; 6 - lymphocyte nucleus, 7 - illuminated cytoplasm.

lymphocytes, the cytoplasm is clear and contains organelles. Mitochondria are hypertrophied with a light matrix.

Perivascular edema is observed. The basement membrane of hemocapillaries, venules, and arterioles is thickened, stratified, and their lumen is somewhat narrowed. Endotheliocyte nuclei in the vessel wall are somewhat swollen, the lumenal surface of the plasmalemma forms numerous microvilli, which actually narrow the lumen of the vessel (Fig. 6). Organelles in the cytoplasm of endotheliocytes lose their contours.

Discussion

So, after four weeks of sodium glutamate action on histological preparations of mesenteric lymph nodes, intensive formation of germinal centers, increased proliferation and differentiation of lymphoid cells is observed. These are signs of antigenic stimulation. There is an immunoinducing effect with increased proliferation of activated lymphocytes and their subsequent differentiation into plasma cells. This is the morphological prerequisite for increased synthesis of immunoglobulins.

We believe that all changes in this term of the experiment are the primary reaction of immune organs to the daily administration of monosodium glutamate, similar changes have been described under the influence of other factors [15, 16]. Changes in the vascular bed are non-specific for this organ. Signs of edema of the parenchyma of lymph nodes are that the intercellular space is expanded and contains vacuole-like structures [16].

From the studies described in the literature, it is known that the administration of monosodium glutamate in a dose of 30 mg/kg of body weight leads to the accumulation of an excessive amount of substances of low and medium molecular weight in the body and a decrease in the ability of the kidneys to excrete toxic products. The shift of markers of intoxication syndrome towards catabolic substances was revealed. After a week of the experiment, the results correspond to the phase of partial compensation, characterized by an increased concentration of substances of low and medium molecular weight in erythrocytes and blood plasma. After two weeks and up to one month of the experiment, catabolic markers of endogenous intoxication prevail, which continue to accumulate in erythrocytes and plasma, which indicates the transition to the phase of partial decompensation of all systems and organs involved in detoxification [12]. Based on these results, the organs of the immune system are affected by intoxication of the body, as a side effect of monosodium glutamate.

Similar changes were found in other lymphoid organs under the influence of a high-calorie diet. An increase in the number of lymphocytes in the thymus parenchyma was found in rats. In the spleen of rats, the volume fraction of white pulp decreased, the number of cells in it also decreased, and the mass of the spleen increased. On the part of the vessels, hematuria and swelling of the parenchyma in both the thymus and the spleen were found, which once again confirms the non-specificity of changes in the vascular bed. The author explains the above changes as a manifestation of the body's general adaptive response [18].

As is well known, the population of "naïve" T-cells (helpers) decreases quantitatively with age, which leads to deterioration of the immune system. In animal model studies, high-calorie diet and obesity compromise the immune system through effects on T-cells due to increased adipogenesis in primary lymphoid organs and systemic inflammation in general. Given the fact that obesity increases the risk of many age-related diseases, impaired immune competence is a possible link between obesity and the development of diseases in the elderly and senile [5].

The results of a study in which experimental animals were fed a high-calorie diet consisting of 20 % protein, 20 % carbohydrates and 60 % fat for two weeks indicate that the proportion of macrophages and stromal cells that contain lipid inclusions increases in the parenchyma of lymph nodes. For comparison, a group of animals was used that received a low-calorie diet that included 20 % protein, 70% carbohydrates and 10 % fat for two weeks. The authors proved that stromal cells express a large number of genes related to lipid metabolism, which suggests that lymph nodes are involved in lipid metabolism [15]. The presence of lipid inclusions in the organs of the immune system is described in obesity.

Changes at the submicroscopic level were found in the lymph nodes during long-term use of the opioid nalbuphine. The authors describe that the six-week and eight-week administration of the opioid nalbuphine leads to pathological changes in the lymph nodes at the submicroscopic level: the number of lymphoblasts with signs of mitosis decreases, the number of lymphocytes with significant nuclear changes and damaged organelles in the cytoplasm of cells increases, which leads to the appearance of lymphoid cells with phenomena of preapoptosis and apoptosis, the intercellular spaces increase [16].

From the study conducted by the authors, it is known that the addition of monosodium glutamate to the diet of rats causes a delay in the removal of Na, K and water from the body. This, in turn, causes arterial hypertension [4].

Conclusions

It was found that even short-term daily exposure of male and female rats of reproductive age to monosodium glutamate, namely four weeks, causes changes in the structural organization of mesenteric lymph nodes. Swelling of the parenchyma of nodes and signs of immune activity are observed. There is a significant decrease in the relative area of lymphoid nodules and the mantle zone, an increase in the relative area of the medulla of the node, cortico-medullar index, germinal centers, paracortical area, and medullar cords. Arteries with a thickened wall are full-blooded, veins are deformed full-blooded. Submicroscopically, the proportion of apoptically changed cells increased.

References

[1] Abdel Moneim, W. M., Yassa, H. A., Makboul, R. A., & Mohamed, N. A. (2018). Monosodium glutamate affects cognitive functions in male albino rats. *Egypt J. Forensic Sci,* 8(1), 1-10. doi: 10.1186/s41935-018-0038-x

[2] Bautista, R. J. H., Mahmoud, A. M., Konigsberg, M., & Guerrero, N. E. L. D. (2019). Obesity: Pathophysiology, monosodium glutamate-induced model and anti-obesity medicinal plants. *Biomedicine & Pharmacotherapy,* 111, 503-516. doi: 10.1016/j.biopha.2018.12.108

[3] Bhandari, U. (2018). Effect of Embelin in Monosodium Glutamate Induced Obesity in Male Neonatal Wistar Rats. *Atheroscler.* Suppl., 32, 138. doi: 10.1016/j.atherosclerosissup.2018.04.423

[4] Contini, M. C., Fabro, A., Millen, N., Benmelej, A., & Mahieu, S. (2017). Adverse effects in kidney function, antioxidant systems and histopathology in rats receiving monosodium glutamate diet. *Experimental and Toxicologic Pathology*, 69(7), 547-556. doi: 10.1016/j.etp.2017.03.003

[5] Demchenko, G. A., Abdreshov, S. N., & Nurmakhanova, B. A. (2019). Contractile activity of lymph nodes in young, middle-aged, and old rats. *Bulletin of Experimental Biology and Medicine,* 167(2), 194-197. doi: 10.1007/s10517-019-04489-x

[6] Hussein, U., Hassan, N., Elhalwagy, M., Zaki, A. R., Abubakr, H. O., Nagulapalli Venkata, K. C. … Bishayee, A. (2017). Ginger and Propolis Exert Neuroprotective Effects against Monosodium Glutamate-Induced Neurotoxicity in Rats. *Molecules,* 22(11), 1928. doi: 10.3390/molecules22111928

[7] Islam, M. N., Khan, M. Z. I., Jahan, M. R., & Shinoda, K. (2018). Developmental trajectory of the prenatal lymphoid organs in native chickens: a macro anatomical study. *Asian Journal of Medical and Biological Research*, 3(4), 432-436. doi: 10.3329/ajmbr.v3i4.35333

[8] Galeeva, E. N., & Ul'yanov, O. V. (2019). Topographic and anatomical characteristic of visceral lymphatic nodes of the abdomen in the intermediate fetal period of human ontogenesis. *Journal of Anatomy and Histopathology,* 8(2), 38-42. doi: 10.18499/2225-7357-2019-8-2-38-42

[9] Gavrilin, P. N., Lieshchova, M. A., Gavrilina, O. G., & Boldyreva, T. F. (2018). Prenatal morphogenesis of compartments of the parenchyma of the lymph nodes of domestic cattle (Bos taurus). *Regulatory Mechanisms in Biosystems*, 9(1), 95-104. doi: 10.15421/021814

[10] Gavrilin, P. N., Gavrilina, O. G., & Kravtsova, M. V. (2017). The compartments of the parenchyma of the lymph nodes in the newborn bull calves of domestic cattle (Bos taurus). *Regulatory Mechanisms in Biosystems,* 8(2), 169-178. doi: 10.15421/021727

[11] Kolenchenko, O. O., Falalieieva, T. M., Berehova, T. V., & Kuryk, O. N. (2017). Стан ліпідного обміну щурів за умов введення глутамату натрію [The state of lipid metabolism in rats under conditions of monosodium glutamate administration]. *Актуальні проблеми сучасної медицини: Вісник української медичної стоматологічної академії - Actual Problems of Modern Medicine: Bulletin of the Ukrainian Medical Stomatological Academy,* 17(4-2(60), 58-61.

[12] Krynytska, I., Marushchak, M., Naumova, L., & Mazur, L. (2019). The Toxic Impact of Monosodium Glutamate in Rats. *J. Med. J.,* 53(2), 91-101.

[13] Lieshchova, M. A., Oliyar, A. V., Bilyi, D. D, Skliarov, P. M., Masiuk, D. M., Logvinova, V. V., & Bohomaz, A. A. (2020). Dynamics of lymph nodes weight characteristics in cattle during the prenatal period of their ontogenesis. *Theoretical and Applied Veterinary Medicine,* 8(4), 283-288. doi: 10.32819/2020.84042

[14] Nnadoziem, J. O., Chijioke, U. O., Okafor, O. C., Olusina, D. B., Oli, A. N., Nwonu, P. C. … Chijioke, C. P. (2019). Chronic toxicity of low dose monosodium glutamate in albino Wistar rats. *BMC Res Notes,* 12(1), 1-7. doi: 10.1186/s13104-019-4611-7

[15] Streich, K., Smoczek, M., Hegermann, J., Dittrich-Breiholz, O., Bornemann, M., Siebert A. … Buettner, M. (2020). Dietary lipids accumulate in macrophages and stromal cells and change the microarchitecture of mesenteric lymph nodes. *Journal of Advanced Research,* 24, 291-300. doi: 10.1016/j.jare.2020.04.020

[16] Valko, O. O., & Holovatskyi, A. S. (2018). Changes in the cell squad of iliac lymph nodes of white rats in case of longterm influence of nalbufin. *EUREKA: Health Sciences,* 2, 8-16. doi: 10.21303/2504-5679.2018.00573

[17] Vorhees, C. V. (2018). A Test of Dietary Monosodium Glutamate Developmental Neurotoxicity in Rats: A Reappraisal. *Ann. Nutr. Metab.,* 73(5), 36-42. doi: 10.1159/000494781

[18] Yakubtsova, I. V., Khilko, T. D., Savytska, I. M., Konopelniuk, V. V., Preobrazhenska, T. D., & Makai, Sh. (2016). Вплив Trigonella Foenum Graecum L. на стан імунокомпетентних органів за умов дієтіндукованого ожиріння у щурів [The effect of Triogenella Foenum Graecum L. on the state of immunocompetent organs under conditions of diet-induced obesity in rats]. *Scientific Journal "ScienceRise: Biological Science",* 3(3), 53-60. doi: 10.15587/2519-8025.2016.83579

[19] Zanfirescu, A., Cristea, A. N., Nitulescu, G. M., Velescu, B. S., & Gradinaru, D. (2017). Chronic monosodium glutamate administration induced hyperalgesia in mice. *Nutrients,* 10(1), 1. doi: 10.3390/nu10010001

ЗМІНИ СТРУКТУРНОЇ ОРГАНІЗАЦІЇ ЛІМФАТИЧНИХ ВУЗЛІВ ПРИ КОРОТКОТРИВАЛІЙ ДІЇ ГЛУТАМАТУ НАТРІЮ

Матешук-Вацеба Л. Р., Головацький А. С., Гарапко Т. В., Форос А. І., Литвак Ю. В.

Глутамат натрію є поширеною харчовою добавкою, котра відноситься до групи підсилювачів смаку, які використовують у широкому асортименті продуктів харчової промисловості. Потенційно негативний вплив глутамату натрію на здоров'я людини спонукає поставити під сумнів безпеку його широкого застосування. В статті наведено та проаналізовано дані експериментального дослідження, проведеного на 40 білих щурах-самцях і самках репродуктивного віку (2,5-3,5-місячних) масою 120-190 г. Мета дослідження - вивчити гістологічні, морфометричні та ультраструктурні зміни лімфатичних вузлів щурів в умовах короткотривалого впливу глутамату натрію. Експериментальній групі тварин (10 щурів-самців, 10 щурів-самок), котра перебувала на стандартному харчовому раціоні віварію, впродовж чотирьох тижнів щодня в один і той же час піпеткою додавали глутамат натрію в дозі 0,07 г/кг маси тіла щура з подальшим вільним доступом до води та їжі. У тварин інтактної групи будова брижових лімфатичних вузлів відповідала видовій нормі. В експериментальній групі тварин через чотири тижні дії глутамату натрію виявлено, що прикіркова ділянка містила більшу кількість закапілярних венул з високим ендотелієм порівняно з інтактною та контрольними групами тварин. Встановлено зміни в судинному руслі, зокрема, артерії як в товщі органа, так і в його воротах містять потовщену стінку, їх просвіт повнокровний. Вени

також повнокровні, розширені та деформані. Спостерігається набряк паренхіми вузлів та ознаки імунної активності. Відбувається достовірне зменшення відносної площі лімфоїдних вузликів та плащової зони, збільшення відносної площі мозкової речовини вузла, кірково-мозкового індексу, зародкових центрів, прикіркової ділянки, мозкових тяжів. Частина лімфоцитів всіх популяцій з ознаками апоптозу. Інша частина має нерівний контур каріолеми, ядерце візуалізується не у всіх лімфоцитах, цитоплазма просвітлена, містить органели. Мітохондрії гіпертрофовані зі світлим матриксом. Отже, навіть короткотривалий щоденний вплив на організм глутамату натрію, а саме чотири тижні, викликає зміни структурної організації брижових лімфатичних вузлів.

Ключові слова: *експеримент, глутамат натрію, ліматичний вузол, кіркова речовина, мозкова речовина, лімфоцити.*

DOI: 10.31393/morphology-journal-2022-28(4)-06 Reports of Morphology, Vol. 28, №4, Pages 41-47

ISSN 1818-1295 eISSN 2616-6194

REPORTS OF MORPHOLOGY

Official Journal of the Scientific Society of Anatomists, Histologists, Embryologists and Topographic Anatomists of Ukraine

journal homepage: https://morphology-journal.com

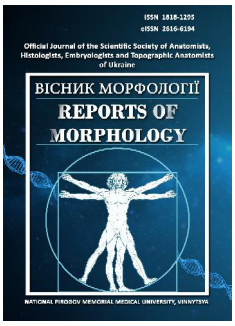

Teleroentgenometric parameters of the soft palate in young men and young women with an orthognathic bite without and taking into account the type of face

Kostiuchenko-Faifor O. S., Gunas I. V., Kyrychenko I. M., Vakhovskyi V. V., Kosianenko S. M.
National Pirogov Memorial Medical University, Vinnytsya, Ukraine

ARTICLE INFO
Received: 22 August 2022
Accepted: 26 September 2022

UDC: 616.21:616.314.26-053.81-073.75

CORRESPONDING AUTHOR
e-mail: kostyuchenko.olha.91@gmail.com
Kostiuchenko-Faifor O. S.

CONFLICT OF INTEREST
The authors have no conflicts of interest to declare.

FUNDING
Not applicable.

The study of the features of the upper respiratory tract and the relationship of their parameters with other anatomical formations and structures of the human body is one of the promising areas of modern science. Since numerous anatomical components are involved in the functioning of the respiratory tract, their detailed study should be carried out separately. One of these components that is of direct interest to science and practice is the soft palate. The purpose of the study is to establish the peculiarities of the teleroentgenometric parameters of the soft palate in Ukrainian young men and young women without pathology of the upper respiratory tract with an orthognathic bite without and taking into account the type of face. Determination of teleroentgenometric parameters of the soft palate was carried out in 72 young women and 46 young men with no pathology of the upper respiratory tract with an orthognathic bite (primary lateral teleroentgenograms were taken from the database of the research center and the Department of Pediatric Dentistry of the National Pirogov Memorial Medical University, Vinnytsya). For all young men and young women face type was determined using Garson's morphological index. The analysis of the obtained results was carried out in the statistical package "Statistica 6.0" using non-parametric estimation methods. As a result of the conducted research, pronounced gender differences were found (significantly greater, or a tendency to greater values in young men): the value of the PM-U distance in representatives without taking into account the type of face by 7.1 %, with very wide - by 9.2 %, with wide - by 8.4 % and with narrow - by 7.4 % face types; values of the SPT distance in representatives without taking into account the face type by 10.3 %, with very wide - by 16.4 % and with narrow - by 23.1 % face types; the values of the NL/PM-U angle in representatives without taking into account the face type by 7.6 % and by 11.5 % with wide face types; the size of the SPA area in representatives without taking into account the type of face by 17.2 %, with very wide - by 24.4 %, with wide - by 13.4 % and with narrow - by 32.2 % of face types. When analyzing the value of teleradiographic parameters of the soft palate in young men between different types of faces, it was established that significantly higher values or trends towards higher values in representatives with a narrow face of the SPT distance and SPA area than in young men with a very wide (respectively by 8.9 % and 13.0 %) and average (by 13.9 % and 22.2 %), respectively, face types, and in young men, regardless of face type, there is a tendency for greater values of the PM-U distance than in representatives with an average face (by 4.2 %). In young women with a narrow face, only a tendency to greater values of the NL/PM-U angle was established than in young women with a wide face (by 6.2 %). The results of the study are an integral element of determining the normative values of various parameters of the upper respiratory tract, which enables practicing doctors to more correctly distinguish the norm from pathology.

Keywords: *teleroentgenography, cephalometry, soft palate, young men, young women, facial types, orthognathic bite.*

Introduction

The study of the upper respiratory tract is a complex and complex process, because this anatomical complex includes a lot of structures of a different nature - both bony, cartilaginous and soft tissue. If we talk about the latter, the

soft palate has a special place among them.

The soft palate is a group of five muscles, and is an extension of the hard palate that hangs over the base of the tongue. In general, it occupies about a third of the roof of the oral cavity and has a unique for mammals (except some primates) process - the uvula. Intrauterine development of the palate includes the formation of the primary and secondary palate. If a small part of the hard palate is formed from the primary palate, then the majority of both the hard and soft palate is formed from the secondary. The rudiments of the secondary palate are formed at the 6th week of intrauterine development, and it is its developmental pathology that later leads to the formation of a cleft palate defect. Later in life, the soft palate takes part in the act of breathing and swallowing, where it plays one of the key roles. In addition, the function of voice production and speech production is important [13].

As an object of cephalometric research, the soft palate has been studied as an independent component for quite some time. This led to the formation of a classification of forms of the soft palate, which is still a subject of debate in the scientific world. One of the common ones is the classification that distinguishes 6 forms of the soft palate during cephalometric examination: leaf-shaped (the middle part is raised on both sides), rat-tail-shaped (inflated front part and free edge), pillow-shaped (short and thick), rectilinear, S-type, curved (the back part bends upwards from the front) [3, 7, 16].

The prevalence of such forms is quite heterogeneous in different populations. So, on the example of Indian, the first type is the most common and occurs in about half of the cases, the second and third types are less common, and all other types occur in less than 10 % of the population. At the same time, the presence of manifestations of sexual dimorphism regarding one or another type of palate is still debatable [3, 7]. However, these data raise an equally important question - can the features of the structure of the soft palate be interconnected with other structures of the respiratory tract or head, sex and other parameters?

Equally important is the fact that the size of the soft palate varies significantly in people with respiratory tract diseases. An increase in the length of PNS-U of the soft palate with a more severe course of obstructive sleep apnea [14]. In addition, certain forms of soft palate occur more often in people with this disease [5].

According to other studies, not only the parameters of the soft palate, but also other elements of the respiratory tract in the complex affect the severity of obstructive sleep apnea. Such a parameter is also a linear distance along a plane perpendicular to the plane of the hyoid bone of the lower jaw [4].

Thus, it becomes especially important to determine the normative indicators of the soft palate for individuals of a certain population, taking into account such parameters as gender and age. An equally important direction may be the search for the relationship between the parameters of the soft palate and other craniofacial structures.

The purpose of the study is to establish the peculiarities of the teleroentgenometric parameters of the soft palate in Ukrainian young men and young women without pathology of the upper respiratory tract with an orthognathic bite without and taking into account the type of face.

Materials and methods

Primary lateral radiographs of 46 Ukrainian young men (YM) (aged 17 to 21 years) and 72 Ukrainian young women (YW) (aged 16 to 20 years) with an orthognathic bite and the absence of upper respiratory tract pathology were taken from the database of the Scientific Research Center and Department of Pediatric Dentistry National Pirogov Memorial Medical University, Vinnytsya. All of them, after applying for dental care, underwent a teleradiographic examination (effective radiation dose up to 0.001 mSv) using a dental cone-beam tomograph Veraviewepocs 3D Morita (Japan) on the basis of the private dental clinic "Vinintermed" (Vinnytsia). Cephalometric analysis was performed using the licensed medical software OnyxCeph^{3}™, version 3DPro (Image Instruments GmbH, Germany) and the diagnostic program "UniqCeph" created at the National Pirogov Memorial Medical University, Vinnytsya.

Committee on Bioethics of National Pirogov Memorial Medical University, Vinnytsya (protocol № 8 From 30.09.2021) found that the studies do not contradict the basic bioethical standards of the Declaration of Helsinki, the Council of Europe Convention on Human Rights and Biomedicine (1977), the relevant WHO regulations and laws of Ukraine.

Using Garson's morphological index [17], the face type was determined in Ukrainian YM and YW: in YW - 25 with a very wide face, 25 with a wide face, 10 with an average face and 12 with a narrow face; in YM, 5 with very wide face, 22

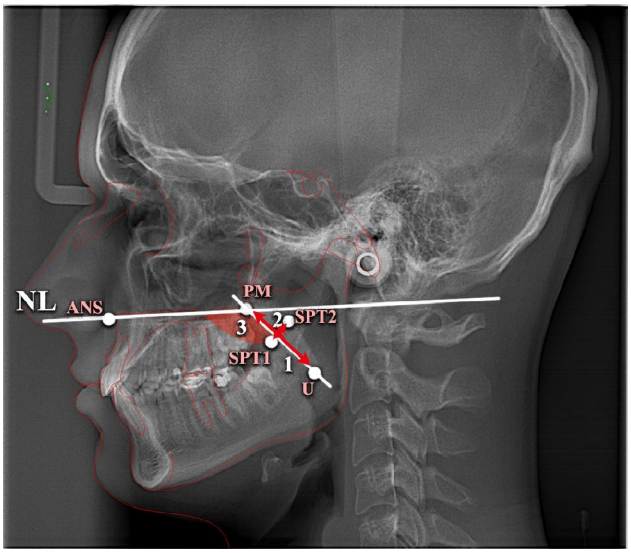

Fig. 1. Linear parameters used in teleroentgenometric examination of the soft palate: 1 - distance PM-U, 2 - distance SPT, 3 - angle NL/PM-U, NL - nasal plane (passes through the ANS and PM points).

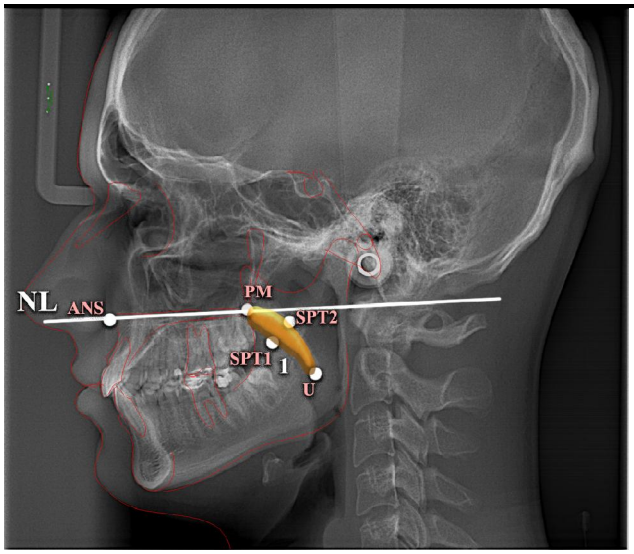

Fig. 2. The area of the soft palate (area SPA).

with wide face, 11 with medium face and 8 with narrow face.

The following teleroentgenometric parameters of the soft palate were determined (Fig. 1, 2):

distance **PM-U** (also known as Soft palate length) - distance between points PM and U (mm);

distance **SPT** (also known as Maximum soft palate thickness) - the distance between the most distant points perpendicular to the line PM-U (mm);

angle **NL/PM-U** (also known as Soft palate inclination Angle) - the angle formed by the lines PM-U and NL (°);

area **SPA** (also known as Soft palate area) - outlined by a contour through points PM and U (mm^2).

The analysis of the obtained results was carried out in the licensed statistical package "Statistica 6.0" using non-parametric estimation methods. Means and standard deviations were determined for each trait. The significance of the difference in values between independent quantitative values was determined using the Mann-Whitney U-test.

Results

When comparing the value of the **PM-U** distance between Ukrainian YM and YW without pathology of the upper respiratory tract with an orthognathic bite without and taking into account the type of face, it was established (Fig. 3) that in YM without taking into account the type of face (31.45±3.43 mm), with a very wide with a face (32.01±1.31 mm), with a wide face (31.81±3.92 mm) and with a narrow face (31.88±3.03 mm), the value of this distance is significantly greater or tends to greater values than in YW without taking into account the type of face (29.23±2.84 mm, p<0.001), with a very wide face (29.06±2.87 mm, p<0.05), with a wide face (29.15±3.33 mm, p<0.01) and a narrow face (29.53±2.29 mm, p=0.076).

When comparing the value of the **PM-U** distance in Ukrainian YM or YW without pathology of the upper respiratory tract with an orthognathic bite between different types of face, it was established (see Fig. 1) that only in YM without taking into account the type of face the value of this distance has a tendency (p=0.062) to greater values than in YM with an average face type (30.13±3.59 mm).

When comparing the value of the **SPT** distance between Ukrainian YM and YW without pathology of the upper respiratory tract with an orthognathic bite without and taking into account the type of face, it was established (Fig. 4) that in YM without taking into account the type of face (7.340±1.460 mm), with a very wide face (7.656±1.175 mm) and with a narrow face (8.400±1.436 mm), the value of this distance is significantly greater than in YW without taking into account the type of face (6.587±1.169 mm, p<0.01), with a very wide face (6.397±1.142 mm, p <0.05) and a

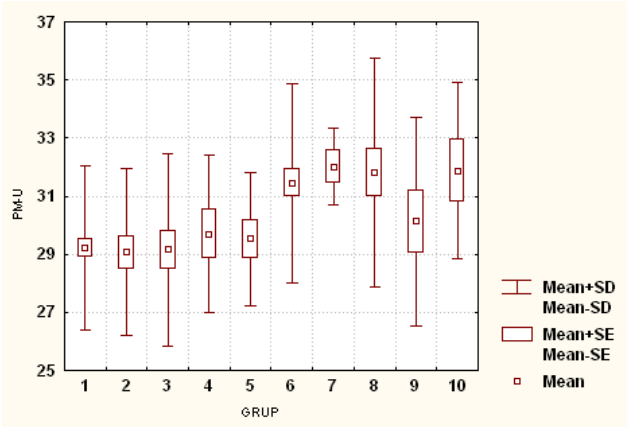

Fig. 3. The value of the **PM-U** distance (length of the soft palate) in YM and YW with orthognathic bite without and taking into account the type of face (mm). Notes: Here and in subsequent figures, 1 is YW excluding face type; 2 - YW with a very wide face type; 3 - YW with a wide face type; 4 - YW with an average face type; 5 - YW with a narrow face type; 6 - YM without taking into account the type of face; 7 - YM with a very wide face type; 8 - YM with a wide face type; 9 - YM with an average face type; 10 - YM with a narrow face type; Mean - sample mean; ±SE - error of the mean; ±SD - standard deviation.

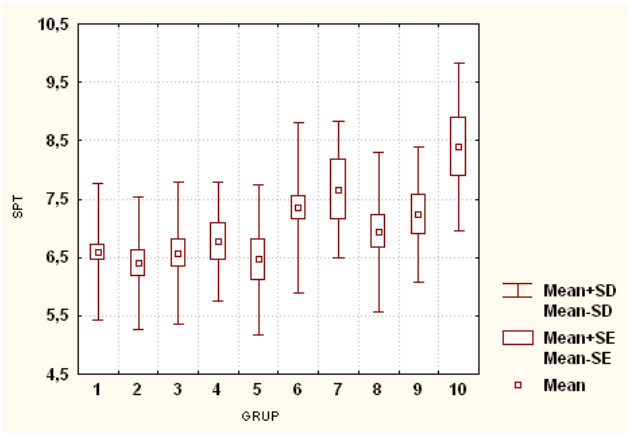

Fig. 4. The magnitude of the **SPT** (soft palate thickness) distance in YM and YW with orthognathic bite without and taking into account the type of face (mm).

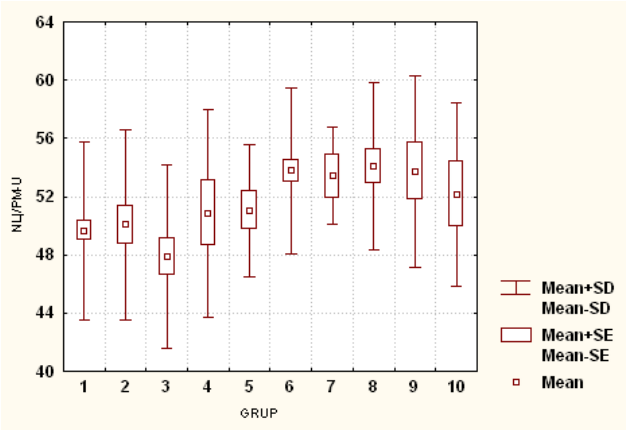

Fig. 5. The value of the **NL/PM-U** angle (angle of inclination of the soft palate) in YM and YW with orthognathic bite without and taking into account the type of face (°).

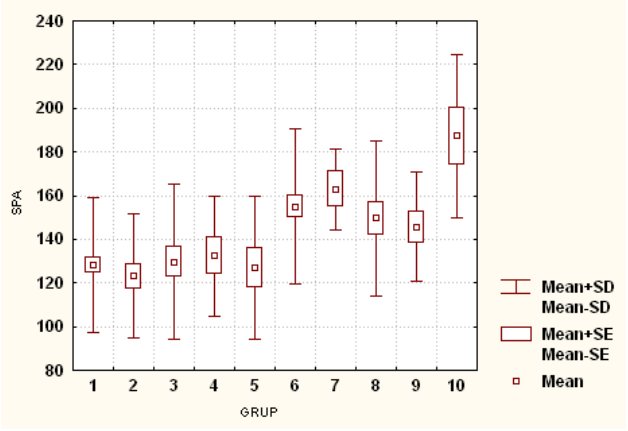

Fig. 6. The size of the **SPA** area (area of the soft palate) in YM and YW with an orthognathic bite without and taking into account the type of face (mm^2).

narrow face (6.458±1.275 mm, p<0.01).

When comparing the value of the **SPT** distance in Ukrainian YM or YW without pathology of the upper respiratory tract with an orthognathic bite between different types of face, it was established (see Fig. 2) that only in YM with a narrow face type, the value of this distance is significantly (p<0.05) greater, than in YM with a very wide face type and has a slight tendency (p=0.083) to greater values than in YM with an average face type (7.235±1.152 mm).

When comparing the value of the **NL/PM-U** angle between Ukrainian YM and YW without pathology of the upper respiratory tract with an orthognathic bite without and taking into account the type of face, it was established (Fig. 5) that in YM without taking into account the type of face (53.77±5.68 °) and with a wide face (54.08±5.71 °), the value of this angle is significantly greater than in YW regardless of face type (49.66±6.09 °, p<0.001) and with a wide face (47.88±6.26 °, p<0.01).

When comparing the value of the **NL/PM-U** angle in Ukrainian YM or YW without pathology of the upper respiratory tract with an orthognathic bite between different types of face, it was established (see Fig. 3) that only in YW with a narrow face type (51.07±4.54 °) the value of this angle has a tendency (p=0.064) to greater values than in YW with a wide face type (47.88±6.26 °).

When comparing the size of the **SPA** area between Ukrainian YM and YW without pathology of the upper respiratory tract with an orthognathic bite without and taking into account the type of face, it was established (Fig. 6) that in YM without taking into account the type of face (155.0± 35.5 mm^2), with a very wide face (162.8±18.7 mm^2), with a wide face (149.6±35.6 mm^2) and with a narrow face (187.2±37.2 mm^2), the value of this area is significantly greater or tends to greater values than in YW regardless of face type (128.3±30.7 mm^2, p<0.001), with a very wide face (123.0±28.4 mm^2, p<0.01), with a wide face (129.6± 35.6 mm^2, p=0.061) and a narrow face (127.0±32.7 mm^2, p<0.01).

When comparing the size of the **SPA** area in Ukrainian YM or YW without pathology of the upper respiratory tract with an orthognathic bite between different types of face, it was established (see Fig. 4) that only in YM with a narrow face type, the size of this area is reliable (p<0.05 in both cases) is greater than in YM with very wide and medium (145.6±25.0 mm^2) facial types.

Discussion

Thus, in Ukrainian YM and YW without pathology of the upper respiratory tract with an orthognathic bite without and taking into account the type of face, pronounced manifestations of sexual dimorphism (higher values in young men) of teleroentgenometric parameters of the soft palate were found: **PM-U** distance in YM without taking into account the type of face by 7.1 %, with a very wide face - by 9.2 %, with a wide face - by 8.4 % and with a narrow face - by 7.4 %; values of the **SPT** distance in YM without taking into account the type of face by 10.3 %, with a very wide face - by 16.4 % and with a narrow face - by 23.1 %; the values of the **NL/PM-U** angle in YM without taking into account the type of face by 7.6 % and with a wide face by 11.5 %; the size of the **SPA** area in YM without taking into account the type of face by 17.2 %, with a very wide face - by 24.4 %, with a wide face - by 13.4 % and with a narrow face - by 32.2 %.

When analyzing the teleroentgenometric parameters of the soft palate in Ukrainian YW or YM without pathology of the upper respiratory tract with an orthognathic bite between different facial types, in YM with a narrow facial type, significantly greater or trends to greater values of the **SPT** distance value were established than in YM with a very wide (by 8.9 %) and medium (by 13.9 %) face types and the size of the **SPA** area than in YM with very wide (by 13.0 %) and medium (by 22.2 %) face types, as well as in YM without taking into account the face type of the distance value **PM-U** tends to higher values than YM with an average face type (by 4.2 %); and in YWs with a narrow face type, a tendency to greater values of the **NL/PM-U** angle was established

than in YWs with a wide face type (by 6.2 %).

Works on the study of the relationship between the parameters of the soft palate and other structures of the human body are quite few in the scientific literature. Thus, Kulshrestha R. and co-authors [12] found significant differences for the value of the angle of inclination of the soft palate in groups with hypo- and hyperdivergent patterns of facial growth ($p<0.003$).

The first type of soft palate is significantly more common ($p=0.001$) in people with an average type of facial growth, and the second type in people with horizontal and vertical types of facial growth [21].

A statistically significant difference was found between all groups with different values of the Needs coefficient. The highest coefficient was observed with a curved type of soft palate (average value 0.9). The vertical growth type in all six types of soft palate demonstrated a higher Needs coefficient than the average and horizontal growth types [9]. Similar data were also obtained in another study [6].

If we talk about the pathology of the maxillofacial system and its relationship with the features of the soft palate, it has been established that in persons with a skeletal malocclusion of class I, a leaf-like form of the soft palate is most often found, and in class II - a rat's tail, in class III - leaf-like and curved forms in equal proportions [2].

In a study on another sample of patients, the following interdependencies were found: patients with a Class I malocclusion most often had a rat-tail type soft palate, Class II patients had a leaf-like soft palate, and Class III patients had a curved soft palate [18].

As for the study of the features of age or sexual dimorphism when studying the indicators of the soft palate, such work is more numerous. For the Iraqi population, adolescent females have been found to have higher soft palate thickness (SPT) values than adult females [1].

In a study of an Indian population, it was found that the velar length increased with age, and the length and width of the soft palate was greater in men than in women. However, a reliable correlation regarding the belonging of one or another type of soft palate to gender was not found [8].

In another study conducted by Indian scientists, the relationship between different types of soft palate in different age groups turned out to be insignificant. The highest values of the average length of the soft palate were found in men aged 46-55 years (and in all age groups higher values in men). In addition, a positive correlation was found between age and the type of soft palate [10].

No correlations were found between the age of the person and the characteristics of the type of soft palate within the studied group, residents of the state of Vikarabad (India) [23].

For the Indian population, the average values of the total average anterior-posterior length of the soft palate were 30.31±3.39 mm, and the upper-lower one was 10.72±1.71 mm [15]. The presence of significant differences in most size indicators within the Indian population is confirmed by the results of other studies [19, 20]. However, the question of why the data of different studies show different results regarding the presence or absence of certain manifestations of sexual dimorphism in the investigated indicators still remains open. Probably, one of the explanations for this phenomenon can be the regional difference in the normative indicators of the Indian population, which is not taken into account by the authors of the mentioned studies.

In the American population, a statistically significant difference was noted for age in relation to the shape of the soft palate ($p=0.014$). At the same time, gender and race have no significant effect on its shape [11].

Nepalese researchers examined and analyzed 263 lateral teleroentgenograms of ethnic residents of Nepal. Statistical analysis of the obtained data did not reveal any manifestations of gender or age dimorphism regarding the features of the forms of the soft palate [22].

Conclusions

1. Pronounced manifestations of sexual dimorphism of teleroentgenometric parameters of the soft palate were established in the Ukrainian youth population without pathology of the upper respiratory tract with an orthognathic bite - in most cases, higher values in young men without and taking into account the type of face (with the exception of the average face type).

2. Differences in teleroentgenometric parameters of the soft palate between young men and young women with different facial types are established mainly in young men - representatives with a narrow face have larger values of the **SPT** distance and the **SPA** area than in young men with very wide and medium facial types, as well as representatives regardless of face type have larger values of the **PM-U** distance than young men with an average face type; and young women with a narrow face type only have larger values of the **NL/PM-U** angle than young women with a wide face type.

References

[1] Al-Sayagh, N. M. (2012). A cephalometric comparison of pharynx and soft palate in Iraqi adolescents and adults population. *Al-Rafidain Dental Journal,* 12(1), 32-42. doi: 10.33899/rden.2012.4

[2] Bhambri, E., Ahuja, V., Ahuja, S., Bhambri, G., Choudhary, A., & Sukhija, S. (2018). The association between soft palate shape and Need's ratio in various sagittal skeletal malocclusions: A digital lateral cephalometric study. *International Journal of Orthodontic Rehabilitation,* 9(1), 8-13. doi: 10.4103/ijor.ijor_41_17

[3] Chalkoo, A. H., Naikoo, F. A., Ahmad, M. B., & Oberoi, I. S. (2015). Morphological varieties of soft palate in normal subjects: a digital cephalometric study. *Indian J. Dent. Adv.,* 7(4), 241-245. doi: 10.5866/2015.7.10241

[4] Cho, S. H., Jeon, J. Y., Jang, K. S., Kim, S. Y., Kim, K. R., Ryu, S., & Hwang, K. G. (2019). Gender-specific cephalometric features related to obesity in sleep apnea patients: trilogy of soft palate-mandible-hyoid bone. *Maxillofacial Plastic and Reconstructive Surgery,* 41, 58. doi: 10.1186/s40902-019-0242-0

[5] Deepa, V., & Ramnarayan, B. K. (2015). Morphological varieties of soft palate in normal individuals, cleft palate patients and obstructive sleep apnea patients with reference to Indian population: a preliminary digital cephalometric study. *World Journal of Dentistry*, 4(4), 241-249. doi: 10.5005/jp-journals-10015-1239

[6] Elkunchwar, G., Gulve, N., Nehete, A., Shah, K., & Aher, S. (2018). Evaluation of airway in different types of soft palate according to growth pattern. *IOSR J. Dent. Med. Sci.,* 17, 53-58. doi: 10.9790/0853-1709035358

[7] Farhadi, N., Zaheri, T., Anjam, N., & Naderi, L. (2018). Evaluation of Morphological Variants of the Soft Palate on Digital Lateral Cephalometric Image among Iranian Patients. *Jundishapur Scientific Medical Journal,* 17(2), 179-186. doi: 10.22118/jsmj.2018.66433

[8] Guttal, K. S., Breh, R., Bhat, R., Burde, K. N., & Naikmasur, V. G. (2012). Diverse morphologies of soft palate in normal individuals: a cephalometric perspective. *Journal of Indian Academy of Oral Medicine and Radiology*, 24(1), 207-210. doi: 10.5005/jp-journals-10015-1084

[9] Jayaprakash, P. K., Modi, P., Sapawat, P., Thakur, R. S., Choudhari, T., & Chandrakar, J. (2019). Correlation of soft palate morphology to growth pattern: A retrospective cephalometric study. *Journal of Family Medicine and Primary Care,* 8(7), 2468-2472. doi: 10.4103/jfmpc.jfmpc_322_19

[10] Khaitan, T., Pachigolla, R., Uday, G., Balmuri, P. K., Chennoju, S. K., & Pattipati, S. (2015). Digital cephalometric analysis illustrating morphological variation of the soft palate. *Journal of Indian Academy of Oral Medicine and Radiology,* 27(4), 532-538. doi: 10.4103/0972-1363.188745

[11] Kotlarek, K. J., Haenssler, A. E., Hildebrand, K. E., & Perry, J. L. (2019). Morphological variation of the velum in children and adults using magnetic resonance imaging. *Imaging Science in Dentistry,* 49(2), 153-158. doi: 10.5624/isd.2019.49.2.153

[12] Kulshrestha, R., Tandon, R., Singh, K., & Chandra, P. (2015). Analysis of pharyngeal airway space and tongue position in individuals with different body types and facial patterns: A cephalometric study. *Journal of Indian Orthodontic Society,* 49(3), 139-144. doi: 10.4103/0301-5742.165555

[13] Li, J., Rodriguez, G., Han, X., Janeckova, E., Kahng, S., Song, B., & Chai, Y. (2019). Regulatory mechanisms of soft palate development and malformations. *Journal of dental research,* 98(9), 959-967. doi: 10.1177/002203451985

[14] Lim, J. S., Lee, J. W., Han, C., & Kwon, J. W. (2018). Correlation of soft palate length with velum obstruction and severity of obstructive sleep apnea syndrome. *Auris Nasus Larynx,* 45(3), 499-503. doi: 10.1016/j.anl.2017.07.023

[15] More, C. B., Saha, N., & Vijayvargiya, R. (2015). Morphological study of soft palate by using computed tomography-a prospective study. *Journal of Clinical and Diagnostic Research: JCDR,* 9(8), ZC71-ZC74. doi: 10.7860/JCDR/2015/14194.6354

[16] Praveen, B. N., Shubhasini, A. R., Vaseemuddin, S., Amrutesh, S., & Pal, S. (2012). Various shapes of soft palate: a lateral cephalometric study. *World Journal of Dentistry*, 2, 207-210. doi: 10.5005/jp-journals-10015-1084

[17] Proffit, U. R., Fildz, G. U., & Saver, D. M. (2006). *Современная ортодонтия* (перевод с английского Д. С. Персина) [*Modern orthodontics* (translation from English by D. S. Persina)]. М.: МЕДпресс-информ - M.: MEDpress-inform.

[18] Samdani, D., Saigal, A., & Garg, E. (2015). Correlation of morphological variants of soft palate and types of malocclusion: A digital lateral cephalometric study. *Journal of Indian Academy of Oral Medicine and Radiology,* 27(3), 366-371. doi: 10.4103/0972-1363.170451

[19] Santosh, V. K., Singh, P., & Pagare, S. S. (2015). Normative soft palate dimensions and morphology in a subset of Indian population: a digital cephalometric study. *Indian Journal of Oral Health and Research,* 1(2), 48-51. doi: 10.4103/2393-8692.172022

[20] Smriti, K., Pai, K. M., Vineetha, R., & Pentapati, K. C. (2015). Radiographic evaluation of soft palate morphology and correlation with gender on lateral cephalograms. *World Journal of Dentistry,* 6(3), 147-149.

[21] Susan, T. C., Sudhakar, S. S., Harshitha, V., Shetty, K. N., Thomas, B., & Rai, K. (2021). Correlation of Morphological Variants of Soft Palate and Different Facial Divergence-a CBCT Study. *Annals of the Romanian Society for Cell Biology,* 25(6), 20449-20454.

[22] Upadhyaya, C., Neupane, I., Sapkota, B., & Srivastava, S. (2017). Morphological diversity of soft palate in Nepalese population: A retrospective cephalometric study. *Orthodontic Journal of Nepal,* 7(1), 18-22. doi: 10.3126/ojn.v7i1.18896

[23] Vani, C., Lakshmi, T. V., & Roy, V. D. (2017). Morphological variations of soft palate and influence of age on it: A digital cephalometric study. *IAIM,* 4(10), 72-76.

ТЕЛЕРЕНТГЕНОМЕТРИЧНІ ПАРАМЕТРИ М'ЯКОГО ПІДНЕБІННЯ В ЮНАКІВ І ДІВЧАТ ІЗ ОРТОГНАТИЧНИМ ПРИКУСОМ БЕЗ ТА З УРАХУВАННЯМ ТИПУ ОБЛИЧЧЯ

Костюченко-Файфор О. С. Гунас І. В., Кириченко І. М., Ваховський В. В., Косьяненко С. М.

Дослідження особливостей верхніх дихальних шляхів та взаємозв'язку їх параметрів з іншими анатомічними утвореннями та структурами тіла людини є одним з перспективних напрямків сучасної науки. Так як у функціонуванні дихальних шляхів приймають участь численні анатомічні компоненти, слід проводити їх детальне дослідження окремо. Одним з таких компонентів, що безпосередньо представляє інтерес для науки та практики є м'яке піднебіння. Мета дослідження - встановити особливості телерентгенометричних параметрів м'якого піднебіння в українських юнаків і дівчат без патології верхніх дихальних шляхів із ортогнатичним прикусом без та з урахуванням типу обличчя. Визначення телерентгенометричних параметрів м'якого піднебіння проведено у 72 українських дівчат і 46 юнаків із відсутністю патології верхніх дихальних шляхів із ортогнатичним прикусом (первинні бокові телерентгенограми взяті з бази даних науково-дослідного центру та кафедри стоматології дитячого віку Вінницького національного медичного університету ім. М. І. Пирогова). Усім юнакам і дівчатам проведено визначення типу обличчя за допомогою морфологічного індексу Гарсона. Аналіз отриманих результатів проведений у статистичному пакеті "Statistica 6.0" з використанням непараметричних методів оцінки. В результаті проведених досліджень виявлені виражені статеві розбіжності (достовірно більші, або тенденція до більших значень в юнаків): величини відстані PM-U у представників без урахування типу обличчя на 7,1 %, з дуже широким - на 9,2 %, з широким - на 8,4 % і з вузьким - на 7,4 % типами обличчя; величини відстані SPT у

представників без урахування типу обличчя на 10,3 %, з дуже широким - на 16,4 % і з вузьким - на 23,1 % типами обличчя; величини кута NL/PM-U у представників без урахування типу обличчя на 7,6 % і з широким - на 11,5 % типами обличчя; величини ділянки SPA у представників без урахування типу обличчя на 17,2 %, з дуже широким - на 24,4 %, з широким - на 13,4 % і з вузьким - на 32,2 % типами обличчя. При аналізі величини телерентгенометричних параметрів м'якого піднебіння в юнаків між різними типами обличчя встановлено достовірно більші або тенденції до більших значень у представників із вузьким обличчям величини відстані SPT і ділянки SPA, ніж в юнаків із дуже широким (відповідно на 8,9 % і на 13,0 %) і середнім (відповідно на 13,9 % і на 22,2 %) типами обличчя, а в юнаків без урахування типу обличчя - тенденцію до більших значень величини відстані PM-U, ніж у представників із середнім обличчям (на 4,2 %). У дівчат із вузьким обличчям встановлено лише тенденцію до більших значень величини кута NL/PM-U, ніж у представниць із широким обличчям (на 6,2 %). Результати дослідження є складовим елементом визначення нормативних значень різних параметрів верхніх дихальних шляхів, що дає змогу практичним лікарям більш коректно відрізняти норму від патології.

Ключові слова: *телерентгенографія, цефалометрія, м'яке піднебіння, юнаки, дівчата, типи обличчя, ортогнатичний прикус.*

DOI: 10.31393/morphology-journal-2022-28(4)-07 Reports of Morphology, Vol. 28, №4, Pages 48-53

ISSN 1818-1295 eISSN 2616-6194

REPORTS OF MORPHOLOGY

Official Journal of the Scientific Society of Anatomists, Histologists, Embryologists and Topographic Anatomists of Ukraine

journal homepage: https://morphology-journal.com

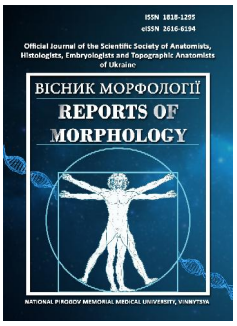

Features of functional changes in blood vessels during the period of early recovery after static physical exercise

Malyuga S. S., Lukyantseva H. V., Bakunovsky O. O.
National University of Ukraine on Physical Education and Sport, Kyiv, Ukraine

ARTICLE INFO
Received: 23 August 2022
Accepted: 28 September 2022

UDC: 612.13:613.73(045)

CORRESPONDING AUTHOR
e-mail: lukjantseva@gmail.com
Lukyantseva H. V.

CONFLICT OF INTEREST
The authors have no conflicts of interest to declare.

FUNDING
Not applicable.

The cardiovascular system is one of the leading functional systems of the body, which ensure and maintain the proper level of physical performance of the body during physical exertion. Bodybuilding is one of the areas of sports activity in which taking into account the individual characteristics of the adaptation of the circulatory system to powerful muscle work of significant intensity is decisive for building an optimal training regimen. Anatomical and physiological remodeling of the heart as a result of regular sports leads to changes in the pumping function of the myocardium, as well as indicators of central and peripheral hemodynamics. Currently, there is a problem of insufficient study of the functional changes of blood vessels in response to a static regime of physical exertion in the early post-workout period. The purpose of the research is to study the characteristics of the reaction of blood vessels during the early recovery period after dosed physical exertion of a static nature. During the study, 34 young men were examined in the following groups: 1 group - persons engaged in bodybuilding; 2 group - young men engaged in fitness; 3 group - untrained persons. Maximum arbitrary static force was determined in all examined persons using a static dynamometer DS-500, static load was modeled by holding on a static dynamometer for 30 seconds an effort corresponding to 50 % of the maximum static force. Functional changes of blood vessels and central hemodynamics were registered by the method of tetrapolar thoracic impedance rheoplethysmography using the computerized diagnostic complex "Cardio+" (Ukraine). Statistical data processing was carried out using the computer program IBM SPSS Statistics (version 26), using non-parametric methods of evaluating the obtained results. It was established that static exercise in young bodybuilders leads to an increase in minute blood volume due to optimal physiological changes in central hemodynamic parameters. In persons engaged in fitness and in untrained young men, the minute volume of blood decreases and circulation conditions deteriorate immediately after exercise, which complicates the processes of rapid recovery after physical exercise in a static mode. A decrease in vascular resistance to blood flow with a simultaneous increase in minute blood volume was revealed immediately after static exercise in young bodybuilders compared to individuals engaged in fitness and untrained individuals. It was established that the circulatory system of young bodybuilders is most optimally adapted to static loads compared to persons engaged in fitness and untrained young men.
Keywords: *blood vessels, central hemodynamics, static load.*

Introduction

The cardiovascular system (CVS) is one of the most important functional systems of the body, which determine and limit the physical performance of an athlete's body [9, 10, 27]. Adaptation of the components of the circulatory system to different modes of physical exertion is one of the central issues of biological and sports science due to the fact that the reduced adaptive capabilities of the specified system limit the realization of the functional reserves of the athlete's body during various types of physical exertion [19, 22, 28]. Bodybuilding, as one of the directions of health-improving motor activity, is characterized by a significant intensity and volume of training loads [11, 26]. Without proper consideration of the individual characteristics of the adaptation of the circulatory system to powerful muscle work, this can lead to pre-pathological, and sometimes even to pathological changes in the activity of the heart and

blood vessels [18, 24], which, with suboptimal physical exertion, can lead to deaths during sports [6, 20].

Regular physical exertion during bodybuilding classes leads to the occurrence of specific changes in the circulatory system. Morphological and functional remodeling of the sports heart is accompanied by changes in the pumping capacity of the myocardium, as well as indicators of central and peripheral hemodynamics [8, 15, 25]. Bodybuilding as a sport with a highly static component of muscle exercises is characterized by an insufficient study of the problems of functional changes in blood vessels in response to a static mode of physical exertion and actualizes the appearance of detailed studies of the impact of loads on the indicators of the circulatory system.

The purpose of our study was to study the characteristics of the reaction of blood vessels during the early recovery period after dosed physical exertion of a static nature.

Materials and methods

The work is a fragment of the research work of the department of medical and biological disciplines of the National University of Physical Education and Sports of Ukraine "The influence of exogenous and endogenous factors on the course of adaptive reactions of the body to physical exertion of various intensities" (state registration number 012U108187). Practically healthy young men (21 years old) without bad habits took part in the study. Examination of young men was carried out in the morning, after at least 15 minutes of passive rest after arriving at the laboratory. The research was conducted in two stages. At the first stage, in order to determine the type of reaction of the circulatory system to physical exertion, representatives of all groups were subjected to a modified Martine functional test (a test with 20 squats for 30 seconds). Only persons with a normotonic type of response of the circulatory system to stress were admitted to further research. In total, 34 such persons took part in the study, who were divided into 3 groups: 1 group - persons engaged in bodybuilding; 2 group - young men engaged in fitness; 3 group - untrained persons.

The Bioethics Committee of the National University of Physical Education and Sports of Ukraine (protocol No. 2 dated 16.12.2020) established that the research does not contradict the basic bioethical standards of the Helsinki Declaration, the Council of Europe Convention on Human Rights and Biomedicine (1977), relevant WHO resolutions and laws of Ukraine.

At the second stage of the study, the reaction of the circulatory system to the dosed static load (SL) was determined. The maximum voluntary static force was determined in all persons involved in the examination using a static dynamometer DS-500. Static load was modeled by holding on a static dynamometer for 30 seconds a force corresponding to 50% of the maximum static force. Functional changes of blood vessels and central hemodynamics were registered by the method of tetrapolar thoracic impedance rheoplethysmography using the computerized diagnostic complex "Cardio+" (Ukraine). The following indicators of hemodynamics were evaluated - minute blood volume (MBV), specific peripheral resistance (SPR), total peripheral resistance (TPR), dicrotic index (DicIn), diastolic index (DiaIn), tone of all arteries (TAA), tone of large arteries caliber (TLAC), tone of medium and small caliber arteries (TMSAC). The indicated indicators were recorded before the load, immediately after the load, as well as 1, 2 and 3 minutes after the load.

Statistical data processing was carried out using the computer program IBM SPSS Statistics (version 26), using non-parametric methods of evaluating the obtained research results.

Results

Table 1 presents the dynamics of the reaction of the blood vessels of the examined persons to a static load and in the early period of recovery after it.

In the initial state, young men engaged in bodybuilding differ from representatives of groups 2 and 3 in significantly lower parameters of SPR and TPR, DisIn and DiaIn, as well as reduced tone of arterial vessels of all calibers ($p<0.05$). The MBV parameter in bodybuilders at rest significantly exceeds the value of the similar indicator in young men engaged in fitness by 13.6%, and by 24.8% the similar parameter in untrained individuals (all with $p<0.05$).

Untrained individuals, on the contrary, are characterized by the largest values of all the hemodynamic parameters we studied, except for the MBV parameter, which is the smallest compared to the values of the other groups. Indicators of functioning of blood vessels of young men engaged in fitness in the initial state are characterized by intermediate values compared to individuals from groups 1 and 3.

After static loading, there is a significant increase in MBV in young bodybuilders both immediately after SL (by 6.9%, $p<0.05$) and 1 minute after it (by 30.2%, $p<0.05$). In contrast to them, the determined indicator of representatives of groups 2 and 3 immediately after SL decreases by 24.5% and 13.1%, respectively ($p<0.05$). However, 1 min after exercise, a significant increase in minute blood volume was observed by 22.9% (group 2, $p<0.05$) and 22.1% (group 3, $p<0.05$). Further observation periods (2 and 3 min after SL) were characterized by a gradual return of the MBV value to the initial state.

Immediately after SL, representatives of all groups observed an increase in SPR, the least expressed in bodybuilders (by 1.5%) compared to individuals engaged in fitness, in which the degree of increase in SPR was 33.6% ($p<0.05$). An increase in the specified parameter by 30.5% ($p<0.05$) was registered in untrained young men. However, already 1 min after the static load, the SPR parameter significantly and reliably decreases in all examined persons - by 21.6% (group 1), 7.9% (group 2), 6.1% (group 3) compared to the initial state. After 2 and 3 min after SL, the SPR index gradually returned to initial values in all examined

Table 1. Changes in indicators of the functioning of blood vessels during the period of early recovery after static exercise.

Parameter	Group	Before SL	Immediately after SL	1 minute after SL	2 minutes after SL	3 minutes after SL
MBV	1	6.484±0.391	6.930±0.340*	8.435±0.380*	7.470±0.340*	6.536±0.390
	2	5.604±0.680^	4.757±0.472^*	6.883±0.710^*	6.330±0.463^*	5.825±0.494^
	3	4.874±0.364^#	4.232±0.270^#*	5.948±0.341^#*	5.476±0.352^#*	5.038±0.330^#
SPR	1	27.69±3.65	28.09±3.22	21.68±2.54*	24.16±2.85*	27.46±3.38
	2	31.39±2.38^	42.30±4.18^*	28.18±3.57^*	29.14±2.63	30.39±2.13^
	3	37.21±6.48^#	50.78±7.31^#*	34.42±5.23^#*	35.53±5.92	36.77±6.12^#
TPR	1	1128±89	1146±76	884.4±51.9*	984.3±52.8*	1119±78
	2	1312±46^	1769±87^*	1175±71^*	1218±43^*	1272±38^
	3	1475±176^#	2034±124^#*	1378±129^#*	1420±114^#	1470±134^#
DicIn	1	48.23±1.85	42.14±1.65*	44.26±1.75*	46.24±1.75	48.10±1.80
	2	55.52±1.79^	69.22±2.09^*	50.72±1.93^*	52.91±2.03^*	55.24±1.97^
	3	60.83±1.89^#	72.38±1.89^#*	55.75±2.03^#*	57.76±1.98^#*	60.03±1.78^#
DiaIn	1	50.61±1.27	45.59±1.41*	47.12±1.41*	48.82±1.51*	50.44±1.23
	2	55.02±2.02^	61.19±1.82^*	58.83±1.62^*	57.23±1.59	55.73±1.84^
	3	60.44±1.74^#	66.71±1.82^#*	64.81±1.35#*	62.84±1.25^#	61.41±1.43^#
TAA	1	19.67±0.35	21.08±0.73*	18.81±0.35*	19.25±0.25	19.64±0.37
	2	22.32±1.60^	27.10±1.18^*	19.51±1.94^*	20.78±1.97^*	21.98±1.67^
	3	27.05±2.76^#	30.43±3.04^#*	25.27±3.17^#	26.12±2.31^#	26.98±2.59^#
TLAC	1	6.868±0.179	7.548±0.278*	7.335±0.216*	7.127±0.176	6.918±0.181
	2	8.123±0.319^	9.457±0.241^*	9.172±0.295^*	8.776±0.278^*	8.364±0.408^
	3	10.36±0.48^#	11.60±0.39^#*	11.31±0.29^#	10.99±0.39^#	10.62±0.52^#
TMSAC	1	11.83±0.48	11.24±0.46*	11.50±0.49	11.63±0.48	11.77±0.48
	2	14.07±0.96^	17.24±0.86^*	12.30±0.34^*	13.15±0.31	13.81±0.92^
	3	16.64±0.78^#	19.39±0.93^#*	15.02±0.48^#*	15.70±0.69^#	16.08±0.80^#

Notes: here and hereafter, * - p<0,05 compared to the value before the static load of its own group; ^ - p<0,05 compared to the similar indicator of 1st group; # - p<0,05 compared to the similar indicator of the 2nd group.

young men. A similar trend characterizes the parameter of total peripheral resistance, which also increased immediately after SL in different ways - it almost did not change in bodybuilders (the degree of unreliable growth was 1.7%), it increased most significantly in people of group 2 (by 34.8%, p<0.05) and untrained young men (by 30.3%, p<0.05). After the specified initial increase, a decrease in TPR was observed in all examined persons - by 21.6% in group 1, by 10.5% in group 2, by 6.3% in group 3 (all with p<0.05).

Changes in DicIn have a slightly different character between the representatives of group 1 and the other examinees - in bodybuilders it decreases by 12.7% immediately after SL with a gradual return to initial values 3 min after exercise. In contrast, in representatives of groups 2 and 3, DisIn increased sharply immediately after SL - by 24.7% (group 2, p<0.05) and by 19.1% (group 3, p<0.05). In the subsequent periods of observation, DisIn in these individuals gradually decreased to baseline values.

A similar trend characterizes the dynamics of the DiaIn parameter. In the group of bodybuilders, after an initial decrease of 9.3% (p<0.05) immediately after SL, a gradual return of DiaIn to baseline values is observed. An increase in the specified parameter by 11.3% and 10.4%, respectively (all with p<0.05), was registered in persons engaged in fitness and untrained young men, with a further return to normal 3 min after SL.

The tone of all arterial vessels immediately after exercise in all examined persons changes in the same direction - immediately after SL it increases to a different extent depending on the group, then decreases to the initial values. Thus, the specified parameter increases by 7.1% in people of group 1, by 21.5% in group 2, and by 12.2% in group 3 (all with p<0.05). The tone of large-caliber arteries also shows a similar trend of changes - immediately after SL it increases to varying degrees (by 9.9% in individuals of group 1, by 16.4% in young men of group 2, by 12.0% in individuals of group 3, all - p<0.05).

Some distinctive features distinguish the dynamics of the tone of the arteries of small and medium caliber, which

in the group of bodybuilders immediately after SL decreases by 5.0%, then gradually returns to the initial value. In contrast, in individuals of groups 2 and 3, there is a significant increase in the tone of small and medium-sized arteries (by 21.9% and 16.5%, respectively, $p<0.05$), which already 1 minute after SL is replaced by a similar sharp decrease in tone (by 12.8 % in the 2nd group and by 9.6% in the 3rd group, $p<0.05$). In the subsequent periods of observation, the return of the tone to the initial values was registered.

Discussion

In the initial state, representatives of group 1 are characterized by lower values of SPR and TPR, which indicates a reduced tone of pre- and postcapillary resistance vessels in bodybuilders compared to untrained individuals and young people engaged in fitness. This is confirmed by lower values of the dicrotic index, which characterizes the tone of the vessels of the precapillary bed, as well as the diastolic index, which depends on the tone of the postcapillary vessels, compared to groups 2 and 3. It should be noted that before exercise, the tone of small, medium and large arterial vessels in bodybuilders is also statistically significantly lower compared to untrained young men and those engaged in fitness. All of the above indicates that the blood vessels of bodybuilders at rest are characterized by a lower tone of the smooth muscles of the walls of blood vessels, which makes the latter more expanded compared to individuals of groups 2 and 3. Perhaps this phenomenon ensures the creation of the most optimal conditions for more intensive blood flow during active muscle work [4]. Most likely, this is a consequence of reduced sympathetic nervous influences that provide basal vascular tone [7, 12], and can also be explained by the systematic powerful release of vasodilator metabolites from the hypertrophied skeletal muscles of bodybuilders during regular strength training.

It is also worth noting that untrained young men are characterized by the highest values of all analyzed parameters (except MBV), which gives grounds for asserting that the tone of their blood vessels is formed due to stronger, compared to group 1, sympathetic influences [23]. In persons engaged in fitness, central hemodynamic indicators differ by intermediate values compared to representatives of groups 1 and 3, which may be a consequence of the balance between sympathetic influences and the action of biologically active substances-vasodilators, which are metabolites of skeletal muscles.

Immediately after a static load, a significant decrease in MBV is observed in individuals of groups 2 and 3, which can be explained by the effect of straining when performing a static effort, as well as by squeezing the walls of blood vessels with a simultaneous decrease in the venous return of blood to the heart. Accordingly, thanks to the myogenic and nervous mechanisms of heart regulation, cardiac output will be reduced, which leads to a decrease in MBV [2, 21]. In young bodybuilders, on the contrary, there is an increase in MBV even in the conditions of a powerful static effort, which was mainly provided by an increase in the force of contractions of the left ventricle and a corresponding increase in stroke volume [1, 16].

The growth of MBV in young bodybuilders is a physiologically appropriate reaction of the cardiovascular system to static physical exertion, this phenomenon is a manifestation of a high degree of functional reserves of the heart. These reserves are caused by an increase in the force of heart contractions (due to physiological hypertrophy of the myocardium of the left ventricle with a sufficient degree of capillarization) and physiological dilatation of the chambers of the heart, in particular, the left ventricle, which provides the necessary end-diastolic volume [13, 29].

Immediately after a static load, an increase in SPR and TPR parameters, as well as the tone of large-caliber arteries, was registered in all the examined persons. Thus, there is a narrowing of main large arteries, as well as pre- and post-capillary resistance vessels (mainly arterioles and venules), which is a consequence of the vasoconstrictor effect of hormones and mediators of the sympatho-adrenal system [3]. This is most significant in the fitness group and the least in bodybuilders, which is evidence that it is the young men who are engaged in bodybuilding who are the most adapted to static loads, in contrast to persons who are engaged in fitness and show the least degree of training of the circulatory system to physical exercises of a static nature.

It is worth noting that TPR reflects not only the state of the tone of the resistive vessels, but also the volume of blood entering them. If at the same time there is an increase in MBV against the background of a slight increase in mean dynamic pressure, as in the representatives of the group of bodybuilders, it can be assumed that the resistance of arterioles and venules is not high. However, this is not evidence of a change in the lumen of resistive vessels. Perhaps this is a consequence of the growth of the volumetric velocity of expulsion and the increase in the power of the left ventricle, which we observe in individuals of group 1. That is, it is a physiological mechanism of maintaining optimal conditions for the exchange of water and nutrients between blood plasma and tissue fluid.

Already 1 min after SL, all examined young men observed a decrease in the SPR, TPR, and tone of large-caliber arteries, which is evidence of the fact that the initial narrowing of the main arteries, arterioles, and venules is replaced by their significant expansion. This phenomenon can be explained by the leveling of the effect of catecholamines under the action of the powerful release of metabolites-vasodilators from skeletal muscles, a greater proportion of beta- than alpha-adrenoceptors in the cell membranes of myocytes of blood vessels of skeletal muscles and a local increase in temperature in actively working skeletal muscles [5, 9]. This is most pronounced in bodybuilders, who have the most developed and hypertrophied muscles, compared to untrained young men and those who engage in fitness.

DisIn and DiaIn parameters are characterized by quite interesting dynamics - in individuals of group 1, they decrease

immediately after SL, in contrast to the values of similar parameters in individuals of groups 2 and 3, in which a rather significant increase was registered. The marked initial decrease in DisIn and DiaIn, which reflect the tone of arterioles and venous outflow, respectively, can be explained by the features of better adaptation of bodybuilders to SL, associated with the functioning of arterio-venous shunts in actively working skeletal muscles [14, 17]. The consequence of this will be a redistribution of the volume of circulating blood with an increase in the volume of blood in the collateral vessels, which will provide blood flow in the "bypass" of the compressed vessels.

In general, the most pronounced change in hemodynamic indicators in untrained individuals and young people engaged in fitness is a manifestation of the Lingard phenomenon and demonstrates a powerful postoperative increase in the functioning of the components of the circulatory system. It is due to the effect of straining during static effort, powerful squeezing of blood vessels and a decrease in the venous return of blood to the heart under the specified conditions. In contrast, body builders do not have a decrease in venous return due to a well-developed system of arterio-venular shunts. Against the background of the hypertrophied myocardium of the left ventricle and better adaptation to static efforts, this makes it possible for the circulatory system of bodybuilders not only not to decrease, but even to ensure the growth of such an integral parameter as minute blood volume. Thus, in young men who are engaged in bodybuilding, there is a decrease in the manifestation of the Lingard phenomenon.

Conclusions

1. In response to a static load, bodybuilding individuals experience an increase in minute blood volume and the most optimal physiological change in the hemodynamic parameters that provide it. In contrast to them, in young people engaged in fitness and in untrained individuals, the minute blood volume decreases and the conditions of central hemodynamics deteriorate immediately after exercise, which complicates the processes of rapid recovery after physical exercise in a static mode.

2. A decrease in vascular resistance to blood flow with a simultaneous increase in minute blood volume provides a better state of perfusion of the capillary bed of working skeletal muscles immediately after static exercise in young bodybuilders compared to young men engaged in fitness and untrained individuals.

3. The circulatory system of young bodybuilders is most optimally adapted to static loads compared to young men engaged in fitness and untrained individuals.

References

[1] Bakunovsky, O. M., Lukyantseva, H. V., & Kotlyarenko, L. T. (2021). Different features of changes in central hemodynamics during early recovery after different exercise regimes. *Фізіологічний журнал - Physiological Journal*, 67(6), 13-20. doi: 10.15407/fz67.06.013

[2] Beaumont, A., Grace, F., Richards, J., Hough, J., Oxborough, D., & Sculthorpe, N. (2017). Left ventricular speckle tracking-derived cardiac strain and cardiac twist mechanics in athletes: a systematic review and meta-analysis of controlled studies. *Sports Medicine,* 47(6), 1145-1170. doi: 10.1007/s40279-016-0644-4

[3] Chen, H., Chen, C., Spanos, M., Li, G., Lu, R., Bei, Y., & Xiao, J. (2022). Exercise training maintains cardiovascular health: signaling pathways involved and potential therapeutics. *Signal Transduction and Targeted Therapy,* 7(1), 1-18. doi: 10.1038/s41392-022-01153-1

[4] D'Andrea, A., Formisano, T., Riegler, L., Scarafile, R., America, R., Martone, F., ... Calabro, R. (2017). *Acute and chronic response to exercise in athletes: the "supernormal heart".* In Exercise for Cardiovascular Disease Prevention and Treatment (pp. 21-41). Springer, Singapore. doi: 10.1007/978-981-10-4307-9_2

[5] DeLorey, D. S., & Clifford, P. S. (2022). Does sympathetic vasoconstriction contribute to metabolism: Perfusion matching in exercising skeletal muscle? *Frontiers in Physiology,* 1873. doi: 10.3389/fphys.2022.980524

[6] Doleeb, S., Kratz, A., Salter, M., & Thohan, V. (2019). Strong muscles, weak heart: testosterone-induced cardiomyopathy. *ESC Heart Failure,* 6(5), 1000-1004. doi: 10.1002/ehf2.12494

[7] Ehlers, T. S., Sverrisdottir, Y., Bangsbo, J., & Gunnarsson, T. P. (2020). High-intensity interval training decreases muscle sympathetic nerve activity in men with essential hypertension and in normotensive controls. *Frontiers in Neuroscience,* 14, 841. doi: 10.3389/fnins.2020.00841

[8] Fagerberg, P. (2018). Negative consequences of low energy availability in natural male bodybuilding: A review. International *Journal of Sport Nutrition and Exercise Metabolism,* 28(4), 385-402. doi: 10.1123/ijsnem.2016-0332

[9] Flück, M., Kramer, M., Fitze, D. P., Kasper, S., Franchi, M. V., & Valdivieso, P. (2019). Cellular Aspects of Muscle Specialization Demonstrate Genotype-Phenotype Interaction Effects in Athletes. *Frontiers in Physiology,* 8(10), 526. doi: 10.3389/fphys.2019.00526

[10] Franchi, M. V., Reeves, N. D., & Narici, M. V. (2017). Skeletal muscle remodeling in response to eccentric vs. concentric loading: morphological, molecular, and metabolic adaptations. *Frontiers in Physiology,* 4(8), 447. doi: 10.3389/fphys.2017.00447

[11] Howe, L. P., Read, P., & Waldron, M. (2017). Muscle hypertrophy: A narrative review on training principles for increasing muscle mass. *Strength & Conditioning Journal*, 39(5), 72-81. doi: 10.1519/SSC.0000000000000330

[12] Katayama, K., & Saito, M. (2019). Muscle sympathetic nerve activity during exercise. *The Journal of Physiological Sciences,* 69(4), 589-598. doi: 10.1007/s12576-019-00669-6.

[13] Koshy, S. K., George, K. K., & George, L. K. (2018). Changes in right ventricular morphology and function in athletes. *Echocardiography* (Mount Kisco, NY), 35(6), 767-768. doi: 10.1111/echo.14027

[14] Korytko, Z., Kulitka, E., Bas, O., Chornenka, H., Zahidnyy, V., & Yakubovskyi, T. (2020). Adequacy criteria of physical loadings and their use in sports, physical education, and physical rehabilitation. *Physical Education, Sport and Health Culture in Modern Society,* 2(50), 68-77. doi: 10.29038/2220-7481-2020-02-68-77

[15] Lavin, K. M., Coen, P. M., Baptista, L. C., Bell, M. B., Drummer, D., Harper, S. A., ... & Buford, T. W. (2022). State of Knowledge on

Molecular Adaptations to Exercise in Humans: Historical Perspectives and Future Directions. *Comprehensive Physiology,* 12(2), 3193-3279. doi: 10.1002/cphy.c200033

[16] Lukyantseva, H. V., Bakunovsky, O. M., Malyuga, S. S., Oliinyk, T. M., Manchenko, N. R., Manchenko, Y. R., & Korolyova, D. O. (2021). Comparative characteristics of changes in central hemodynamics during early recovery after different exercise regimes. *Reports of Morphology,* 27(2), 47-52. doi: 10.31393/morphology-journal-2021-27(2)-07

[17] Maden-Wilkinson, T. M., Balshaw, T. G., Massey, G. J., & Folland, J. P. (2020). What makes long-term resistance-trained individuals so strong? A comparison of skeletal muscle morphology, architecture, and joint mechanics. *Journal of Applied Physiology,* 128(4), 1000-1011. doi: 10.1152/japplphysiol.00224.2019

[18] Marrakchi, S., Kammoun, I., Bennour, E., Laroussi, L., Ben Miled, M., & Kachboura, S. (2020). Inherited primary arrhythmia disorders: cardiac channelopathies and sports activity. *Herz,* 45(2), 142-157. doi: 10.1007/s00059-018-4706-2

[19] Martino, F., Perestrelo, A. R., Vinarsky V., Pagliari, S., & Forte, G. (2018). Cellular mechanotransduction: from tension to function. *Frontiers in Physiology,* 5(9), 824. doi: 10.3389/fphys.2018.00824

[20] Mont, L., Pelliccia, A., Sharma, S., Biffi, A., Borjesson, M., Terradellas, J. B., ... & Corrado, D. (2017). Pre-participation cardiovascular evaluation for athletic participants to prevent sudden death: Position paper from the EHRA and the EACPR, branches of the ESC. Endorsed by APHRS, HRS, and SOLAECE. *Ep. Europace,* 19(1), 139-163. doi: 10.1093/europace/euw243

[21] Moore, J. P., Simpson, L. L., & Drinkhill, M. J. (2022). Differential contributions of cardiac, coronary and pulmonary artery vagal mechanoreceptors to reflex control of the circulation. *The Journal of physiology,* 600(18), 4069-4087. doi: 10.1113/JP282305

[22] Mueller, P. J., Clifford, P. S., Crandall, C. G., Smith, S. A., & Fadel, P. J. (2011). Integration of central and peripheral regulation of the circulation during exercise: acute and chronic adaptations. *Comprehensive Physiology,* 8(1), 103-151. doi: 10.1002/cphy.c160040

[23] Notarius, C. F., Millar, P. J., & Floras, J. S. (2015). Muscle sympathetic activity in resting and exercising humans with and without heart failure. *Applied Physiology, Nutrition, and Metabolism,* 40(11), 1107-1115. doi: 10.1139/apnm-2015-0289

[24] Pelliccia, A., Sharma, S., Gati, S., Back, M., Borjesson, M., Caselli, S., & Collet, J-P. (2021). Corrigendum to: 2020 ESC Guidelines on Sports Cardiology and Exercise in Patients with Cardiovascular Disease. *European Heart Journal,* 42(5), 548-549. doi: 10.1093/eurheartj/ehaa605

[25] Prieto-Gonz?lez, P., & Sedlacek, J. (2022). Effects of Running-Specific Strength Training, Endurance Training, and Concurrent Training on Recreational Endurance Athletes' Performance and Selected Anthropometric Parameters. *International Journal of Environmental Research and Public Health,* 19(17), 10773. doi: 10.3390/ijerph191710773

[26] Rossow, L. M., Fukuda, D. H., Fahs, C. A., Loenneke, J. P., & Stout, J. R. (2013). Natural bodybuilding competition preparation and recovery: a 12-month case study. *International Journal of Sports Physiology & Performance,* 8(5), 582-592. doi: 10.1123/ijspp.8.5.582

[27] Schoenfeld, B., & Grgic, J. (2018). Evidence-based guidelines for resistance training volume to maximize muscle hypertrophy. *Strength & Conditioning Journal,* 40(4), 107-112. doi: 10.1519/SSC.0000000000000363

[28] Smith, D. L., & Fernhall, B. (2022). Advanced cardiovascular exercise physiology. Human Kinetics.

[29] Schuttler, D., Clauss, S., Weckbach, L. T., & Brunner, S. (2019). Molecular mechanisms of cardiac remodeling and regeneration in physical exercise. *Cells,* 8(10), 11-28. doi: 10.3390/cells8101128

ОСОБЛИВОСТІ ФУНКЦІОНАЛЬНИХ ЗМІН КРОВОНОСНИХ СУДИН В ПЕРІОД РАННЬОГО ВІДНОВЛЕННЯ ПІСЛЯ СТАТИЧНОГО ФІЗИЧНОГО НАВАНТАЖЕННЯ

Малюга С. С., Лук'янцева Г. В., Бакуновський О. О.

Серцево-судинна система є однією з провідних функціональних систем організму, які забезпечують та підтримують належний рівень фізичної працездатності організму при фізичних навантаженнях. Бодібілдинг є одним з напрямів спортивної діяльності, в якому урахування індивідуальних особливостей адаптації системи кровообігу до потужної м'язової роботи значної інтенсивності є визначальним для побудування оптимального тренувального режиму. Анатомо-фізіологічне ремоделювання серця внаслідок регулярних занять спортом призводить до змін насосної функції міокарда, а також показників центральної та периферичної гемодинаміки. Наразі існує проблематика недостатньої вивченості функціональних змін кровоносних судин у відповідь на статичний режим фізичного навантаження в ранньому післяробочому періоді. Мета дослідження - вивчення особливостей реакції кровоносних судин у період раннього відновлення після дозованих фізичних навантажень статичного характеру. Під час дослідження було обстежено 34 юнаків у наступних групах: 1 група - особи, які займаються бодібілдингом; 2 група - юнаки, які займаються фітнесом; 3 група - нетреновані особи. У всіх обстежених осіб за допомогою станового динамометра ДС-500 визначали максимальну довільну станову силу, статичне навантаження моделювали шляхом утримання на становому динамометрі протягом 30 секунд зусилля, яке відповідало 50 % від максимальної станової сили. Функціональні зміни кровоносних судин та центральної гемодинаміки реєстрували методом тетраполярної грудної імпедансної реоплетизмографії за допомогою комп'ютеризованого діагностичного комплексу "Кардіо+" (Україна). Статистичну обробку даних проведено за допомогою комп'ютерної програми IBM SPSS Statistics (версія 26), із використанням непараметричних методів оцінки отриманих результатів. Встановлено, що статичне навантаження у юнаків-бодібілдерів призводить до збільшення хвилинного об'єму крові за рахунок оптимальних фізіологічних змін параметрів центральної гемодинаміки. У осіб, які займаються фітнесом та у нетренованих юнаків, відбувається зменшення хвилинного об'єму крові та погіршення умов циркуляції одразу після навантаження, що ускладнює процеси швидкого відновлення після фізичного навантаження у статичному режимі. Виявлено зменшення опору судин току крові з одночасним зростанням хвилинного об'єму крові одразу після статичного навантаження у юнаків-бодібілдерів порівняно з особами, які займаються фітнесом та нетренованими особами. Встановлено, що система кровообігу юнаків-бодібілдерів найбільш оптимальним чином адаптована до статичних навантажень порівняно з особами, які займаються фітнесом та нетренованими юнаками.

Ключові слова: *кровоносні судини, центральна гемодинаміка, статичне навантаження.*

DOI: 10.31393/morphology-journal-2022-28(4)-08 Reports of Morphology, Vol. 28, №4, Pages 54-63

ISSN 1818-1295 eISSN 2616-6194

REPORTS OF MORPHOLOGY

Official Journal of the Scientific Society of Anatomists, Histologists, Embryologists and Topographic Anatomists of Ukraine

journal homepage: https://morphology-journal.com

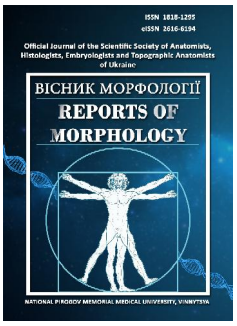

Morphological changes of sexually mature rat's pineal gland and cerebellar cortex under long-term exposure to heavy metal salts

Hryntsova N. B.[1], Romaniuk A. M.[2], Kiptenko L. I.[1], Sulym L. G.[1]

[1]Department of Morphology, Medical Institute, Sumy State University, Sumy, Ukraine
[2]Department of Pathological Anatomy, Medical Institute, Sumy State University, Sumy, Ukraine

ARTICLE INFO
Received: 29 August 2022
Accepted: 3 October 2022

UDC: 611.42+611.018.83]:616-092.9:613.63

CORRESPONDING AUTHOR
e-mail: natalia.gryntsova@gmail.com
Hryntsova N. B.

CONFLICT OF INTEREST
The authors have no conflicts of interest to declare.

FUNDING
This study was supported by the scholarship of the Slovak Republic Government (2020), the research project "Modern views on the morphogenesis of general pathological processes", state registration No. 0119U100887 (2019-2024).

Pollution with heavy metal salts is an important environmental problem today, having an adverse effect on public health. The endocrine system maintains homeostasis in the body. The purpose of the work is to study the morphological changes of the cerebellar cortex and epiphyses of sexually mature male rats under the condition of long-term exposure to the body of a complex of heavy metal salts. The morphological changes in the cerebellar cortex and epiphysis of sexually mature male rats under the condition of long-term exposure to heavy metal salts was studied. Animals of the experimental group were simulated microelementosis by adding to drinking water a mixture of heavy metal salts for 60 days: zinc ($ZnSO_4x7H_2O$) - 5 mg/l, copper ($CuSO_4x5H_2O$) - 1 mg/l, iron ($FeSO_4$) - 10 mg/l, manganese ($MnSO_4x5H_2O$) - 0.1 mg/l, lead ($Pb(NO_3)_2$) - 0.1 mg/l and chromium ($K_2Cr_2O_7$) - 0.1 mg/l. Morphological, morphometric and statistical research methods were used. Long-term (60-days) intake of heavy metal salts mixture in the body of experimental animals leads to the development of the general adaptation syndrome, the stage of chronic stress "subcompensation" in the pineal gland. Morphological changes in the organs had a nonspecific polymorphic character, such as a sharp violation of hemodynamics, a violation of the morphology of the vascular wall, the state of pinealocytes and Purkinje cells, the development of tissue hypoxia, processes of apoptosis and reactive astrogliosis as a response to the action of a damaging agent. The pineal gland of the experimental animals showed signs of indole production, but the evacuation of hormones (including melatonin) into the vascular bed was hampered due to the violation of the morphology of the vascular wall and the cell membrane of pinealocytes. This led to a deficiency of this hormone in the body of the experimental animals, which negatively affected the adaptive processes in the cerebellar cortex in response to the action of the stress agent. Compensatory and adaptive processes in the pineal gland and cerebellar cortex had signs of functional stress. Adaptive processes were observed both in a small number of pinealocytes and in Purkinje cells, as well as an active adaptive glial reaction in both organs.

Keywords: *pineal gland, heavy metals, cerebellar cortex, reactive astrogliosis.*

Introduction

Pollution by salts of heavy metals is an important environmental problem today, which negatively affects the health of the population. Such a negative impact determines the development of various pathologies, disruption of the body's homeostasis and morphological transformations in various tissues [24, 25], since each trace element is potentially toxic in case of excessive exposure [5]. Various human diseases and toxicity are often associated with oxidative stress [5].

To date, the human pineal gland is the least studied endocrine gland, which occupies one of the central places in the endocrine regulation of the vital activity of all organs and systems, carries out adaptive reactions of the body to the changing conditions of the external environment. It is known that the hormone melatonin (indole metabolite of the amino acid tryptophan, which is mainly produced by the pineal gland) is the strongest natural inhibitor of free radical processes in the body [5, 23].

Melatonin is a neuropeptide that is synthesized by the pineal gland and with the help of which the pineal gland participates in the organization and regulation of cyclic processes [19]. It is believed that the pineal gland secretes

the hormone in the form of two separate portions: one, at a low concentration, enters the blood and connects with peripheral organs, and the other, at a higher concentration, enters the cerebrospinal fluid and binds to brain receptors [29]. The pineal gland, with the help of melatonin, controls the endocrine, nervous and immune systems, integrates the systemic response to adverse factors affecting the body's resistance [9]. At the same time, another property of melatonin was discovered - optimization of brain activity and at the same time counteracting pathological processes that cause its disturbances. Improvement of brain activity under the influence of melatonin is associated with several mechanisms: antioxidant effect, weakening of glutamate neurotoxicity, activation of neuron growth factor and limitation of apoptosis of nerve cells. Melatonin provides protection of brain cells by decomposition of hydrogen peroxide into water and oxygen, by utilization of free hydroxyl radicals, activation of the natural system of antioxidant protection, by activation of superoxide dismutase and catalase [3, 13]. In addition, melatonin neuroprotection is based on the limitation of various forms of neurotoxicity (glutamate, nitric oxide, p-amyloid peptide, metals, etc.), as well as synchronization of biorhythms, changes in endocrine status [4].

Thus, it has been proven that a number of diseases of the nervous system are directly related to melatonin deficiency: Parkinson's disease, Alzheimer's disease. It should also be added that melatonin reduces the neurotoxicity of glutamate in brain tissues, the aggressiveness of nitric oxide, activates neuron growth factors, and at the same time limits the apoptosis of nerve cells [19].

Biological activity of melatonin in most cases is mediated by interaction with specific membrane and nuclear receptors. Membrane melatonin receptors (MT1, MT2) coupled to G proteins have a high affinity for their ligand and are localized in the suprachiasmatic nucleus (SCN) and other nuclei of the hypothalamus, hippocampus, cerebral cortex, and cerebellum [27].

To date, it is known about environmental factors that can cause negative changes in various structures of the cerebellum: bisphenol A (contained in plastic dishes), alcohol, methylazoxymethanol salts, hyperdynamia, hypoxia, hypodynamia, radiation [17], the sweetener aspartame [2, 11], methyl chloride, methyl bromide, thiophene [14, 16]. However, the study of histopathomorphological changes in the cerebellum under the influence of various negative factors showed that the most pronounced changes are observed in Purkinje neurons [12, 26]. Melatonin is also known to prevent radiation-induced reduction in Purkinje cell volume and number [18].

To date, it has been established that a violation of the melatonin-producing function of the pineal gland can be both congenital and acquired during life, as a result of the action of various negative factors of the external and internal environment. The reaction of pinealocytes to a certain influence depends not only on the intensity and duration of its action, but also on the hormonal saturation of the body, against the background of which this influence is carried out [19].

The aim of the work is to study morphological changes in the cerebellar cortex and epiphyses of sexually mature male rats under the condition of long-term exposure to a complex of heavy metal salts.

Materials and methods

Animals

The experiment was performed on 12 white sexually mature male rats weighing 200-250 g, aged 7-8 months, which were divided into 2 groups (the control and the experimental ones). Animals of the both groups were kept in the normal vivarium conditions, where the equal keeping conditions, nutrition, proper care and natural light (day/night) were maintained, with a constant ambient temperature (20-22°C). The animals had free access to drinking water. The study was carried out in the autumn-winter period.

Experimental microelementosis model

The experimental group included of rats, which for 60 days of drinking water mixture with heavy metal salts: zinc ($ZnSO_4x7H_2O$) - 5 mg/l, copper ($CuSO_4x5H_2O$) - 1 mg/l, iron ($FeSO_4$) - 10 mg/l, manganese ($MnSO_4x5H_2O$) - 0.1 mg/l, lead ($Pb(NO_3)_2$) - 0.1 mg/l and chromium ($K_2Cr_2O_7$) - 0.1 mg/l. The selected concentration of salts in the mixture was due to the presence of such concentrations of these salts in the soil and drinking water of Ukraine some regions according to literature sources [24, 25].

Removing animals from the experiment

Groups of experimental animals were removed from the experiment after previous thiopental anesthesia (at the dose of 30-40 mg/10 g body weight) on the 60th day of the experiment, in compliance with national and international standards on bioethics. All animal studies were conducted in accordance with the provisions of the European Convention for the Protection of Vertebrate Animals for Experimental and Scientific Purposes (Strasbourg, 1986) and the "General Ethical Rules for Animal Experiments" approved by the First National Congress of Bioethics (Kyiv, 2001, Ukraine), Protocol No. 4 of 06/03/2020 Commission of Bioethics of Sumy State University. The subject of the study is the pineal gland and cerebellum cortex of experimental and control animals.

Extraction technique and histological studies

To study the morphological changes in the structural components of the pineal gland and cerebellum cortex conventional procedures of microanatomical (histological, histochemical and cytochemical) study method were used. Hematoxylin-eosin staining was used to assess the morphological state of the pineal gland, according to Van Gieson and Einarson. Studies of the cerebellar cortex were performed on histological preparations stained with hematoxylin-eosin and acridine-orange. Assessment of the cerebellum cortex and pineal gland's morphological state was performed by a number of microscopic indices: state

of stromal and parenchymal components, state of the vascular bed, changes in blood rheology, state of pinealocytes, astrocytic glia, Purkinje cells. General morphological and morphometric analysis was performed using the "Leica DM 500" light-optical microscope and with x4, x10, x40 lenses, binoculars 7 and 10; fluorescent microscope "Mikmed-2". Lenses 40, 90, 100; glasses - 7 and 10, immersion medium - non-fluorescent oil. Photo documentation of the results obtained was performed with a digital video camera "Leica DM IC C50 HD Camera". "Leica Application Suite LAS EZ version 20.0 [Build: 292] Copyright @ 2010" software was used.

Statistics

Processing of digital results was performed by applied statistical methods using the Microsoft Word Excell 2010 text editor with AtteStat 12.0.5 application. Reliability of the difference between the experimental and control data of morphometric parameters was assessed using the Student's test, the probability of error less than 5 % ($p<0.05$) was considered sufficient.

Results

After 60 days of the experiment, the epiphysis of the experimental animals had an oval shape, preserved its anatomical integrity and connection with the vascular plexus. Heavy metal salts caused noticeable negative changes in all structural components of the gland: stromal, vascular and parenchymal.

The length of the gland increased by 5.6 % (1.186±0.061 mm; $p>0.05$), the width by 2.7 % (0.838±0.072 mm; $p>0.05$) in comparison with the indicators of control animals.

Long-term administration of heavy metal salts to the body of rats caused vascular congestion. The vessels of the epiphysis, especially the capsule and subcapsular zone were dilated, significantly full of blood, with the initial stages of violation of the rheological properties of blood (stasis and initial stages of blood coagulation). The vascular wall thickened, especially in the large supplying vessels of the subcapsular zone. The lumen area of blood vessels increased by 2.25 times ($p<0.001$) relative to the indicators of control animals (Table 1). Around the vessels of the subcapsular zone, a rather pronounced active glial reaction was observed in the form of reactive astrogliosis, which is an adaptive reaction of neuroglia to the action of heavy metal salts [10]. In addition to the local, a general diffuse glial reaction was also observed (Fig. 1). Vascular engorgement of the gland was accompanied by swelling of the intertrabecular connective tissue component (Fig. 2), capillary engorgement in some areas was accompanied by their spasm in others. The capsule of the gland was significantly thickened (see Fig. 2), its thickness was 2.5 times greater than that of the control animals ($p<0.05$) (see Table 1).

Parenchyma of the pineal gland of the experimental animals was slightly spongy. Moderate disruption of the cytoarchitectonics of cellular trabeculae were observed. The

Table 1. Results of the pineal gland structural components' morphometric study in sexually mature rats under the heavy metal salts impact (X±CD).

Index	Groups of laboratory animals	
	Rats of the control group, n=6	Rats of the experimental group, n=6
Large diameter of pinealocyte nuclei, mm	3.831±0.192	5.182±0.246**
Small diameter of pinealocyte nuclei, mm	2.733±0.441	3.621±0.272
Cross-sectional area of pinealocyte nuclei, mm^2	7.270±1.240	25.18±3.09***
Large diameter of pinealocyte bodies, mm	6.019±0.931	8.817±0.498*
Small diameter of pinealocyte bodies, mm	4.374±0.383	4.613±0.142
Cross-sectional area of pinealocyte bodies, mm	23.04±1.83	51.62±3.05***
Area of the pinealocyte cytoplasm, mm^2	15.77±0.39	26.38±1.63***
Nuclear cytoplasmic ratio	1:0.461±0.224	1:0.142±0.213
Optical density of the nucleus, RU	110.1±1.1	83.17±5.39***
Optical density of cytoplasm, RU	132.6±1.3	85.61±2.86***
Vessels area, mm^2	61.27 ±0.67	137.8±1.6***
Absolute number of pinealocytes	113.7±1.5	71.51±1.83***
Absolute number of astrocytic glia cells	42.25±1.48	92.04±3.29***
Glyocyto-neuronal index	0.374±0.122	1.227±0.579
The average diameter of the caryon	3.228±0.374	4.327±0.711
Capsule thickness, mm	1.537±0.716	3.887±0.561*

Note: reliable compared to the control - * $p<0.05$; ** $p<0.01$; *** $p<0.001$.

nuclei and cytoplasm of pinealocytes underwent morphological changes. Pinealocytes with signs of indoleamine production prevailed on samples stained by Einarson's gallocyanin. Light pinealocytes with lightened, vacuolated cytoplasm and oval, enlarged nuclei were detected only in certain fields of view. The increase in terms of heavy metal salts entering the body of rats caused polymorphic rearrangements of the chromatin of pinealocyte nuclei. Thus, a sufficient number of cells with deformed, irregularly shaped, homogeneous nuclei were visualized in the preparations. However, some cells had hypertrophied nuclei, with lightened chromatin meshwork, chromatin margination, and hypertrophied, hyperchromic nucleolus on the background of lightened karyoplasm. In addition, the preparations contained a sufficient number of cells with fine- and coarse-grained condensation of chromatin, which were diffusely located in the enlightened nucleus in the form of blocks of various sizes.

The general morphometric indicators of the nucleus and cytoplasm of pinealocytes also underwent changes. Linear indicators, as well as the area of nuclei and bodies of

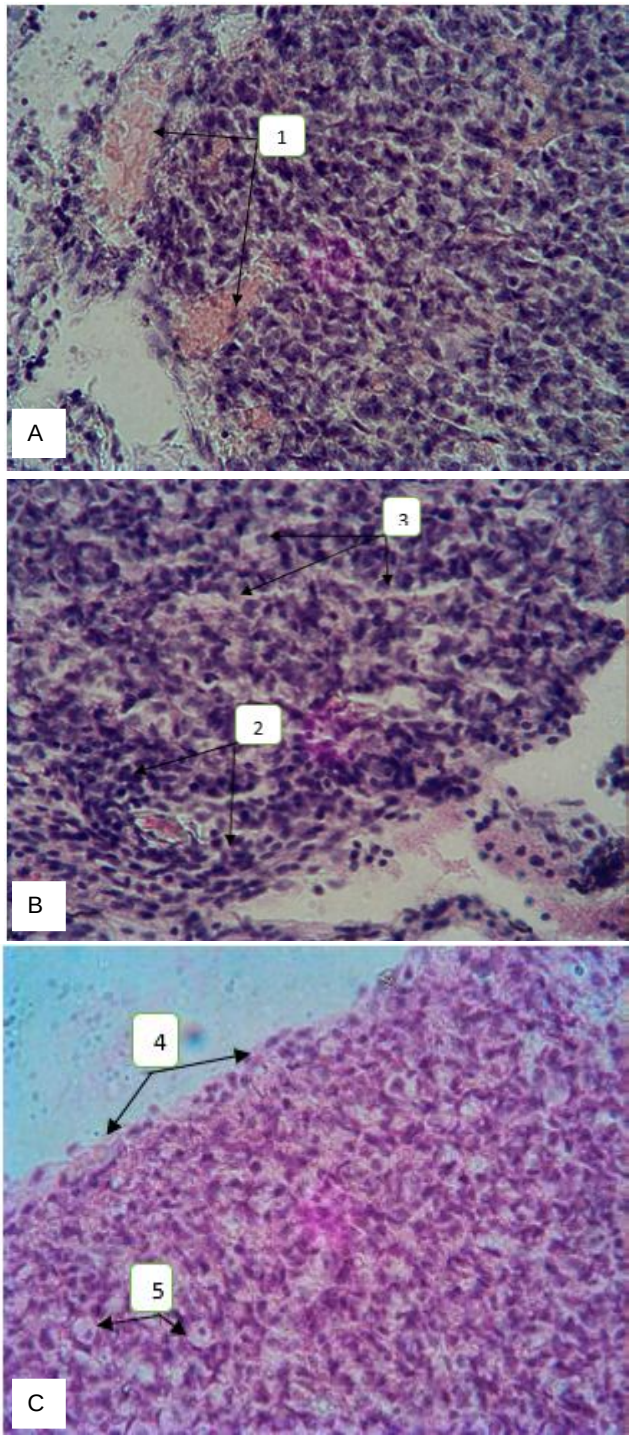

Fig. 1. Morphological rearrangements of the structural components in the pineal gland of experimental (A, B) and control (C) animals under the conditions of 60-day exposure to of heavy metal salts: A: 1 - plethora of the subcapsular zone vessels with signs of the blood rheological properties impairment; B: 2 - reactive astrogliosis; 3 - expansion of intertrabecular spaces; C: 4 - connective tissue capsule; 5 - light pinealocyte. Hematoxylin-eosin staining. x400.

pinealocytes underwent a dynamic increase in comparison with the indicators of control animals. The large and small diameters of pinealocyte nuclei increased, respectively, by 35.2 % ($p<0.01$) and 32.6 % ($p>0.05$), and the large and small diameters of pinealocyte bodies increased, respectively, by 46.5 % ($p<0.05$) and 5.5 % ($p>0.05$) in comparison with indicators of control animals. The cross-sectional area of nuclei, cytoplasm, and bodies of pinealocytes increased, respectively, by 3.5 times ($p<0.001$), 2.2 times ($p<0.001$) and 67.4 % ($p<0.001$) relative to the indicators of control animals. The average diameter of the karyon increased by 34.0 % relative to the control animals ($p<0.001$). The general indicators of the nuclear-cytoplasmic ratio were 1:0.142 and decreased relative to the control animals by 69.5 % ($p>0.05$). The optical density of nuclei and cytoplasm of pinealocytes decreased, respectively, by 24.4 % ($p<0.001$) and 35.5 % ($p<0.001$) compared to control animals. Long-term ingestion of heavy metal salts into the body of rats caused apoptotic rearrangements of pinealocytes and a decrease in their absolute number by 37.0 % ($p<0.001$), while the absolute number of astrocytic glia cells, on the contrary, increased by 2.2 times ($p<0.001$). The glial-neuronal index increased and exceeded the indicators of control animals by 3.3 times ($p>0.05$) (see Table 1).

In the experimental animals of the 60-day period of the experiment, morphological changes in the cerebellar cortex had a pronounced and progressive character. The number of neurons with reversible morphological changes decreased and, at the same time, the number of dystrophically changed cells, in which the processes were irreversible, increased.

As in the pineal gland, hemodynamic disorders, among which hypoxic changes predominated, were the primary morphological changes in the cerebellar cortex. The vessels of the cerebellar cortex (mainly the venous channel) were dilated and filled with cellular elements of blood, with the development of a morphological pattern of stagnant phenomena. Violation of the rheological properties of blood

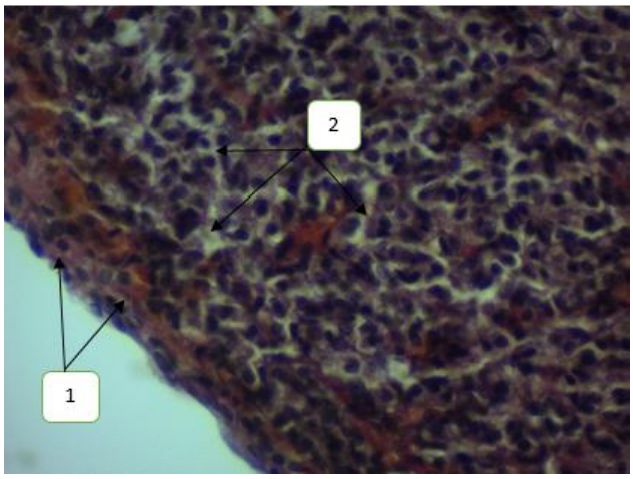

Fig. 2. Morphological changes in the structural components of the pineal gland under conditions of 60-day exposure to heavy metal salts: 1 - thickening of the gland capsule; 2 - growth of the connective tissue component of the stroma. Van Gieson staining. x400.

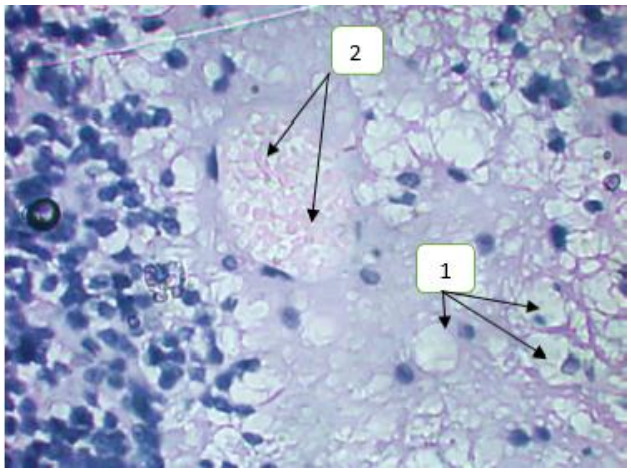

Fig. 3. Cerebellar cortex of experimental group rats after 60-day exposure to heavy metal salts. 1 - sponginess of the substance of the cerebellar cortex; 2 - venous congestion. Hematoxylin-eosin staining. x400.

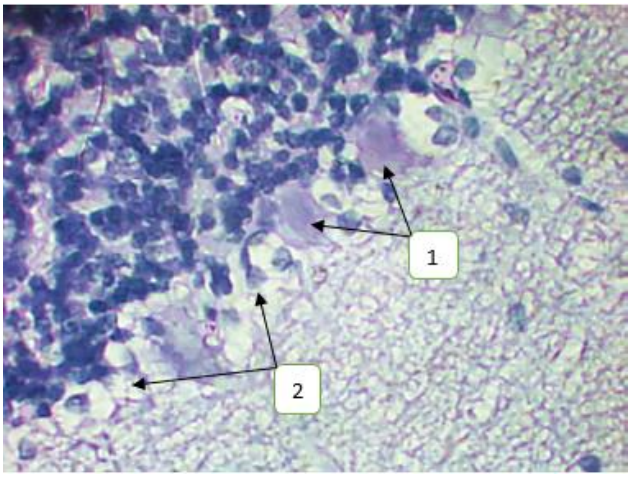

Fig. 4. Cerebellar cortex of an experimental rat after 60-day exposure to salts: 1 - karyocytolysis and karyolysis of Purkinje cells; 2 - area of partial loss of Purkinje cells. Hematoxylin-eosin staining. x400.

in the form of stasis and initial stages of sweetening of blood cells was observed. Hemocapillaries were unevenly filled with blood, dystonic (in some areas they were expanded, in others - spasmodic). The wall of hemocapillaries showed signs of impaired permeability, which was accompanied by the release of blood and plasma elements into the perivascular space with the formation of perivascular edema. After the 60-day period of the experiment, sponginess of the parenchyma of the cerebellar cortex and disruption of the cytoarchitectonics of the cells of the cerebellar cortex were noted. Zones of desolation (lacunae) were formed in the granular layer (Fig. 3).

The state and morphological features of the Purkinje cells of experimental animals were studied, taking into account their special vulnerability to various negative influences [12, 26]. Salts of heavy metals caused in Purkinje cells rather pronounced and widespread various morphological changes characterized by polymorphism.

Acute swelling of a part of Purkinje cells and their nuclei with the formation of pericellular edema was observed. Blurredness and roundness of cell contours, lightness of the cytoplasm were noted. The nuclei were hypochromic, indistinct, enlarged, in some places eccentrically located and had a well-contoured, hypertrophied and hyperchromic nucleolus, which was located in the center of part of the nuclei. In individual neurons, the nucleus occupied almost the entire cytoplasm. Chromatin margination was noted in some nuclei.

Along with the cells in a state of acute edema, there was a small number of neurons in a state of hypoxic changes (homogenizing splitting of Purkinje cells) and deeply changed cells with the formation of cells - shadows. Neurons with signs of homogenizing splitting of Purkinje cells had pale, homogeneous cytoplasm, the tigroid of which was in a state of partial or complete chromatolysis. Nuclei were sharply hyperchromic. Nuclei were not contoured, or, in individual cells, were hyperchromic and hypertrophied. In some places, Purkinje cells were surrounded by gliocytes.

In the cerebellum of the experimental animals, during the 60-day period of the experiment, neurons that were in a state of karyocytolysis and karyolysis with the formation of shadow cells prevailed. Attention was drawn to multiple foci of loss of Purkinje cells with preservation of the molecular and granular layers of the cerebellar cortex (Fig. 4).

At this time of the experiment, an increase in glial reaction was noted, especially around pathologically changed cells and vessels, in the form of hyperplasia processes (satellitosis and neuronophagy). Neurons with a pronounced process of karyocytolysis, which turned into shadow cells, underwent neurophagy with the formation of numerous foci of loss of Purkinje cells.

According to the data of morphometric studies, the indicators of the large diameter of the bodies of pear-shaped neurons increased by 9.7 % ($p>0.05$). The linear indicator of the small diameter of neuron bodies increased by 7.6 % ($p>0.05$), the outer perimeter of neuron bodies increased by 17.5 % ($p<0.01$). The cross-sectional area of neuron bodies increased by 31.7 % ($p<0.01$). The cross-sectional area of the cytoplasm of neurons increased by 27.6 % ($p<0.01$). The morphometric indicators of the state of the nucleus at this time of the experiment acquired a slight stabilization relative to the indicators of the control animals. Thus, the morphometric index of the large diameter of the nuclei of pear-shaped neurons decreased by 1.8 % ($p>0.05$), and the small one by 7.0 % ($p>0.05$), the outer perimeter of the nuclei was smaller than the indicators of control animals by 12.6 % ($p>0.05$). The cross-sectional area of the nuclei of neuron bodies exceeded the indicators of control animals by 39.0 % ($p<0.05$). The nuclear-cytoplasmic ratio was 1:0.552±1.119 and increased by 10.0 % ($p>0.05$) compared to the indicators of control animals (Table 2).

When studying the cytochemical state of Purkinje cells of experimental animals (acridine orange staining), a decrease

Table 2. Results of a morphometric study of Purkinje cells in the mature rats cerebellar cortex under the heavy metal salts impact.

Index	Groups of laboratory animals	
	Rats of the control group, n=6	Rats of the experimental group, n=6
Large diameter of the neuron's bodies, mm	6.418±0.412	7.036±0.258
Small diameter of the neuron's bodies, mm	4.012±0.076	4.311±0.132
Large diameter of the neuron's nuclei, mm	1.105±0.083	1.079±0.031
Small diameter of the neuron's nuclei, mm	0.793±0.101	0.741±0.012
Cross-sectional area of neurons, mm^2	406.9±31.5	536.1±19.9**
Cross-sectional area of neuron's nuclei, mm^2	135.8±18.4	190.0±1.2*
Cytoplasmic area of neurons, mm^2	271.1±13.2	346.1±18.7**
Nuclear-cytoplasmic index	1:0.51±1.086	1:0.552±1.119
The outer perimeter of neuron bodies, mm	39.95±1.71	46.93±0.87**
The outer perimeter of the neurons nuclei, mm	3.182±0.173	2.783±0.082
Normochromic neurons, %	48.63±1.83	31.63±1.72***
Hyperchromic neurons, %	46.48±0.94	30.04±1.53***
Hypochromic neurons, %	4.867±1.289	38.33±0.31***

Note: reliable compared to the control - * p<0.05; ** p<0.01; *** p<0.001.

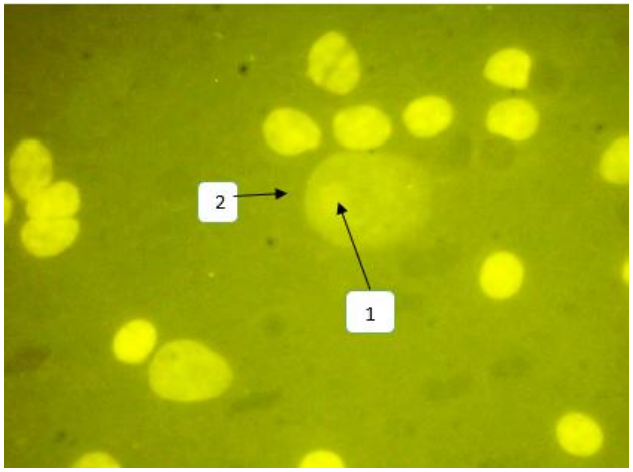

Fig. 5. Cerebellar cortex after 60-day exposure to heavy metal salts: Disappearance of RNA structures in the nucleus (1) and cytoplasm (2) of Purkinje cells. Acridine orange staining. x900.

in the content of RNA structures in the cytoplasm of part of the cells, an increase in the size of the nucleoli, an increasing condensation of the chromatin network of the nuclei, and destruction of the nuclei were observed. The level of saturation with RNA structures of the cytoplasm of neurons decreased, which was reflected in a decrease in the degree of saturation of the cytoplasm of neurons with red dusting (Nissl's substance) (Fig. 5). Evaluation according to the Keplow

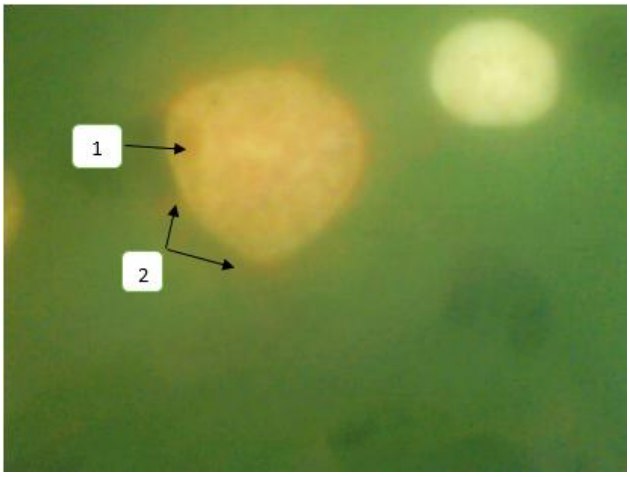

Fig. 6. Rat cerebellar cortex after 60-day exposure to heavy metal salts: Sufficient level of RNA structures in the nucleus (1) and cytoplasm (2) of Purkinje cells. Acridine orange staining. x900.

formula: + and ++ conditional units, which indicated an average and low degree of RNA saturation of Purkinje cells. Against the background of neurons with a medium and low degree of luminescence of RNA structures in the cytoplasm, there was a small number of cells with a high degree of luminescence of RNA structures (++++), which indicated the development of reparative processes in these cells.

Nuclei had increasing condensation of chromatin in the form of multiple clumps with chromatin margination. In cells with a small content of RNA structures in the cytoplasm, and the vast majority of them, nucleoli in the nuclei were weakly contoured or not at all detected, luminescence was noted with a bright yellow or pale red glow, depending on their saturation with RNA structures. This indicated an insufficient number of RNA structures in the nuclei. In single neurons that had sufficient saturation of cytoplasmic RNA structures (+++), the nucleoli also had a sufficient number of these structures, were hypertrophied, with the presence of bright red luminescence (+++) and sometimes shifted to the inner karyolemma of the nucleus (Fig. 6).

The number of hyperchromic neurons decreased by 35.4 % (p<0.001) and normochromic neurons by 34.9 % (p<0.001) compared to the control. Compared with control animals, hypochromic neurocytes increased their number by 7.9 times (p<0.001) (see Table 2).

Discussion

It is common knowledge that the neuroendocrine system is a regulator of all vital processes of the body. At the same time, this system is subject to the primary threat of intoxication and destabilization, the consequences of which are extremely dangerous for vital functions [7]. At the current stage of the development of natural knowledge, the interest of many researchers is focused on the problem of stress, especially its role in the processes of adaptation of the body to endogenous and exogenous influences, as well as in the occurrence of some diseases. According to modern data

[7], the pineal gland is an organ that combines the processes of adaptogenesis and immunogenesis, participates in the initiation of stress reactions and determines the sequence of disorders in the body at different stages of stress development.

Experimental and clinical data indicate a close connection of the pineal gland with the cerebellum [27]. Thus, the hormone of the pineal gland melatonin, which has an anti-stress, antioxidant effect, suppresses the formation of nitric oxide, the initiation of apoptosis, regulates circadian rhythms [22], has membrane melatonin receptors in various structures of the brain, including the cerebellum [27]. In our opinion, a comprehensive study of morphological features of the pineal gland and cerebellar cortex of sexually mature rats under conditions of 60-day exposure to a complex of heavy metal salts is interesting. The study of organometric indicators of the pineal gland during the 60-day period of the experiment indicated a slight hypertrophy of the organ in comparison with the indicators of control animals, which indicated the development of adaptive processes in response to the action of heavy metal salts.

Morphological changes in the epiphysis and cortex of the cerebellum were related to changes in all structural components of the studied organs: stromal, parenchymal, and vascular, which was confirmed by their morphological, morphometric, and cytochemical indicators. At the same time, both in the pineal gland and in the cerebellar cortex, the morphological changes had a non-specific polymorphic character. The basis of the occurrence of destructive changes in the structural components of the pineal gland and the cerebellar cortex was hypoxia, which is caused by both direct and indirect (mediated) effects of heavy metals on the vascular endothelium [28]. Thus, both in the pineal gland and in the cerebellar cortex, the pathogenetically morphological basis for negative changes was circulatory disorders, namely, vascular congestion (mainly venous), violation of the permeability of the vascular wall with the formation of perivascular edema, sponginess, and edematous processes, both in the cerebellar cortex, as well as in the pineal gland.

At the same time of the experiment, the rheological properties of blood in the form of stasis and the initial stages of blood clotting were disturbed in the bloodstream of both organs. Most likely, disorders of the rheological properties of blood were caused by the direct action of heavy metal salts on the capillary endothelium. At the same time, there was a violation of the functions of intracellular organelles, transport, metabolic, synthetic and adhesive functions of the endothelium. And as a result, there was a violation of hemorheology and microcirculation (changes in the number of active functioning capillaries, stasis, erythrocyte sludge, microthrombosis, paresis and vascular dystonia) [21, 28]. In addition, about 90 % of lead ions (which are part of the studied complex of heavy metal salts) entering the blood are bound by erythrocytes [20]. The absence of a blood-brain barrier in this organ can be considered an additional link of hemodynamic disturbances in the pineal gland [1].

The described morphological disorders in the vascular bed of the pineal gland indicated the gradual development of chronic hypoxia in the organ, which led to the further development of sclerotic changes due to hypoxia of collagen synthesis by fibroblasts [6]. Sclerotic changes, edema, and blood circulation disorders negatively affected the state of pinealocytes, including their secretory activity and the processes of releasing hormones into the blood due to impaired permeability of the vascular wall and disruption of the plasmalemma membrane of pinealocytes.

After a 60-day period of exposure to heavy metal salts on the pineal gland, morphologically, indole production prevailed in the gland, and the nuclear apparatus of part of the glandulocytes showed signs of hypertrophy of both the nucleus and the nucleolus, with an increase in the number of the latter. This undoubtedly indicated a significant stress on the controlling properties of the nucleus on synthetic processes in cells.

Morphometric indicators (area of nuclei, cytoplasm of pinealocytes and the average diameter of their karyon) remained increased compared to the indicators of control animals and confirmed the results of light-optical studies. The optical density of chromatin nuclei, on the contrary, decreased by 24.4 %, which according to Bulyk R. E. et al. [8]: "increased nuclear volume and low optical density of nuclear chromatin staining indicates the activation of genetic material and is regarded as an increase in cell function". But part of the pinealocytes still had morphological signs of chromatin margination, which are harbingers of apoptosis. Confirmation of the initial stages of apoptotic rearrangements in pinealocytes is a further decrease in their absolute number by 37.0 % in comparison with the indicators of control animals. That is, an increase in the synthetic activity of a part of pinealocytes against the background of a decrease in their absolute number indicated a general high load on the gland and, according to Gubina-Vakulyk G. I. [15], had a compensatory nature in connection with a decrease in the number of pinealocytes under conditions of chronic exposure to the complex salts of heavy metals. All this indicates a gradual decrease in reserve mechanisms of physiological adaptation in the pineal gland of experimental animals.

In response to the action of heavy metal salts, an active glial reaction was detected in the peripheral areas of the gland, which can be considered an active adaptive reaction of neuroglia to the action of heavy metal salts, and during the 60-day period of the experiment, the reaction of astroglia intensified, and both diffuse and local astrogliosis were detected around the vessels of the subcapsular zone, with the formation of "couplings". Such morphological formations, in our opinion, contributed to delaying the diffusion of heavy metal salts through the vascular wall into the parenchyma of the pineal gland. The formed perivascular astroglial proliferates [15], may indirectly testify to more intense processes of pinealocyte apoptosis in response to the action of a damaging agent. However, other properties

of astrocytic neuroglia in glial proliferates cannot be eliminated. In our opinion, they are aimed at achieving water-ion homeostasis in the gland by improving the trophicity of pinealocytes, their barrier function, preventing the penetration of heavy metals into the parenchyma of the gland. It is impossible to overestimate the contribution of astrocytes in the protection of the gland parenchyma from oxidative stress by synthesizing the gaseous gliotransmitter hydrogen sulfide (H_2S), which has the properties of a synaptic modulator and neuroprotector, protecting the organ from oxidative stress [10]. An increase in the number of glial elements in the pineal gland definitely has a certain compensatory and adaptive value, especially in the processes of transfer of RNA, amino acids and growth factors to pinealocytes [10]. Morphological changes in the body were confirmed by their morphometric indicators. Thus, a gradual dynamic increase in the absolute number of astrocytic glial cells by 2.2 times and the gliocyto-neuronal index by 3.3 times was observed in comparison with the indicators of control animals.

Thus, long-term (60-day) administration of a mixture of heavy metal salts to the body of experimental animals led to the development of a general adaptation syndrome and the stage of "subcompensation" of chronic stress in the pineal gland and the body as a whole.

Therefore, the morphological changes in the pineal gland had a non-specific polymorphic character in the form of a sharp violation of hemodynamics in the organ, the morphology of the vascular wall, the development of tissue hypoxia, a delay in the release of hormones into the blood as a result of a violation of the permeability of the cell membrane and vessel wall, processes of accelerated apoptosis of a part of pinealocytes, reactive astrogliosis in response to the action of a damaging agent.

Along with negative changes in the pineal gland, compensatory and adaptive processes with signs of functional stress were also noted. A slight hypertrophy of the organ and pinealocytes, an increase in the average diameter of the karyon, an active adaptive glial reaction and activation of synthetic processes in the part of pinealocytes were revealed.

In our opinion, the delay in the release of indole-containing hormones of the pineal gland (including melatonin) into the blood had negative consequences for endocrine regulation and preservation of homeostasis in the cerebellar cortex. Although, this aspect of the regulation of adaptive mechanisms in the cerebellum can be considered an addition to other, no less significant.

Morphological changes of Purkinje cells were quite distinct and widespread, had a versatile, non-specific, polymorphic character, and some cells had an irreversible character. The morphological indicators of the cells of the cerebellar cortex were characterized by the development of swelling due to a decrease in the relative density of cells and their nuclei. The trend towards an increase in all morphometric indicators of the bodies of pyriform neurons remained. Morphometry of the state of the nucleus in this term of the experiment showed signs of slight stabilization relative to the parameters of the control animals. Thus, the morphometric indicators of the nuclei of pear-shaped neurons decreased unreliably. At the same time, the cross-sectional area of the nuclei of neurons exceeded the indicators of intact animals by 39.0 %.

The number of neurons with reversible morphological changes decreased and, at the same time, the number of dystrophically changed cells, in which the processes were irreversible, increased. This is evidenced by the gradual and increasing inhibition of protein synthesis in the cytoplasm of neurons (chromatolysis), as well as the increase in reactive changes in neurons (the state of the nucleus and nucleoli, which were in a state of deep irreversible changes (rhexis, lysis), the formation of heterochromatin lumps in the chromatin of the nucleus, the decrease amount of RNA in nucleoli). Thus, the number of hyperchromic neurons decreased by 35.4 % compared to the control, and the number of normochromic neurons decreased by 34.9 %. Hypochromic neurocytes, in comparison with intact animals, increased their number by 7.9 times.

A fairly high level of RNA structure content was still preserved in some neuron nuclei, and their hyperplasia was observed. This, in our opinion, can be explained both by a compensatory and adaptive increase in the synthesis of RNA structures and proteins in individual cells (adaptive and adaptive changes), and by inhibition of the transition of substances from the nucleolus to the nucleus and further into the cytoplasm (this can lead to inhibition of synthesis protein in the nucleus and in the cytoplasm).

In the conditions of the experiment, glial hyperplasia was noted in the cerebellar tissue with the development of the process of satellitosis and neuronophagy around deeply altered neurons. Taking into account the works of a number of authors [21], hyperplasia of glia under the influence of Pb, due to its high plastic and adaptive properties to the surrounding microenvironment, should be considered as the ability to maintain high functional activity of the neuron-glia system and neuron-glia-capillary relationships. In addition, the glial reaction of the cells can be a sign of the compensatory and protective reaction of the cerebellar tissue. Forming a protective barrier around blood vessels, glial proliferates are thus likely to be able to prevent the penetration of the toxin into the brain substance.

Conclusions

1. Prolonged (60 days) ingestion of a complex of heavy metal salts into the experimental animals body led to the development of a general adaptation syndrome in the epiphysis and cerebellar cortex, the stage of "subcompensation" of chronic stress.

2. Morphological changes in the organs had a non-specific polymorphic character, such as a sharp violation of hemodynamics, a violation of the morphology of the vascular wall, the state of pinealocytes and Purkinje cells, the development of tissue hypoxia, processes of apoptosis

and reactive astrogliosis as a response to the action of a damaging agent.

3. Although the pineal gland of the experimental animals showed signs of indole production, the evacuation of hormones (including melatonin) into the vascular bed was hampered due to a violation of the morphology of the vascular wall and the cell membrane of pinealocytes. Most likely, this led to a deficiency of this hormone in the body of the experimental animals, which negatively affected the adaptive processes in the cerebellar cortex in response to the action of the stress agent.

4. Along with negative changes in the pineal gland and cerebellar cortex, compensatory and adaptive processes with signs of functional stress took place. Adaptive processes were observed both in a small number of pinealocytes and in Purkinje cells, as well as an active adaptive glial reaction in both organs. The signs listed above can probably indicate the possibility of regenerative processes in the studied organs after the termination of the negative effect of the complex of heavy metal salts.

References

[1] Acuna-Castroviejo, D., Escames, G., Venegas, C., Diaz-Casado, M. E., Lima-Cabello, E., Lopez, L. C., ... Reiter, R. J. (2014). Extrapineal melatonin: sources, regulation, and potential functions. *Cellular and Molecular Life Sciences,* 71(16), 2997-3025. doi: 10.1007/s00018-014-1579-2

[2] Ajayi, S. A., Ofusori, D. A., Ojo, G. B., Ayoka, O. A., Abayomi, T. A., & Tijani, A. A. (2011). The microstructural effects of aqueous extract of Garcinia kola (Linn) on the hippocampus and cerebellum of malnourished mice. *Asian Pacific Journal of Tropical Biomedicine,* 1(4), 261-265. doi: 10.1016/S2221-1691(11)60039-7

[3] Albarran, M. T., Lopez-Burillo, S., Pablos, M. I., Reiter, R. J., & Agapito, M. T. (2001). Endogenous rhythms of melatonin, total antioxidant status and superoxide dismutase activity in several tissues of chick and their inhibition by light. *Journal of Pineal Research,* 30(4), 227-233. doi: 10.1034/j.1600-079x.2001.300406.x

[4] Arushanyan, E. B. (2005). Гормон шишкоподібної залози мелатонін - новий ноотроп? [Pineal hormone melatonin - a new nootropic?]. *Експериментальна і клінічна фармакологія - Experimental and Clinical Pharmacology*, 68, 74-79.

[5] Bharti, V. K., Srivastava, R. S., Kumar, H., Bag, S., Majumdar, A. C., Singh, G., ... Brown, G. M. (2014). Effects of melatonin and epiphyseal proteins on fluoride-induced adverse changes in antioxidant status of heart, liver, and kidney of rats. *Advances in Pharmacological Sciences,* 2014. doi: 10.1155/2014/532969

[6] Blagodarov, V. M. (1997). *Патологічна анатомія (загальнопатологічні процеси) [Pathological Anatomy (general pathological processes)].* Київ: ТОВ "Генеза" - Kyiv: Ltd "Genesis".

[7] Bondarenko, A. A. (2013). Гіпофізарно-епіфізарні відносини: вплив кортикотропіну на метаболізм серотоніну та формування нічного піку мелатоніну [Hypophysis-epiphyseal interactions: effects of corticotropin on metabolism of serotonin and formation of a melatonin night-time peak]. *Нейрофізіологія - Neurophysiology,* 45(2), 128-132. doi: 10.1007/s11062-013-9347-8

[8] Bulyk, R. E., Krivchanskaya, M. I., & Khomenko, V. G. (2016). Морфологічні та морфометричні зміни в епіфізі під дією пропранололу та їх корекція мелатоніном [Morphological and morphometric changes in the pineal gland under the action of propranolol and their correction with melatonin]. *Символ науки - Symbol of Science*, 3, 22-25.

[9] Chuang, J. I., Chen, S. S., & Lin, M. T. (1993). Melatonin decreases brain serotonin release, arterial pressure and heart rate in rats. *Pharmacology,* 47(2), 91-97. doi: 10.1159/000139083

[10] Drozdova, G. A., Samigullina, A. F., & Nurgaleeva, E. A. (2017). Постгипоксическая реакция клеток астроглии зрительной коры в эксперименте [Posthypoxic reaction of astroglia cells of the visual cortex in the experiment]. *Казанский медик - Kazan Doctor,* 98(6), 984-988.

[11] Eluwa, M., Inyangmme, I., Akpantah, A., Ekanem, T., Ekong, M. B., Asuquo, O., & Nwakanma, A. A. (2013). A comparative study of the effect of diet and soda carbonated drinks on the histology of the cerebellum of adult female albino Wistar rats. *African Health Sciences*, 13(3), 541-545. doi: 10.4314/ahs.v13i3.1

[12] Emel'yanchik, S. V., & Zimatkin, S. M. (2014). Structural and histochemical changes in Purkinje cells in the rat cerebellum in cholestasis. *Neuroscience and Behavioral Physiology*, 44(4), 467-471. PMID: 23898717

[13] Escames, G., Macias, M., Leon, J., Garcia, J., Khaldy, H., Martin, M., ... Acuna-Castroviejo, D. (2001). Calcium-dependent effects of melatonin inhibition of glutamatergic response in rat striatum. *Journal of Neuroendocrinology*, 13(5), 459-466. doi: 10.1046/j.1365-2826.2001.00656.x

[14] Fonnum, F., & Lock, E. A. (2004). The contributions of excitotoxicity, glutathione depletion and DNA repair in chemically induced injury to neurones: exemplified with toxic effects on cerebellar granule cells. *Journal of Neurochemistry*, 88(3), 513-531. doi: 10.1046/j.1471-4159.2003.02211.x

[15] Gubina-Vakulik, G. I. (2006). Попытка обобщить результаты гистопатологического исследования эпифизов головного мозга [An attempt to generalize the results of histopathological examination of the epiphysis of the brain]. *Буковинский медицинский вестник - Bukovinian Medical Bulletin,* 10(4), 34-36.

[16] Hazarika, R. (2014). Neurotoxic impact of organophosphate pesticide phosphomedon on the albino rat. *Journal of Environmental Biology,* 35(2), 427-430. PMID: 24665773

[17] Ipastova, I. D. (2015). Нормальная и патологическая количественная морфология мозжечка белых крыс (обзор литературы) [Normal and pathological quantitative morphology of the white rat cerebellum (literature review)]. *Ульяновский медико-биологический журнал - Ulyanovsk Medical Biological Journal*, 2, 8-14.

[18] Ivanenko, M. O., Nikiforova, N. A., Gromakova, I. A., & Kuzmenko, O. V. (2007). Радіозахисні властивості мелатоніну: експериментальні та клінічні аспекти [Radioprotective properties of melatonin: experimental and clinical aspects]. *Український радіологічний журнал - Ukrainian Radiological Journal,* 15, 483-488.

[19] Korshniak, V. O. (2016). Роль мелатоніну в нейроендокринній регуляції нервової системи у хворих з наслідками закритих черепно-мозкових травм [The role of melatonin in neuroendocrine regulation of the nervous system in patients with consequences of closed craniocerebral injuries (literature review)]. *Міжнародний журнал неврології - International Neurological Journal,* 4, 108-113.

[20] Kramarenko, V. F. (1989). *Токсикологічна хімія [Toxicological chemistry]*. Київ: Вища школа - Kyiv: High school.

[21] Luhovsky, S. P. (2005). Морфофункциональные особенности головного мозга крыс при хроническом воздействии малых доз свинца [Morpho-functional characteristics of the rat brain under chronic exposure to small doses of lead]. *Современные проблемы токсикологии - Modern Problems of Toxicology,* 3, 21-25.

[22] Pishak, V. P. (2000). *Клінічна анатомія шишковидного тіла [Clinical Anatomy of the Pineal Body].* Тернопіль: Укрмедкнига - Ternopil: Ukrmedkniga.

[23] Reiter, R. J. (2000). Melatonin: lowering the high price of free radicals. *Physiology,* 15(5), 246-250. doi: 10.1152/physiologyonline.2000.15.5.246

[24] Romaniuk, A. M., Hryntsova, N. B., Karpenko, L. I., Kiptenko, L. I., Ustianskii, O. O., & Dunaieva, M. M. (2019). The long-term effect of the complex of heavy metal salts on the morphofunctional changes in the structural components of the intermediate lobe of the mature rat's pituitary gland-the female. Problems Endocrinol. *Pathol.,* 2, 98-103. doi: 10.21856/j-PEP.2019.2.14

[25] Romaniuk, A., Lyndin, M., Lyndina, Y., Sikora, V., Hrintsova, N., Timakova, O. ... Gladchenko, O. (2018). Changes in the hematopoietic system and blood under the influence of heavy metal salts can be reduced with vitamin E. *Turk Patoloji Derg,* 34(1), 73-81. doi: 10.5146/tjpath.2017.01412

[26] Smirnov, A. V., Evsiukov, O. Iu., Snigur, G. L., Shmidt, M. V., Gurov, D. Iu., Mednikov, D. S., & Kharitonova, M. V. (2013). Особенности структурных изменений головного мозга при моделировании алиментарного дефицита магния [Features of structural changes in the brain when modeling alimentary magnesium deficiency]. *Современные проблемы науки и образования - Modern problems of science and education,* 4, 119-126.

[27] Stankov, B., Capsoni, S., Lucini, V., Fauteck, J., Gatti, S., Gridelli, B., ... & Fraschini, F. (1993). Autoradiographic localization of putative melatonin receptors in the brains of two Old World primates: Cercopithecus aethiops and Papio ursinus. *Neuroscience,* 52(2), 459-468. doi: 10.1016/0306-4522(93)90172-C

[28] Trakhtenberg, I. M., & Lugovskoy, S. P. (2005). The role of endothelium in the mechanisms of development of vasotoxic effects of lead. *Journal of the Academy of Sciences of Ukraine,* 1, 63-74.

[29] Weekley, L. B. (1995). Pharmacologic studies on the mechanism of melatonin-induced vasorelaxation in rat aorta. *Journal of Pineal Research,* 19(3), 133-138. doi: 10.1111/j.1600-079x.1995.tb00182.x

МОРФОЛОГІЧНІ ПЕРЕБУДОВИ ШИШКОПОДІБНОЇ ЗАЛОЗИ ТА КОРИ МОЗОЧКА СТАТЕВОЗРІЛИХ ЩУРІВ ПРИ ТРИВАЛОМУ ВПЛИВІ СОЛЕЙ ВАЖКИХ МЕТАЛІВ

Гринцова Н. Б., Романюк А. М., Кіптенко Л. І., Сулім Л. Г.

Забруднення солями важких металів є актуальною екологічною проблемою сучасності, яка негативно впливає на здоров'я населення. Ендокринна система підтримує гомеостаз в організмі, в тому числі й у нервовій системі. Метою роботи є дослідження морфологічних змін кори мозочка та епіфізів статевозрілих самців-щурів за умови тривалого впливу на організм комплексу солей важких металів. Досліджено морфологічні зміни кори мозочка та епіфізів статевозрілих самців щурів за умов тривалого впливу солей важких металів. Тваринам дослідної групи моделювали мікроелементоз шляхом додавання до питної води суміші солей важких металів протягом 60 діб: цинку ($ZnSO_4x7H_2O$) - 5 мг/л, міді ($CuSO_4x5H_2O$) - 1 мг/л, заліза ($FeSO_4$) - 10 мг/л, марганцю ($MnSO_4x5H_2O$) - 0,1 мг/л, свинцю ($Pb(NO_3)_2$) - 0,1 мг/л і хрому ($K_2Cr_2O_7$) - 0,1 мг/л. Використовували морфологічні, морфометричні та статистичні методи дослідження. Тривале (60 діб) надходження до організму піддослідних тварин комплексу солей важких металів призводило до розвитку в епіфізі та корі мозочка загального адаптаційного синдрому, стадії "субкомпенсації" хронічного стресу. Морфологічні перебудови в органах мали неспецифічний поліморфний характер, як то різке порушення гемодинаміки, порушення морфології судинної стінки, стану пінеалоцитів та клітин Пуркіньє, розвиток тканинної гіпоксії, процесів апоптозу та реактивного астрогліозу як відповідь на дію пошкоджуючого агенту. В епіфізі піддослідних тварин виявлені ознаки індол-продукції, але евакуація гормонів (в тому числі мелатоніну) до судинного русла була уповільнена внаслідок порушення морфології судинної стінки та клітинної оболонки пінеалоцитів. Це призводило до недостатності цього гормону в організмі піддослідних тварин, що негативно впливало на адаптивні процеси у корі мозочку у відповідь на дію стресорного агенту. Компенсаторно-пристосувальні процеси в епіфізі та корі мозочка мали ознаки функціонального напруження. Спостерігалися адаптивні процеси як у незначної кількості пінеалоцитів, так і у клітинах Пуркіньє, а також активна адаптивна гліальна реакція в обох органах.

Ключові слова: *шишкоподібна залоза, важкі метали, кора мозочка, реактивний астрогліоз.*

DOI: 10.31393/morphology-journal-2022-28(4)-09 Reports of Morphology, Vol. 28, №4, Pages 64-69

ISSN 1818-1295 eISSN 2616-6194

REPORTS OF MORPHOLOGY

Official Journal of the Scientific Society of Anatomists, Histologists, Embryologists and Topographic Anatomists of Ukraine

journal homepage: https://morphology-journal.com

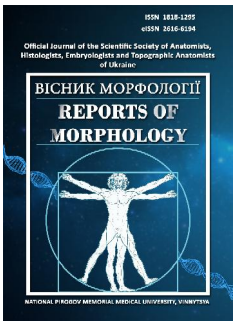

Changes of c-Fos expression and NADPH-d activity in claustrum induced by chronic muscle inflammation in cat (a preliminary study)

Maznychenko A. V., Abramovych T. I., Sokolowska I. V.
Gdansk University of Physical Education and Sport, Gdansk, Poland

ARTICLE INFO
Received: 1 September 2022
Accepted: 5 October 2022

UDC: 612.82+612.884

CORRESPONDING AUTHOR
e-mail: andrii.maznychenko@awf.gda.pl
Maznychenko A. V.

CONFLICT OF INTEREST
The authors have no conflicts of interest to declare.

FUNDING
Not applicable.

ACKNOWLEDGMENTS
The authors thank to Dr. Maisky V.O. and Dr. Pilyavskii O.I from the Bogomolets Institute of Physiology for their assistance in histological processing.

An investigation of the central mechanisms underlying muscle inflammation and musculoskeletal pain is an important step to find means for the prevention or treatment of muscle inflammation. One of the insufficiently studied brain structures involved in the transmission of nociceptive information is the claustrum (CL). Therefore, the aim of the study was to reveal changes in the patterns of Fos-immunoreactivity and NADPH-diaphoreactivity in the nucleus claustrum (CL) and additionally in the ventral putamen (Pu) during chronic inflammation of m. gastrocnemius-soleus in cat, induced by intramuscular injection of complete Freund's adjuvant (CFA). Immunohistochemical and histochemical techniques were used to detect Fos-immunoreactive (Fos-ir) and NADPH-diaphorase reactive (NADPH-dr) neurons within studied structures. It was revealed that nine days after CFA-induced muscle inflammation the level of Fos-immunoreactivity and NADPH-d reactivity within the CL and in the ventral part of Pu increased two-fold in comparison with the control. Because the CL is reciprocally connected with many structures of the brain cortex and subcortical structures, all these structures can be pathways of transmission of nociceptive information, nevertheless, it can be assume that the central amygdala nucleus may make the main nociceptive contribution to the activation of neurons within the CL. It is known that CL is mutually related to Pu, but it was not possible to assess their mutual influence in this study. The results of the study of the Fos-ir neurons distribution in CL and Pu under conditions of long-term muscles inflammation indicate the active involvement of the mentioned structures in the formation of adaptive reactions. The increase in the number of neurons with NADPH-d reactivity in CL and Pu indicates that NO-signals play a significant role in the formation and amplification of the response to painful impulses from inflamed muscles. In addition, further research is needed to accurately identify all possible nociceptive inputs to the CL and to separate the emotional, motor, auditory, and visual components that may accompany nociceptive processes.

Key words: *muscle inflammation, complete Freund's adjuvant, claustrum, putamen, cat.*

Introduction

It is well known that inflammatory muscle diseases lead to a significant decrease in a human's life quality [31]. Musculoskeletal pain or myalgia is the result of muscle inflammation, which leads to a significant modulation of motor activity [18, 20, 30]. In this regard, it is a considerable interest to study the effect of inflammatory processes (occurring in the skeletal muscles) on the brain structures. To study central mechanisms underlying musculoskeletal pain, electrical, mechanical, or chemical excitation of high-threshold group III and IV muscle afferents has been widely explored in tests on humans and animals. Intramuscularly injected agents, such as capsaicin, carrageenan, potassium chloride, hypertonic saline, or others, were used to induce muscle pain and, thereby, to excite thin muscle afferents [30]. Peripheral and central mechanisms underlying chronic pain are still poorly understood; this type of pain is difficult to ameliorate. The induction of persistent inflammatory pain by intramuscular (i.m.) injections of complete Freund's adjuvant (CFA) could be a convenient approach in examination of brain structures involved in muscle nociception [1, 30, 33].

One of the understudied structures of the brain is the claustrum. It is known that claustrum receives input from almost all regions of cortex and projects back to almost all

regions of cortex. Although there are enough studies of this structure, including studies on human under pain conditions, nevertheless, the function of the claustrum remains unclear [4]. Morphological investigations are one of the appropriate ways to study inflammatory pain processes at the CNS level. The best known morphological techniques are the detection of c-Fos protein in the nuclei of activated neurons and detection of nerve cells containing nitric oxide synthase.

The expression of immediate early genes, especially *c-fos*, is widely used for mapping functional pathways, including the circuitry that underlies the transmission of nociceptive information in the CNS. The proto-oncogene *c-fos* is expressed in neurons in response to various stimuli, and its c-Fos-protein product can be easily detected with immunohistochemical techniques [12, 23]. Therefore, the immunohistochemical method of *c-fos* expression (as a marker of neuronal activation) to determine which neural elements are activated. Another method of investigation is the identification of nitric oxide synthase (NO-synthase or NOS-containing neurons) within the spinal and brain structures. The neuronal variant NADPH-diaphorase is known to correspond to a form of nitric oxide synthase [28, 32]. NO-synthase acts as a marker of late changes in gene expression and effects on various physiological and pathophysiological functions of the central and peripheral nervous system [7, 14].

Thus, *the aim of the study* was to reveal changes in patterns of Fos-immunoreactivity and NADPH-diaphorase reactivity within the nucleus claustrum (CL) and additionally in the ventral part of Putamen (Pu) under condition of chronic inflammation of the *m. gastrocnemius-soleus* (GS) (which is most frequently involved in daily life) induced by i.m. injection of CFA.

Materials and methods

Cats weighing 2.4 to 3.8 kg were randomly divided into 2 groups. 1st group - control intact animals (n=4). 2nd groups - adjuvant-injected cats (n=4). The animals were purchased from a state-controlled animal farm through the common animal facility of the Bogomolets Institute of Physiology (Kyiv, Ukraine). The experimental animals were kept in an air-filtered, humidity - (55±5 %) and temperature-controlled (20-22 °C) room with filtered air. The present study was approved by the Bioethics Committee of the Institute and performed in accordance with the European Union Directive of 22 September 2010 (2010/63/EU) for the protection of animals used for scientific purposes.

Inflammation was induced by infiltrating the GS muscles with 1 ml of the CFA modified with *Mycobacterium butyricum* (Calbiochem, USA) dissolved in 1 ml of Ringer's solution. Injections of CFA solution were performed under full inhalation anesthesia into the left GS muscles (three injections of 0.2 ml into each head). Cats were placed in cages with soft bedding and allowed to recover for 9 days [30].

Nine days after the induction of inflammation of GS muscles, all animals were deeply anesthetized with sodium pentobarbital (75 mg/kg, i.p., Sigma, USA) and perfused through the ascending aorta with a 0.9 % physiological saline (500 ml) followed by a fixative solution (1500 ml) containing 4% paraformaldehyde in 0.1 M phosphate buffer (pH 7.4). Samples of the lumbar and sacral spinal cord were quickly removed; blocks were postfixed in the same fixative overnight and cryoprotected in phosphate-buffered sucrose at 4 °C for 48 h. Part of the brain was cut into frontal frozen 40-μm-thick sections. Brain sections were collected in wells with cold phosphate-buffered saline (0.01 M phosphate buffer containing 0.9 % NaCl), to be processed immunohistochemically and histochemically. The Fos immunoreactivity was detected according to a standard avidin-biotin-peroxidase technique [16] using a rabbit polyclonal antibody against c-Fos protein 1:2000 (Ab-5, Oncogene Research, USA) and a commercial kit 1:200 (ABC Kit, PK 4001, Vector Laboratories, USA). Fos-immunoreactive (Fos-ir) neurons were observed as units with black nuclei due to nickel-intensified 3,3'-diaminobenzidine tetrahydrochloride (Sigma, USA), staining. To evaluate the possibility of double labeling of Fos immunoreactivity and NADPH-diaphorase reactivity in neurons, half of the immunostained sections were additionally incubated in 0.1 M phosphate buffer (pH 7.4) containing 0.3 % Triton X-100, 0.2 mg/ml nitroblue tetrazolium (Sigma, USA), and 0.5 mg/ml β-NADPH tetrasodium salt (Sigma, USA) at 37 °C for 30 to 60 min [32]. NADPH-diaphorase reactive (NADPH-dr) neurons were detected as light-blue cells with unstained nuclei. The location of Fos-ir and NADPH-dr cells were controlled according to the stereotaxic atlas [21].

The density of Fos-ir neurons and NADPH-dr cells were counted bilaterally in the cat brain sections (in all animals) at the levels A+11/12 (within 400 x 400 μm^2 areas) and analyzed. Only high intensely stained NADPH-dr neurons were used for statistical analysis. The Shapiro-Wilk test was used to test the normality of the data distribution. The obtained values are expressed as means ±SEM. Intergroup differences were evaluated by two-way ANOVA followed by the Bonferroni's multiple comparison test. Differences of the mean values with $p<0.05$ were considered as significant. Data analysis was performed using software "Origin 8.5" (OriginLab Corporation, USA).

Results

In the intact cats, the mean density of Fos-ir neurons within CL were 6.8±0.8 and 7.2±1.3 (on the left and right side of the section, respectively). Additionally, the labeled neurons were counted in adjacent to CL ventral part of Pu. The density such cells were 13.6±2.1 and 10.2±3.3 units, respectively. Note, difference between amount of activated neurons on left and right sides within these nuclei was not statistically significant ($p>0.05$) (Figs. 1 and 2). In comparison with control animals, increase in the mean

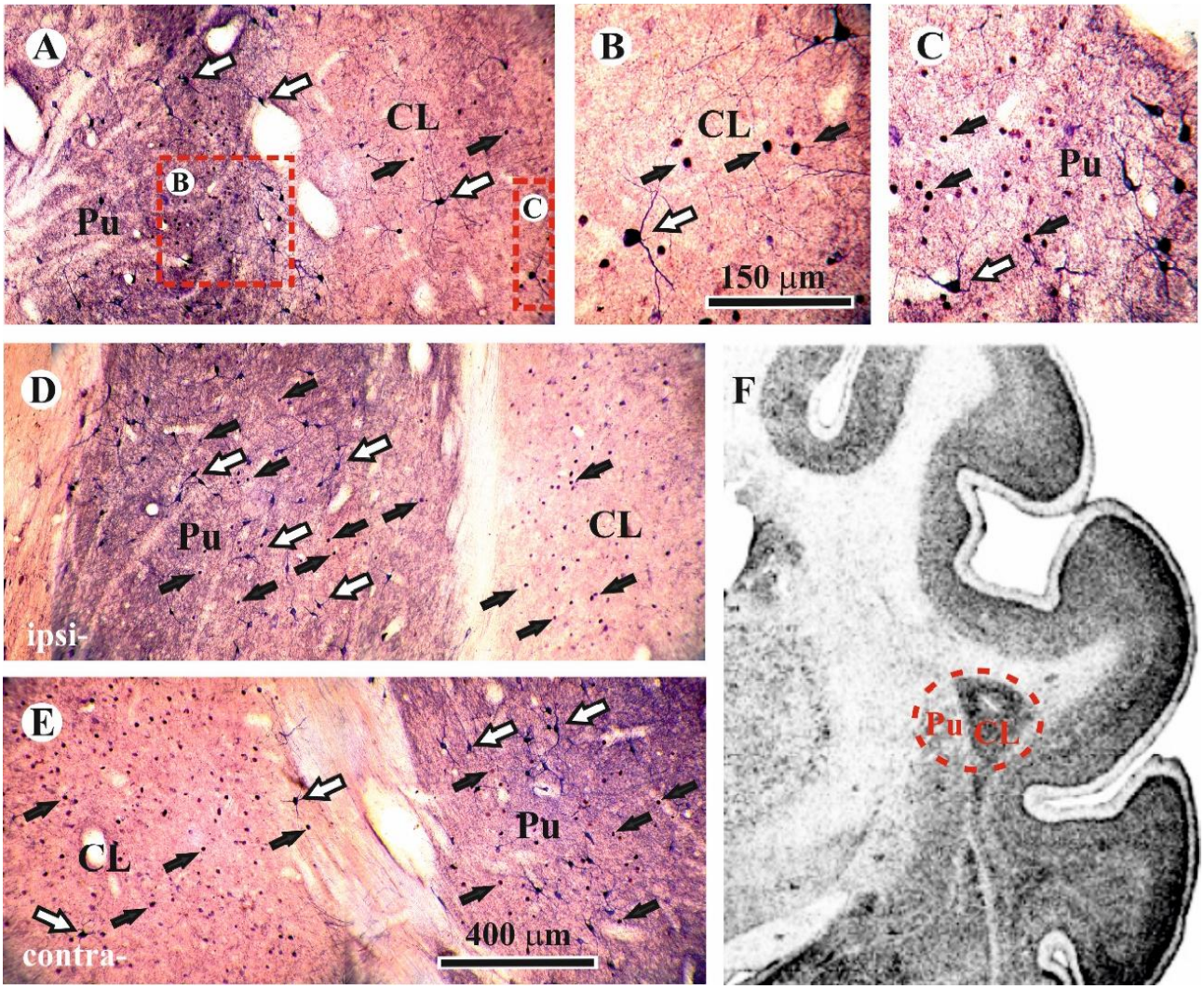

Fig. 1. Distribution of Fos-immunoreactive neurons and NADPH-dr cells in claustrum and putamen: (A-C) unilaterally - in control animals and (D, E) on the ipsil- and contralateral side of the brain in cats after injection of complete Freund's adjuvant. F - frontal section of cat brain according to the atlas [23] at the levels A+11.8. Black and white arrows designates examples of Fos-immunoreactive and NADPH-dr neurons, respectively. Structures: CL - claustrum; Pu - putamen. Scale bars: 150 μm on (B) also appreciated for (C) and 50 μm on (E) appreciated for (A and D).

density of Fos-ir cells was registered in CL and Pu in CFA-injected cats. Maximal density of Fos-ir neurons was recorded within CL and Pu on contralateral side of the brain section (in relation to the CFA-injection side, $p<0.05$). Therefore, mean density of labelled cells were 16.1±1.1 and 20.5±1.6 in CL, and 30.3±4.5 and 42.3±5.8 in ventral part of Pu (on the ipsi- and contralateral side, respectively) (Figs. 1 and 2).

NADPH-d reactivity within CL and Pu were also registered. In the control animals, mean density within these nuclei on left and right sides were 5.1±0.8 and 4.2±2.1 in CL, and 10.8±0.7 and 12.8±1.9 in Pu. Values obtained in CL and Pu were not statistically significant between left and right section side for each nucleus ($p>0.05$) (Figs. 1 and 3). Compared with the control, the level of NADPH-d reactivity was significantly higher ($p<0.05$) in the CFA-injected cats. Thus, mean density within studied nuclei on ipsi- and contralateral side were 8.4±0.9 and 9.7±0.8 in CL, and 11.9±0.7 and 20.5±1.5 in Pu, respectively (Figs. 1 and 3).

It should be noted that in comparison with the control, the average density of labeled Fos-ir as well as NADPH-dr neurons in the contralateral CL and Pu increased by two-fold. Also, note that the Fos-ir and NADPH-dr neurons were intermingled within studied nuclei, but double-labeled cells were not revealed.

Discussion

The results of the study demonstrate that 9 days after CFA-induced muscle inflammation the level of Fos-immunoreactivity and NADPH-diaphorase reactivity within the CL and in the ventral part of Pu increased two-fold

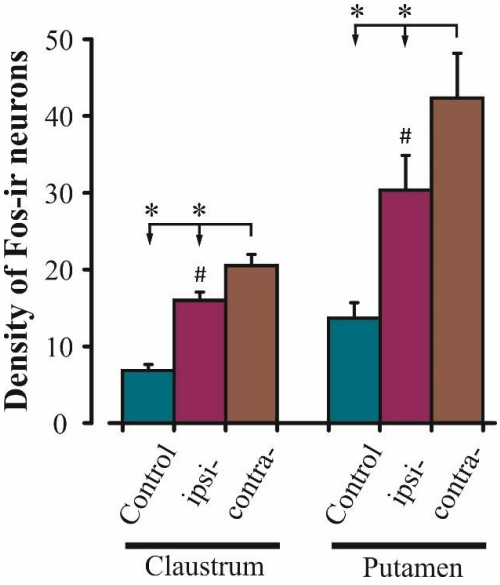

Fig. 2. The mean density ± SEM of Fos-ir neurons in claustrum and ventral part of putamen at the levels A+11/12 (within 400 x 400 μm^2 areas in the cat brain sections) in control animals (unilateraly) and on ipsil- and contralateral side of the cats brain after injection of complete Freund's adjuvant. Asterisks indicate signi?cant differences in the density of labeled cells between those in control animals and cats after injection of complete Freund's adjuvant on contralateral side; sign # - control mean density vs. ipsilateral mean density of adjuvant injected cats.

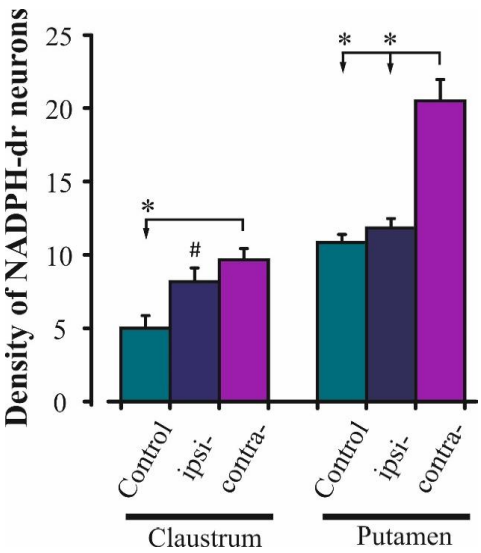

Fig. 3. The mean density ± SEM of NADPH-dr neurons in claustrum and ventral part of putamen at the levels A+11/12 (within 400 x 400 μm^2 areas in the cat brain sections) in control animals (unilateraly) and on ipsil- and contralateral side of the cats brain after injection of complete Freund's adjuvant. Asterisks indicate significant differences in the density of labeled cells between those in control animals and cats after injection of complete Freund's adjuvant on contralateral side; sign # - control mean density vs. ipsilateral mean density of adjuvant injected cats.

compared with the control.

It is known that changes in neuronal activity within the CNS structures are mainly initiated by the inflow of nociceptive signals from high-threshold muscle afferents [5]. Moreover, nociceptive information from inflamed muscles can be transmitted not only through the spinothalamic tract, but also through direct and indirect pathways to the hypothalamus and limbic structures [8, 9, 22]. Also it was shown that intraplantar application of CFA induced expression of microglial and astrocytic markers and proinflammatory cytokines IL1b and IL-6 (involved in inflammation and immune reaction) at the spinal level, brainstem, and forebrain (cerebral hemispheres, limbic system, thalamus, hypothalamus, and corpus callosum) [24].

According to the H. Sherk and K. Shima et al. [26, 27] the claustrum is a telencephalic structure characterized as a subcortical nucleus connected reciprocally with the cerebral cortex. The connections between the CL and the neocortex are well organized. Areas of cortex within one lobe that are interconnected with cortico-cortical connections share afferent and efferent projection zones in the CL, suggesting their interactions by way of convergent inputs. In addition, K. Shima et al. showed that neural activity in the supplementary motor area and precentral motor cortex both projected to the CL [27]. Numerous neuroanatomical studies in the cat and monkey have revealed widespread connections between the claustrum and most allocortical and neocortical regions. Thus, the CL is interconnected with the frontal lobe including motor cortex, prefrontal cortex and cingulate cortex, visual cortical regions in the occipital lobe, temporal and temporopolar cortices, parietooccipital and posterior parietal cortex, the frontoparietal operculum, somatosensory areas, prepiriform olfactory cortex and the entorhinal cortex. The CL is also connected to the hippocampus, amygdala, and caudate nucleus. [4]. In addition, significant influence on neuronal activation under nociceptive stimulation is pain anticipation (medial frontal cortex, cerebellum), attention to pain (anterior cingulate cortex, dorsolateral prefrontal cortex), emotional aspects of pain (CL closely connected to amygdala) and motor control [10]. In our study, apparently, nociceptive information could be transmitted to the CL via the most of the above-mentioned structures. However, it is quite a difficult task to accurately identify all possible nociceptive inputs to the CL and to separate the emotional, motor, as well as auditory and visual components, which requires a lot of additional research.

As mentioned above, significant changes in c-Fos expression levels were also observed in putamen. The Pu, together with the caudate nucleus, makes up the striatum, a major site of cortical and subcortical input into the basal ganglia. Although the putamen is frequently activated during pain, its role during pain has often been assumed to be related to motor processing [29]. However, it was shown that the putamen may contribute to the

processing of sensory aspects of pain. The striatum is rich in opioid receptors and contains nociceptive neurons responsive to graded noxious stimuli [2, 29]. Although the Pu is mutually related to the CL [17], it is quite problematic to assess their mutual influence.

In our study, NADPH-dr/NOS-containing neurons in CL and Pu were found to be twice larger in comparison with the controls. Earlier it was shown that NO is involved in the development of both acute and chronic inflammation, and different NOS inhibitors demonstrate an anti-inflammatory action [6]. An NO-mediated increase/decrease in the cerebral neuronal activity results probably from activation/inhibition of different ion channels in the neuronal membranes [25, 30]. D.V. Hinova-Palova et al. showed that there are two populations of NADPH-dr neurons in the CL. One population, consisting of large and medium-sized positive neurons, represents projection neurons, while the other population of small positive neurons corresponds to local circuit neurons [13] and only the densely stained cells were GABA immunoreactive [11]. In our experiments, it was found that a large number of NADPH-dr neurons are localized in Pu, especially in the ventral part. It was shown that NO-generating interneurons are key modulators of neuronal activity in Pu in rats and are intensely innervated by glutamatergic and dopaminergic-afferent projections from the substantia nigra [15], as well as that NO regulates signaling cascades in intermediate chains of the system central nucleus amygdala-substantia nigra-putamen-thalamus [19].

Conclusions

1. The results of the study of the Fos-ir neurons distribution in CL and Pu under conditions of long-term muscles inflammation indicate the active involvement of the mentioned structures in the formation of adaptive reactions.

2. The increase in the number of neurons with NADPH-d-positivity in CL and Pu indicates that NO-signals play a significant role in the formation and amplification of the response to painful impulses from inflamed muscles.

3. Further research is needed to accurately identify all possible nociceptive inputs to the CL and to separate the emotional, motor, auditory, and visual components that may accompany nociceptive processes.

References

[1] Abbadie, C., & Besson, J. M. (1992). c-fos expression in rat lumbar spinal cord during the development of adjuvant-induced arthritis. *Neuroscience,* (48), 985-993. doi: 10.1016/0306-4522(92)90287-c

[2] Baumgartner, U., Buchholz, H. G., Bellosevich, A., Magerl, W., Siessmeier, T., Rolke, R., & Schreckenberger, M. (2006). High opiate receptor binding potential in the human lateral pain system. *Neuroimage,* 30(3), 692-699. doi: 10.1016/j.neuroimage.2005.10.033

[3] Braz, J. M., Nassar, M. A., Wood, J. N., & Basbaum, A. I. (2005). Parallel "pain" pathways arise from subpopulations of primary afferent nociceptor. *Neuron,* 47(6), 787-793. doi: 10.1016/j.neuron.2005.08.015

[4] Crick, F. C., & Koch, C. (2005). What is the function of the claustrum? *Philosophical Transactions of the Royal Society B: Biological Sciences,* 360(1458), 1271-1279. doi: 10.1098/rstb.2005.1661

[5] Darques, J. L., & Jammes, Y. (1997). Fatigue-induced changes in group IV muscle afferent activity: differences between high- and low-frequency electrically induced fatigues. *Brain Research,* 750(1-2), 147-154. doi: 10.1016/s0006-8993(96)01341-8

[6] Gad, M. Z., & Khattab, M. (2000). Modulation of nitric oxide synthesis in inflammation. Relationship to oxygen-derived free radicals and prostaglandin synthesis. *Arzneimittelforschung,* 50(5), 449-455. doi: 10.1055/s-0031-1300229

[7] Garthwaite, J., & Boulton, C. L. (1995). Nitric oxide signaling in the central nervous system. *Annual Review of Physiology,* (57), 683-706.

[8] Giesler, G. J., Katter, J. T., & Dado, R. J. (1994). Direct spinal pathways to the limbic system for nociceptive information. *Trends in Neurosciences,* 17(6), 244-250. doi: 10.1016/0166-2236(94)90007-8

[9] Govsa, F., Kayalioglu, G., Erdem, B. Maisky, V. A., & Hariri, N. (1998). Laminar distribution of the sources of ascending spino-supraspinal pathways involved in nociceptive transmission and pain modulation. *Turkish Journal of Medical Sciences,* 28(1), 41-46.

[10] Gracely, R. H., Geisser, M. E., Giesecke, T. B., Grant, M. A., Petzke, F., Williams, D. A., & Clauw, D. J. (2004). Pain catastrophizing and neural responses to pain among persons with fibromyalgia. Brain, 127(4), 835-843. doi: 10.1093/brain/awh098

[11] Guirado, S., Real, M. Á., Olmos, J. L., & Dávila, J. C. (2003). Distinct types of nitric oxide-producing neurons in the developing and adult mouse claustrum. *Journal of Comparative Neurology,* 465(3), 431-444. doi: 10.1002/cne.10835

[12] Harris, J. A. (1998). Using c-fos as a neural marker of pain. *Brain Research Bulletin,* 45(1), 1-8. doi: 10.1016/s0361-9230(97)00277-3

[13] Hinova-Palova, D. V., Paloff, A., Christova, T., & Ovtscharoff, W. (1997). Topographical distribution of NADPH-diaphorase-positive neurons in the cat's claustrum. *European Journal of Morphology,* 35(2), 105-116. doi: 10.1076/ejom.35.2.105.13068

[14] Holscher, C. (1997). Nitric oxide, the enigmatic neuronal messenger: its role in synaptic plasticity. *Trends in Neurosciences,* (57), 683-706. doi: 10.1146/annurev.ph.57.030195.003343

[15] Hoque, K. E., Indorkar, R. P., Sammut, S., & West, A. R. (2010). Impact of dopamine-glutamate interactions on striatal neuronal nitric oxide synthase activity. *Psychopharmacology,* 207(4), 571-581. doi: 10.1007/s00213-009-1687-0

[16] Hsu, S.-M., Raine, L., & Fanger, H. (1981). Use of avidin-biotin-peroxidase complex (ABC) in immunoperoxidase techniques: a comparison between ABC and unlabelled antibody (PAP) procedures. *Journal of Histochemistry & Cytochemistry,* 29(4), 577-580. doi: 10.1177/29.4.6166661

[17] Kapakin, S. (2011). The claustrum: three-dimensional reconstruction, photorealistic imaging, and stereotactic approach. *Folia morphologica,* 70(4), 228-234.

[18] Khalsa, P. S. (2004). Biomechanics of musculoskeletal pain: dynamics of the neuromatrix. *Journal of Electromyography*

and Kinesiology, 14(1), 109-120. doi: 10.1016/j.jelekin.2003.09.020

[19] Man'kovskaya, Y. P., Vlasenko, O. V., & Suprunov, K. V. (2012). Expression of c-Fos Protein and Activity of NO Synthase in the Mesolimbic Dopaminergic Structures and Dorsolateral Striatum of Rats Realizing Operant Food-Procuring Reflexes. *Neurophysiology,* 44(6), 433-440.

[20] Mense, S. (1993). Nociception from skeletal muscle in relation to clinical muscle pain. *Pain,* (54), 241-289. doi: 10.1016/0304-3959(93)90027-M

[21] Mikula, S., Trotts, I., Stone, J., & Jones, E. G. (2007). Internet-Enabled High-Resolution Brain Mapping and Virtual Microscopy. *Neuroimage,* 35(1), 9-15. doi: 10.1016/j.neuroimage.2006.11.053

[22] Neugebauer, V., & Li, W. (2002). Processing of nociceptive mechanical and thermal information in central amygdala neurons with knee-joint input. *Journal of Neurophysiology,* 87(1), 103-112. doi: 10.1152/jn.00264.2001

[23] Perrin-Terrin, An-S., Jeton, F., Pichon, A., Frugiere, A., Richalet, Jean-P., Bodineau, L., & Voituron, N. (2016). The c-Fos protein immunohistological detection: A useful tool as a marker of central pathways involved in specific physiological responses in vivo and ex vivo. *Journal of Visualized Experiments,* 110(e), 53613. doi: 10.3791/53613

[24] Raghavendra, V., Tanga, F. Y., & DeLeo, J. A. (2004). Complete Freunds adjuvant-induced peripheral inflammation evokes glial activation and proinflammatory cytokine expression in the CNS. *European Journal of Neuroscience*, 20(2), 467-473. doi: 10.1111/j.1460-9568.2004.03514.x

[25] Schmid, H. A., & Pehl, U. (1996). Regional specific effects of nitric oxide donors and cGMP on the electrical activity of neurons in the rat spinal cord. *Journal of Chemical Neuroanatomy,* 10(3-4), 197-201. doi: 10.1016/0891-0618(96)00143-3

[26] Sherk, H. (1986). *The claustrum and the cerebral cortex.* In: Cerebral Cortex. Sensory-Motor Areas and Aspects of Cortical Connectivity, edited by E. G. Jones and A. Peters, (5), 467-499.

[27] Shima, K., Hoshi, E., & Tanji, J. (1996). Neuronal activity in the claustrum of the monkey during performance of multiple movements. *Journal of Neurophysiology,* 76(3), 2115-2119. doi: 10.1152/jn.1996.76.3.2115

[28] Spike, R. C., Todd, A. J., & Johnston, H. M. (1993). Coexistence of NADPH-diaphorase with GABA, glycine, and acetylcholine in rat spinal cord. *Journal of Comparative Neurology,* 335(3), 320-333. doi: 10.1002/cne.903350303

[29] Starr, C. J., Sawaki, L., Wittenberg, G. F., Burdette, J. H., Oshiro, Y., Quevedo, A. S. ... Coghill, R. C. (2011). The contribution of the putamen to sensory aspects of pain: insights from structural connectivity and brain lesions. *Brain,* 134(7), 1987-2004. doi: 10.1093/brain/awr117

[30] Steffens, H., Schomburg, E. D., Maznychenko, A. V., Maisky, V. A., Kostyukov, A. I., & Pilyavskii, A. I. (2007). Monosynaptic refexes, *c-fos* expression, and NADPH-Diaphorase Activity in the cat spinal cord: changes induced by chronic muscle infammation. *Neurophysiology,* 39(3), 191-200.

[31] Vereshchaka, I. V., Bulgakova, N. V., Maznychenko, A. V., Gonchar, O. O., Prylutskyy, Y. I., Ritter, U., & Kostyukov, A. I. (2018). C60 fullerenes diminish muscle fatigue in rats comparable to N-acetylcysteine or beta-Alanine. *Frontiers in Physiology,* 9(12). doi: 10.3389/fphys.2018.00517

[32] Vincent, S. R., & Kimura, H. (1992). Histochemical mapping of nitric oxide synthase in the rat brain. *Neuroscience,* 46(4), 755-784. doi: 10.1016/0306-4522(92)90184-4

[33] Wei, F., Dubner, R., & Ren, K. (1999). Dorsolateral funiculus-lesions unmask inhibitory or disfacilitatory mechanisms which modulate the effects of innoxious mechanical stimulation on spinal Fos expression after inflammation. *Brain Research,* (820), 112-116. doi: 10.1016/s0006-8993(98)01359-6

ЗМІНИ C-FOS ЕКСПРЕСІЇ ТА NADPH-D АКТИВНОСТІ У КЛАУСТРУМІ, ВИКЛИКАНІ ХРОНІЧНИМ ЗАПАЛЕННЯМ М'ЯЗІВ У КОТІВ (ПОПЕРЕДНЄ ДОСЛІДЖЕННЯ)

Мазниченко А. В. Абрамович Т. І., Соколовска І. В.

Дослідження центральних механізмів, що лежать в основі м'язового запалення і м'язово-скелетного болю, є важливим кроком для пошуку засобів профілактики та лікування м'язового запалення. Однією з недостатньо вивчених структур мозку, котрі приймають участь у передачі ноцицептивної інформації, є клауструм (CL). Тож метою дослідження було виявити зміни патернів Fos-імунореактивності та NADPH-діафореактивності в CL і додатково у вентральній частині ядра путамен (Pu) в умовах хронічного запалення триголового м'яза литки кішки, спричиненого внутрішньом'язовим введенням повного ад'юванта Фроїнда (ПАФ). Імуногістохімічні та гістохімічні методи були використані для виявлення Fos-імунореактивних (Fos-ip) і NADPH-діафоразореактивних (NADPH-dp) нейронів у досліджуваних структурах. З'ясувалося, що через дев'ять днів після запалення м'язів, спричиненого ПАФ, рівень Fos-імунореактивності та NADPH-d-реактивності в CL і у вентральній частині Pu збільшився вдвічі порівняно з контролем. Оскільки CL взаємопов'язана з багатьма структурами кори та підкірковими структурами мозку, всі ці структури можуть бути шляхами передавання ноцицептивної інформації, проте, можна припустити, що центральне ядро мигдалика може вносити основний ноцицептивний внесок до процесу активації нейронів в CL. Відомо, що CL взаємно пов'язана з Pu, проте оцінити їх взаємний вплив у даному дослідженні не було можливим. Результати дослідження розподілу Fos-ip нейронів у CL і Pu в умовах тривалого запалення м'язів свідчать про активну участь зазначених структур у формуванні адаптивних реакцій. Збільшення кількості нейронів з NADPH-d реактивністю в CL і Pu свідчить про те, що NO-сигнали відіграють значну роль у формуванні та посиленні відповіді на больову імпульсацію від запалених м'язів. Крім того, необхідні подальші дослідження для точного визначення всіх можливих ноцицептивних входів у CL і розділення емоційних, моторних, слухових і зорових компонентів, які можуть супроводжувати ноцицептивні процеси.

Ключові слова: *запалення м'язів, повний ад'ювант Фроїнда, клауструм, путамен, кішка.*

DOI: 10.31393/morphology-journal-2022-28(4)-10 Reports of Morphology, Vol. 28, №4, Pages 70-76

ISSN 1818-1295 eISSN 2616-6194

REPORTS OF MORPHOLOGY

Official Journal of the Scientific Society of Anatomists, Histologists, Embryologists and Topographic Anatomists of Ukraine

journal homepage: https://morphology-journal.com

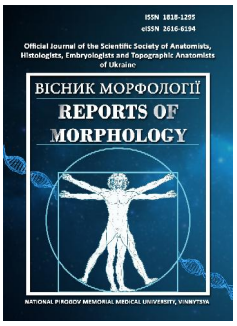

Rats' thyroid gland histological and ultrastructural changes 30 days after the experimental thermal injury on the background of NaCl injection

Tiron O. I.

Odesa National Medical University, Odesa, Ukraine

ARTICLE INFO

Received: 9 September 2022

Accepted: 7 October 2022

UDC: 616.441:599.323.4:615.459

CORRESPONDING AUTHOR

e-mail: chekina.o@ukr.net

Tiron O. I.

CONFLICT OF INTEREST

The authors have no conflicts of interest to declare.

FUNDING

Not applicable.

Very frequent natural and man-made disasters as well as current military conflicts are accompanied by injuries complicated by acute blood loss, burns and shock of different degrees of severity. Thermal injuries are one of the world modern medicine most urgent medical and social problems including the same in Ukraine. In response to a burn injury a significant number of pathological processes develop in the body which manifestation involves almost all organs and systems, leading to an expressed homeostasis disturbance and adaptative processes disorder. Thyroid gland is the one of the first which receives the alterative influence in conditions of both threshold and suprathreshold thermal exposure. The purpose of the work is to establish histological and ultrastructural changes in the thyroid gland of experimental animals 30 days after thermal skin injury. Experimental studies were conducted on 90 white male rats. Skin thermal burns were simulated using four copper plates application to previously depilated lateral surfaces of the rats' body for 10 s. Rats were injected with a 0.9 % saline into the vena cava inferior during the first 7 days of the post-burn period. Thyroid gland pieces were fixed in a 10 % neutral formalin solution, dehydrated in alcohols of increasing concentration and embedded in paraffin blocks. The prepared sections of 5-6 μm thickness were stained with hematoxylin-eosin. In the rats' thyroid gland the presence of complex changes of a destructive, adaptive-compensatory and regenerative nature was established on the 30th day after a skin burn against the background of 0.9 % NaCl administration. These changes indicate a relative organs hemodynamics normalization together with the structure of various diameters vessels walls which creates the basis for the follicular cells typical structure restoration and new follicles synthesis. The expressed osmiophily and thyrocyte nuclei pyknotization, cytoplasm vacuolization and follicle's lumen cells desquamation are revealed in the gland parenchyma. These are signs of the organ fibrosis which are supported by connective tissue amount in the stromal component increase. The thyroid gland parenchyma and the vessels surrounding it micro- and ultrastructural changes caused by the thermal altering influence have a time-dependent expression which transforms from predominantly destructive to predominantly restorative throughout the 30-day post-burn period. The authors are sure that the detected morphological changes of the gland have a time-dependent reversibility which is important to consider from both the time-course and the quantitative aspects taking into account the pathogenetically based scheme of pharmacocorrection. The 30th day of the post-burn pathological process manifestation characterizes by a certain imbalance in the compensatory, restorative and synthetic processes manifestation as well as in the destructive and decompensatory processes manifestation which gives reason to hope for the thyroid gland functioning restoration together with organs and systems in case of pathogenetically determined pharmacological treatment administration. Taking into account the thyroid gland morpho-functional changes wave-like dynamics the authors believe that sanogenetic mechanisms activation might occurs which will allow to prescribe the complex pathogenetically determined correction assuming the above-mentioned patho- and sanogenetic mechanisms dynamics.

Keywords: *thyroid gland, thermal burn, post-burn period, morphological changes, restorative processes, pathogenetic mechanisms.*

Introduction

Very frequent natural and man-made disasters, as well as current military conflicts, are accompanied by injuries complicated by acute blood loss, burns and shock of varying degrees of severity.

Thermal injuries are one of the most urgent medical and social problems of modern medicine in the world, including in Ukraine [4, 10]. In our country, more than 45,000 people suffer from burns every year, they occupy the third place in the structure of mortality, as a result of all received injuries, inferior in frequency only to traffic injuries [13, 18]. The urgency of the burn injury problem is determined by the frequent damage to adults and children, the complexity and duration of treatment, long-term disability and relatively high mortality. Despite the significant progress achieved in the treatment of this pathology, the mortality rate among severely burned patients remains high, especially with critical (40-50% of the body surface) and supercritical (over 50%) deep burns [11, 20].

In response to a burn injury, a significant number of pathological processes develop in the body, the manifestation of which involves almost all organs and systems, leading to a marked violation of homeostasis, disruption of adaptation processes, etc. [9]. One of the most important aspects of a burn injury, which directly affects the severity of its pathogenetic mechanisms, is endocrine dysregulation at the initial stages of the pathological process, which manifests itself as significant metabolic disorders, the direction and severity of which are directly related to the level of endogenous hormones [1].

In this aspect, we were interested in the changes that occur during thermal burns in the thyroid gland, since it plays one of the leading roles in the endocrine regulation of most body functions [2, 3, 14]. Secondly, this gland of internal secretion occupies an important place in the structure of hierarchical hypothalamic-pituitary regulation, and, thirdly, taking into account the anatomical and morphological features of the localization and structure of the thyroid gland, it primarily "takes on" altering traumatic influences, thereby modifying the most functional state of organs and tissues of the human body [7, 9].

We traced the histological changes in the structure of the thyroid gland and the periglandular environment, starting from 24-72 hours post-thermal period [16, 17]. In the first hours and days after a skin burn, the structural changes in the thyroid gland affected mainly the structure of the vascular component of the gland, its stroma and parenchyma and had mainly the character of adaptation and/or compensation [16]. In the urgent aspect, our research lasted 30 days, which prompted us to carefully examine the volume of morphological changes in the structure of the thyroid gland during this time interval. On the other hand, we were guided by a wide range of regulatory hormonal effects of the thyroid gland on organs, organ systems, and regulatory systems of the biological organism, which, in our opinion, determines the primary reactions in response to thermal injuries [1-3, 5, 12, 14].

It is important to imagine that the thyroid gland under the influence of temperature factors of threshold and suprathreshold intensity, taking into account the large-scale redundant feedback mechanisms, the wide spectrum of physiological activity of thyroid hormones, the structural-functional organization and morpho-functional features, is one of the first to fall under thermal shock [12]. With structural and functional changes in the organs of the affected and/or burned organism, including the thyroid gland, dysfunctions of many organs and systems are involved in the mediation of the pathological process, in particular, the blood, cardiovascular, respiratory, and other systems [1, 10, 20]. Pathogenetic mechanisms of the primary and related pathological processes induced by burn damage to the thyroid gland are insufficiently studied, which is a consequence of, firstly, unexplained morpho-functional dysfunctions of the parenchyma of the gland in the dynamics of the burn effect and, secondly, unexplored chains of the "vicious circle" pathological processes that are determined by thyroid dysfunction and occur with the participation of other organs and body systems.

However, studies of the structural reconstruction of the vascular bed of the thyroid gland during burns, especially in the time-delayed stages after the application of thermal exposure, are insufficient and require further research, especially with an emphasis on efforts to correct the morpho-functional disorders formed during a burn injury.

The aim of the work is to determine histological and ultrastructural changes in the thyroid gland of experimental animals 30 days after simulated thermal skin injury.

Materials and methods

Experimental studies were conducted on 90 white male rats weighing 160-180 g (obtained from the vivarium of the Institute of Pharmacology and Toxicology of the National Academy of Sciences of Ukraine) on the basis of the research center of National Pirogov Memorial Medical University, Vinnytsya. Keeping, processing and manipulation of animals was carried out in accordance with the "General Ethical Principles of Animal Experiments" adopted by the Fifth National Congress on Bioethics (Kyiv, 2013), while being guided by the recommendations of the European Convention on the Protection of Vertebrate Animals for Experimental and Other Scientific Purposes (Strasburg, 1985), methodological recommendations of the Ministry of Health of Ukraine "Preclinical studies of drugs" (2001) and the rules of humane treatment of experimental animals and conditions approved by the Bioethics Committee of the National Pirogov Memorial Medical University, Vinnytsya (protocol No. 1 dated January 14, 2010).

Thermal skin burns of the 2nd-3rd degree were simulated by pressing four copper plates (the surface area of each was 13.86 cm^2) to the prematurely depilated lateral surfaces of the body of rats for 10 s. Experimental animals

were heated in water with a temperature of 100°C for 6 minutes before the start of the experiment [6]. The total area of skin damage was equal to 21-23 %. During the first 7 days of the post-burn period, rats were injected with 0.9 % physiological NaCl solution into the inferior vena cava. Rats were shaved, vein catheterized, skin burned, and decapitated under propofol (i/v, 60 mg/kg) anesthesia.

Material collection for microscopic studies was carried out according to generally accepted methods [8]. Pieces of the thyroid gland were fixed in a 10 % neutral formalin solution, dehydrated in alcohols of increasing concentration, and embedded in paraffin blocks. The prepared sections, 5-6 μm thick, were stained with hematoxylin-eosin [8].

Histological preparations were studied with the help of a light microscope MICROmed SEO SCAN ("Sumi Electron Optics", Sumy, Ukraine) and photo-documented with the help of a Vision CCD Camera with a system of image output from histological preparations. For electron microscopic studies, pieces of the thyroid gland were taken, fixed in a 2.5 % glutaraldehyde solution, and postfixed with a 1 % osmium tetroxide solution in a phosphate buffer. Further processing was carried out according to the generally accepted methodology [8]. Semi-thin sections were stained with methylene blue. Ultrathin sections, made on an LKB-3 ultramicrotome, were contrasted with uranyl acetate, lead citrate according to the Reynolds method and studied in a PEM-125K electron microscope.

All morphological studies were carried out within the scope of the Agreements on Scientific Cooperation between the Department of Histology, Cytology and Embryology of Odesa National Medical University and the Research Center of National Pirogov Memorial Medical University, Vinnytsya (from 01.01.2018), as well as the Department of Histology and Embryology of I. Horbachevsky Ternopil National Medical University (from 01.01.2019).

Results

Histologically, 30 days after a skin burn against the background of the introduction of a 0.9 % NaCl solution in the thyroid gland of experimental animals, we found destructive, adaptive-compensatory and regenerative processes in the follicle wall, vascular bed and stromal component.

In this period of the experiment, at the morphological level between the lobes of the organ and in the interfollicular space, wide layers of connective tissue were observed in places, which is a consequence of the activation of fibroblasts and the process of collagen formation in the previous periods. Single neutrophils, basophils, and macrophages were present among the collagen and elastic fibers of the connective tissue framework (Fig. 1).

30 days after the skin burn, against the background of administration of 0.9 % NaCl solution, moderate blood filling and isolated stasis were noted in the vascular network of the organ. The vessel walls were characterized by moderate edema, which was mainly found in the adventitia. Arterioles, hemocapillaries, and venules had a relatively preserved wall

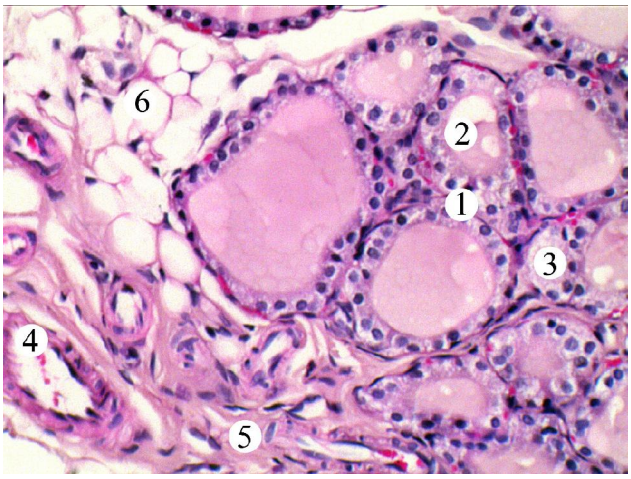

Fig. 1. Histological changes in the thyroid gland of an animal 30 days after a skin burn against the background of administration of a 0.9% NaCl solution. 1 - thyrocytes with areas of light cytoplasm; 2 - colloid with resorption vacuoles, 3 - interfollicular island, 4 - blood vessel, 5 - layers of connective tissue, 6 - adipocytes. Staining with hematoxylin and eosin. Magnification x400.

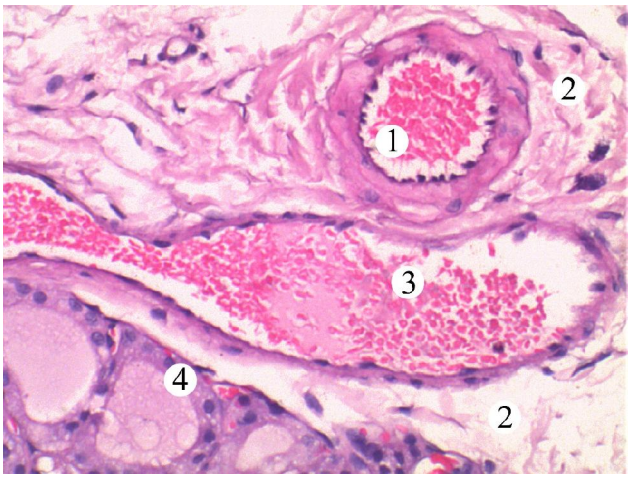

Fig. 2. Microscopic changes in the vessels of the thyroid gland of an animal 30 days after a skin burn against the background of administration of a 0.9 % NaCl solution. 1 - arteriole with 2 - perivascular edema, 3 - venule, 4 - follicle. Staining with hematoxylin and eosin. Magnification x400.

structure, with well-contoured endothelium and moderate lumen width (Fig. 2).

At the microscopic level, 30 days after the skin burn, follicles, mostly of medium size, filled with oxyphilic colloid of a homogeneous structure and lined with low-prismatic thyrocytes, were observed against the background of saline injection. Their rounded-oval nuclei were intensely basophilic, which indicates the predominance of heterochromatin in the karyoplasm. The cytoplasm of many follicular cells had areas of lightening (see Fig. 1). There were also follicles in the composition of the lobes of the organ, the wall of which was formed by flat epitheliocytes with their desquamation into the lumen, and resorption vacuoles were contained in the colloid. It should be noted that interfollicular islands of various sizes were histologically

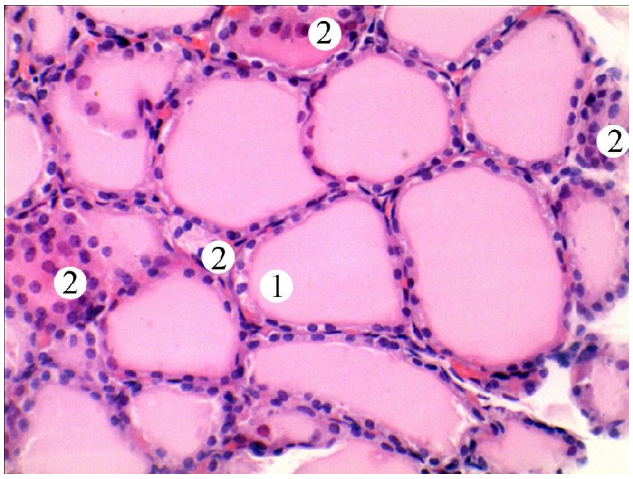

Fig. 3. Histological changes in the thyroid gland of an animal 30 days after a skin burn against the background of administration of a 0.9 % NaCl solution. 1 - follicle lined with flat thyrocytes and 2 - interfollicular islands. Staining with hematoxylin and eosin. Magnification x400.

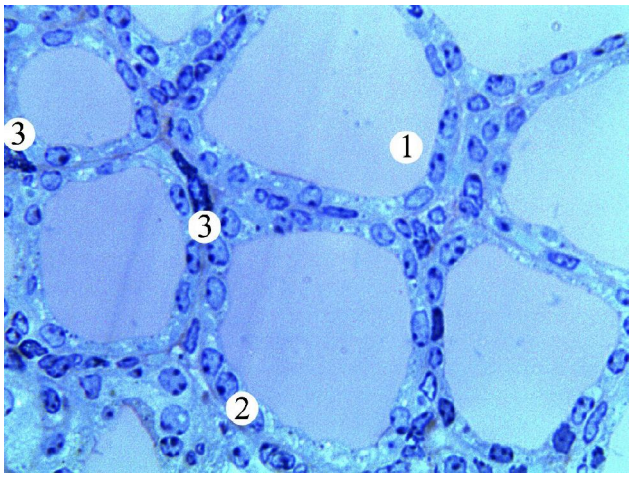

Fig. 4. Microscopic changes in the thyroid gland of an animal 30 days after a skin burn against the background of administration of a 0.9 % NaCl solution. 1 - homogeneous colloid, 2 - thyrocytes, 3 - basophils. Semi-thin cut. Staining with methylene blue. Magnification x400.

detected, the cells of which had moderately basophilic nuclei and moderately oxyphilic cytoplasm. This may indicate reparative processes in the organ (Fig. 3).

On semi-thin sections stained with methylene blue, basophils, the cytoplasm of which contained numerous intensively basophilic granules, were clearly visible in the interfollicular lumens at this time of the experiment. There were thyrocytes with a completely heterochromatin pattern of the nucleus (Fig. 4).

The condition of the thyroid gland of the experimental animals at the ultrastructural level 30 days after the skin burn against the background of the introduction of 0.9 % NaCl solution testified to the changes established by us during microscopic analysis. The low-prismatic thyrocytes of the middle follicles contained an osmiophilic nucleus with numerous lumps of heterochromatin and intussusceptions of karyolemma. A significant number of organelles of the protein-synthesizing apparatus were observed in their cytoplasm.

In particular, most mitochondria were hypertrophied, with partially reduced cristae. The tubules of the granular endoplasmic reticulum are locally significantly expanded, and in some places they are vacuole-like, which could create areas of illumination at the light-optical level. The plasmalemma of the apical pole of thyrocytes formed a moderate number of microvilli. The basement membrane was characterized by tortuosity and contouring (Fig. 5).

Flat thyrocytes contained a pyknotically altered nucleus in the center of the cell. Damaged tubules of the granular endoplasmic reticulum, mitochondria with indistinct cristae and vacuole-like structures with homogeneous content were observed in their cytoplasm, and clusters of osmiophilic lysosomes were observed near the apex of the cell. The plasmalemma at the apical pole contained wide microvilli (Fig. 6).

The ultrastructure of the blood capillaries of the thyroid gland of experimental animals 30 days after a skin burn against the background of administration of a 0.9 % NaCl solution was characterized by the preservation of the wall and the moderate width of the lumen. Endotheliocyte nuclei had shallow invaginations of the karyolemma and a significant amount of heterochromatin in the karyoplasm. In the cytoplasm, the main mass of pinocytotic vesicles is concentrated near the lumenal surface, but the number of microvilli on it is insignificant.

The basement membrane is slightly thickened. Single cells of the leukocyte row and platelets were often observed in the lumen (Fig. 7).

30 days after a skin burn against the background of the

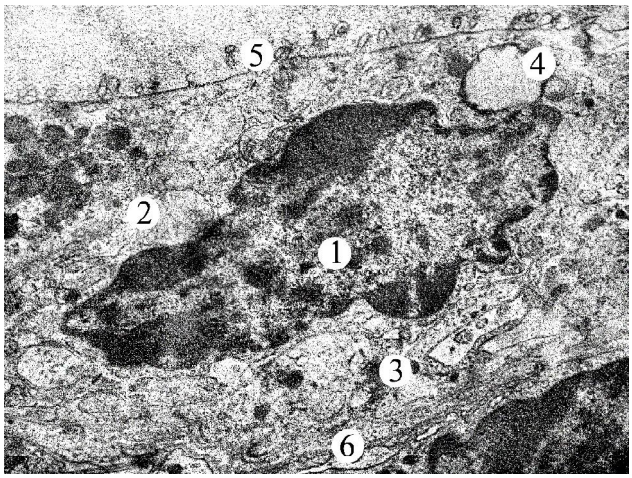

Fig. 5. Ultrastructure of the wall of the follicle of the thyroid gland of an animal 30 days after a skin burn against the background of administration of a 0.9% NaCl solution. 1 - thyrocyte nucleus, 2 - mitochondrion, 3 - tubules of the granular endoplasmic reticulum, 4 - vacuole-like structure, 5 - microvilli on the apical surface, 6 - basement membrane. Electrogram. Magnification x14 000.

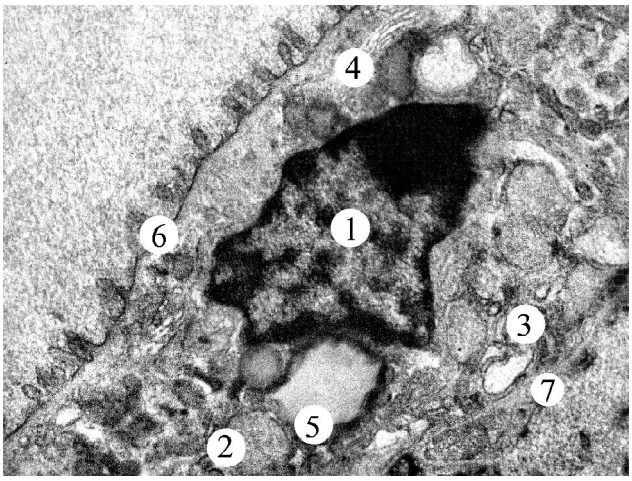

Fig. 6. Ultrastructure of the wall of the follicle of the thyroid gland of an animal 30 days after a skin burn against the background of administration of a 0.9% NaCl solution. 1 - thyrocyte nucleus, 2 - mitochondrion, 3 - tubules of granular endoplasmic reticulum, 4 - Golgi complex, 5 - vacuole-like structure with homogeneous content, 6 - microvilli on the apical surface, 7 - basement membrane. Electrogram. Magnification x14 000.

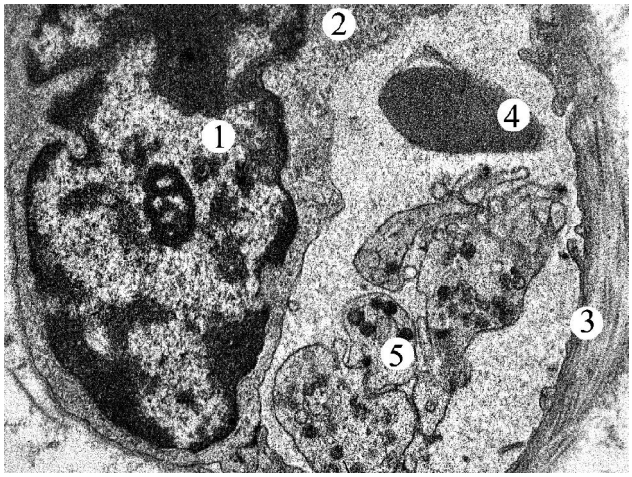

Fig. 7. Ultrastructural organization of the hemocapillary of the thyroid gland of an animal 30 days after a skin burn against the background of administration of a 0.9 % NaCl solution. 1 - nucleus and 2 - cytoplasm of endotheliocyte, 3 - basement membrane, 4 - erythrocyte and aggregation of platelets in the capillary lumen. Electrogram. Magnification x12 000.

introduction of a 0.9 % NaCl solution, a large number of thin collagen fibrils and already well-formed collagen fibers were noted in the stroma of the thyroid gland of experimental animals. The ultrastructure of fibroblasts was characteristic of the state of functional activity: euchromatin pattern of the nucleus, expanded tubules of the granular endoplasmic reticulum in the cytoplasm, with numerous mitochondria between them.

Discussion

Thus, 30 days after skin burn against the background of administration of 0.9 % physiological NaCl solution in the thyroid gland of rats, the presence of complex changes of a destructive, adaptive-compensatory and regenerative nature was established. At the ultrastructural level, the relative normalization of the hemodynamics of the organ and the structure of the vessel walls of various calibers has been proven, which, in our opinion, creates the basis for the restoration of the typical structure of follicular cells and the synthesis of new follicles, which is evidenced by a significant number of interfollicular islands. Therefore, the obtained data can be verified as intensifying synthetic processes in the structural units of the endocrine gland.

However, along with optimistic intraglandular changes, we note that during this period of the experiment, signs of destructive changes are preserved directly in the parenchyma of the gland, which are manifested by significant osmiophily and pyknotization of thyrocyte nuclei, vacuolization of the cytoplasm, and desquamation of cells into the lumen of the follicle. The result of the active activity of fibroblasts in the earlier periods of the experiment are signs of fibrosis of the organ, as evidenced by an increase in the amount of connective tissue in the stromal component.

Summarizing, we note that the 30th day of the course of the post-burn pathological process is characterized by a certain imbalance in the manifestation of both compensatory, restorative and synthetic processes, on the one hand, and destructive, decompensatory processes, on the one hand, which in general gives us reason to hope that in the case of assigning rats model conditions of pathogenetically determined pharmacological treatment of the functioning of the thyroid gland, as well as organs and systems in the animal body will be not only in a compensated, but also in a pronounced restorative state and in the presence of stimulating hormonal and biochemical processes.

Tracking the course of the 30-day period after the skin burn and analyzing the morpho-functional changes of the thyroid gland, we note that they underwent a significant reversal from the supposedly irreversible and degenerative during the first 7 days of the experiment to those noted according to the results of the reported studies and which have a more pronounced restorative effect orientation We will recall that micro- and sub-microscopic studies 1 day after thermal damage revealed only primary and/or reactive auxiliary-compensatory changes and initial manifestations of destruction of the thyroid parenchyma [16]. At the same time, only after 3 days, the initial signs of a heat-induced "stress reaction" in the form of intrathyroidal parenchymal, stromal, and vascular lesions were revealed [17]. Note that the dependence of the morpho-functional changes of the thyroid gland on time that we discovered is, firstly, inherent in such changes during post-traumatic and post-stress periods [19] and, secondly, in a certain way consistent with the dynamics of the secretory activity of the gland and the anterior lobe of the pituitary gland [1, 3, 5, 12, 15].

Logically connecting the obtained results with efforts to develop a scheme for pathogenetically justified pharmacocorrection of burn damage to the thyroid gland,

the following should be stated: micro- and ultrastructural changes in the parenchyma of the thyroid gland and the vessels surrounding it due to the thermal altering effect have a time-dependent severity, which within 30-day post-fire period transforms from predominantly destructive to predominantly restorative. Secondly, the morphological changes of the gland traced by us have a time-dependent reversibility, which is important to take into account from the urgent aspect and from the quantitative aspect of the composition of the scheme of pathogenetically justified pharmacocorrection. Thirdly, we consider it probable, taking into account the wave-like dynamics of changes in the morpho-functional changes of the thyroid gland, to assume the activation of sanogenetic mechanisms by the mechanism of systemic-anti-systemic regulation, which will make it possible, under the conditions of a thorough study of the specified systemic-anti-systemic regulatory mechanisms, to prescribe a complex pathogenetically determined correction taking into account the above-mentioned dynamics patho- and sanogenetic mechanisms.

Conclusions

1. 30 days after a skin burn against the background of administration of a 0.9 % physiological solution of NaCl in the thyroid gland of rats, the presence of complex changes of a destructive, adaptive-compensatory and regenerative nature was established.

2. The indicated changes indicate relative normalization of the hemodynamics of the organ and the structure of the vessel walls of various sizes, which creates the basis for the restoration of the typical structure of follicular cells and the synthesis of new follicles. In the parenchyma of the gland, significant osmiophily and pyknotization of thyrocyte nuclei, vacuolization of cytoplasm, and desquamation of cells in the lumen of the follicle are revealed. There are signs of fibrosis of the organ, which is evidenced by an increase in the amount of connective tissue in the stromal component.

3. The micro- and ultrastructural changes of the parenchyma of the thyroid gland and the vessels surrounding it caused by the thermal altering effect have a time-dependent severity, which during the 30-day post-burn period transforms from predominantly destructive to predominantly restorative.

4. The morphological changes of the gland traced by us have a time-dependent reversibility, which is important to take into account from the urgent aspect and from the quantitative aspect of the composition of the pathogenetically justified pharmacocorrection scheme.

5. 30 days of the course of the post-burn pathological process is characterized by a certain imbalance in the manifestation of compensatory, restorative and synthetic processes, as well as destructive and decompensatory processes, which gives reason to hope for the restoration of the functioning of the thyroid gland, as well as organs and systems in the event of the appointment of pathogenetically determined pharmacological treatment.

6. Taking into account the wave-like dynamics of changes in the morpho-functional changes of the thyroid gland, we consider the activation of sanogenetic mechanisms to be probable, which will make it possible to prescribe a complex pathogenetically determined correction, taking into account the above-mentioned dynamics of patho- and sanogenetic mechanisms.

References

[1] Akmaev, I. G. (2001). *Нейро-иммунно-эндокринные взаимодействия: их роль в дизрегуляторной патологи [Neuro-immuno-endocrine interactions: their role in dysregulatory pathology].* Патол. Физиология - Patol. Physiology, (4), 3-10.

[2] Bassett, J. H. D. (2011). Thyroid hormone action: genomic and non-genomic effects. *Endocrine Abstracts*, (25), 6.1.

[3] Cardoso, L. F., Maciel, L. M., & Paula, F. J. (2014). The multiple effects of thyroid disorders on bone and mineral metabolism. *Arq. Bras. Endocrinol. Metabol,* 58(5), 452-463. doi: 10.1590/0004-2730000003311

[4] Cherniakova, H. M., Minukhin, V. V., & Voronin, Ye. P. (2016). Сучасний погляд на місцеве лікування опіків з інфекційною складовою [A modern view of the local treatment of burns with an infectious component]. *Вісник проблем біології і медицини - Herald of problems of biology and medicine,* 133(4), 68-72.

[5] Evdokimova, O. V., & Gorodetskaya, I. V. (2015). Влияние йодсодержащих тиреоидных гормонов на синтез белков теплового шока в головном мозге крыс при стрессе и адаптации [Influence of iodine-containing thyroid hormones on the synthesis of heat shock proteins in the brain of rats under stress and adaptation]. *Вестник Витебского государственного медицинского университа - Bulletin of Vitebsk State Medical Universitya*, 14(1), 18-25.

[6] Gunas, I., Dovgan, I., & Masur, O. (1997). *Method of thermal burn trauma correction by means of cryoinfluence.* Abstracts are presented in zusammen mit der Polish Anatomical Society with the participation of the Association des Anatomistes Verhandlungen der Anatomischen Gesellschaft, Olsztyn (p. 105). Jena - Munchen: Der Urban & Fischer Verlag.

[7] Hamblin, M. R. (2019). Novel pharmacotherapy for burn wounds: what are the advancements. *Expert opinion on pharmacotherapy,* 20(3), 305-321. doi: 10.1080/14656566.2018.1551880

[8] Horalskyi, L. P., Khomych, V. T., & Kononskyi, O. I. (2019). *Основи гістологічної техніки і морфофункціональні методи досліджень у нормі та при патології [Basics of histological technique and morphofunctional research methods in normal and pathological conditions].* Житомир: ЖНАЕУ - Zhytomyr: GNAEU.

[9] Jeschke, M. G., Gauglitz, G. G., Kulp, G. A., Finnerty, C. C., Williams, F. N., Kraft, R. ... Herndon, D. N. (2011). Long-term persistance of the pathophysiologic response to severe burn injury. *PloS one,* 6(7), e21245. doi: 10.1371/journal.pone.0021245

[10] Jeschke, M. G., van Baar, M. E., Choudhry, M. A., Chung, K. K., Gibran, N. S., & Logsetty, S. (2020). *Burn injury. Nat Rev Dis Primers,* 6(1), 11. doi: 10.1038/s41572-020-0145-5

[11] Kozynets, H. P. Komarov, M. P., & Voronin, A. V. (2014). Нова концепція розвитку комбустіологічної служби в Україні [A new concept of the development of the combustiological service in Ukraine]. *Вестник неотложной и восстановительной*

медицины - Bulletin of Emergency and Restorative Medicine, 15(1), 6-8.

[12] Mosiienko, H. P. (2007). Морфофункціональний стан гіпофізарно-тиреоїдної системи у хворих з функціональними розладами травного каналу [Morphofunctional state of the pituitary-thyroid system in patients with functional disorders of the alimentary canal]. *Лікарська справа - Medical case,* (3), 56-61.

[13] Nebesna, Z. M., & Yeroshenko, H. A. (2015). Гістологічні та гістохімічні зміни легень при експериментальній термічній травмі [Histological and histochemical changes of lungs in experimental thermal injury]. *Світ медицини та біології - World of Medicine and Biology,* 49(2), 106-110.

[14] Robbins, J., & Lakshmanan, M. (1992). The movement of thyroid hormones in the central nervous system. *Acta Medica Austriaca,* 19, 21-25. PMID: 1519446

[15] Strelchenko, Yu. I., Ziablitsev, S. V., & Yelskyi, V. M. (2012). Патофізіолоічні взаємозв'язки гіпофізарно-тиреоїдної та гіпофізарно-надниркової систем під впливом поляризованого світла в щурів із дозованим опіком відкритом полум'ям [Pathophysiological interrelationships of the pituitary-thyroid and pituitary-adrenal systems under the influence of polarized light in rats with a dosed open flame burn]. *Клін та эксперим патологія - Clinical and experimental pathology,* 11(2-3), 156-158.

[16] Tiron, O. I. (2019). Features of morphological changes in the thyroid gland of white male rats 1 day after thermal trauma of the skin on the background of the introduction of 0.9% NaCl solution. *Biomedical and Biosocial Anthropology,* (37), 55-59. doi: https://doi.org/10.31393/bba37-2019-09

[17] Tiron, O. I., Dzygal, O. F., Onufryenko, O. V., Komlevoi, O. M., Shapovalov, V. Yu., & Yatsyna, O. I. (2022). Thyroid gland parenchyma morphological abnormalities in rats on the third day after skin thermal burning. *World of Medicine and Biology,* 81(3), 231-235. doi: 10.26724/2079-8334-2022-3-81-231-235

[18] Ushkalenko, A. O. (2013). *Актуальність питання опікової хвороби та її ускладнень як основних причин летальності при опіках. Актуальні питання теоретичної та клінічної медицини [The relevance of the issue of burn disease and its complications as the main causes of mortality in burns. Current issues of theoretical and clinical medicine].* Тези доп міжн. науково-практ. конф. студентів та молодих вчених, Суми (стор. 264-265). Суми: СумДУ - Theses of additional international scientific and practical conf. students and young scientists, Sumy (pp. 264-265). Sumy: SumSI.

[19] Vastyanov, R. S., Stoyanov, A. N., Demidov, V. M., Bylsky, D. V., Antonenko, S. A., Neskoromnaya, N. V. … Pulyk, A. R. (2016). Повреждения травматического и гипоксического генеза: общность патогенетических механизмов [Injuries of traumatic and hypoxic genesis: common pathogenetic mechanisms]. *Journal of Education, Health and Sport,* 6(9), 285-304.

[20] Zarutskyi, Ya. L., & Bilyi, Y. Ya. (2018). *Воєнно-польова хірургія: підручник [Military field surgery: a textbook].* Київ: ФЕНІКС - Kyiv: FENIX.

ГІСТОЛОГІЧНІ ТА УЛЬТРАСТРУКТУРНІ ЗМІНИ ЩИТОПОДІБНОЇ ЗАЛОЗИ ЩУРІВ ЧЕРЕЗ 30 ДІБ ЗА УМОВ ЕКСПЕРИМЕНТАЛЬНОЇ ТЕРМІЧНОЇ ТРАВМИ НА ФОНІ ВВЕДЕННЯ NaCl

Тірон О. І.

Дуже часті в даний час природні і техногенні катастрофи, а також поточні військові конфлікти супроводжуються травмами, ускладненими гострою крововтратою, опіком і шоком різного ступеня тяжкості. Термічні ураження є однією з найактуальніших медико-соціальних проблем сучасної медицини у світі, в тому числі, в Україні. У відповідь на опікову травму в організмі розвивається значна кількість патологічних процесів, до маніфестації яких залучені практично всі органи і системи, що призводить до вираженого порушення гомеостазу, зриву адаптаційних процесів. Щитоподібна залоза за умов впливу температурних чинників порогової та надпорогової інтенсивності однією з перших підпадає під термічний удар. Мета роботи - встановлення гістологічних та ультраструктурних змін щитоподібної залози експериментальних тварин через 30 діб після змодельованої термічної травми шкіри. Експериментальні дослідження проводили на 90 білих щурах-самцях. Термічні опіки шкіри моделювали шляхом притискання чотирьох мідних пластин до завчасно депільованих бокових поверхонь тіла щурів протягом 10 с. Протягом перших 7 діб післяопікового періоду щурам у нижню порожнисту вену вводили 0,9 % фізіологічний розчин NaCl. Шматочки щитоподібної залози фіксували в 10 % нейтральному розчині формаліну, проводили дегідратацію в спиртах зростаючої концентрації, заливали у парафінові блоки. Виготовлені зрізи, товщиною 5-6 мкм, забарвлювали гематоксиліном-еозином. На 30 добу після опіку шкіри на фоні введення 0,9 % фізіологічного розчину NaCl у щитоподібній залозі щурів встановлено наявність комплексних змін, які мають деструктивний, пристосувально-компенсаторний та регенераторний характер. Вказані зміни свідчать про відносну нормалізацію гемодинаміки органу та структури стінок судин різного діаметра, що створює підґрунтя для відновлення типової структури фолікулярних клітин та синтезу нових фолікулів. В паренхімі залози виявляється значна осміофілія та пікнотизація ядер тироцитів, вакуолізація цитоплазми та десквамація клітин у просвіт фолікула. Наявні ознаки фіброзу органу, про що свідчить збільшення кількості сполучної тканини у стромальному компоненті. Обумовлені термічним альтеруючим впливом мікро- та ультраструктурні зміни паренхіми щитоподібної залози та судин, які її оточують, мають залежну від часу вираженість і упродовж 30-денного післяопікового періоду трансформуються із переважно деструктивних до переважно відновлювальних. Автори впевнені, що виявлені морфологічні зміни залози мають залежну від часу зворотність, що важливо враховувати з термінового аспекту та з кількісного аспекту складу схеми патогенетично обґрунтованої фармакокорекції. 30 доба перебігу післяопікового патологічного процесу характеризується певним дисбалансом у прояві компенсаторних, відновлювальних і синтетичних процесів, а також деструктивних і декомпенсаторних процесів, що дає підстави сподіватися на відновлення функціонування щитоподібної залози, а також органів і систем в разі призначення патогенетично обумовленого фармакологічного лікування. З урахуванням хвилеподібної динаміки морфо-функціональних змін щитоподібної залози, автори вважають ймовірним активацію саногенетичних механізмів, що дасть можливість призначати комплексну патогенетично обумовлену корекцію з урахуванням вищевказаної динаміки пато- та саногенетичних механізмів.

Ключові слова: *щитоподібна залоза, термічний опік, післяопіковий період, морфологічні зміни, відновлювальні процеси, патогенетичні механізми.*

REQUIREMENTS FOR ARTICLES

For publication, scientific articles are accepted only in English only with translation on Ukrainian, which contain the following necessary elements: UDC code; title of the article (in English and Ukrainian); surname, name and patronymic of the authors (in English and Ukrainian); the official name of the organization (institution) (in English and Ukrainian); city, country (in English and Ukrainian); structured annotations (in English and Ukrainian); keywords (in English and Ukrainian); introduction; purpose; materials and methods of research; research results; discussion; conclusions; bibliographic references.

The title of the article briefly reflects its contents and contains no more than 15 words.

Abstract. The volume of the annotation is 1800-2500 characters without spaces. The text of an annotation in one paragraph should not contain general phrases, display the main content of the article and be structured. The abstract should contain an introductory sentence reflecting the relevance of the study, the purpose of the study, a brief description of the methods of conducting research (2-3 sentences with the mandatory provision of the applied statistical methods), a description of the main results (50-70% of the volume of the abstract) and a concise conclusion (1 sentence). The abstract should be clear without familiarizing the main content of the article. Use the following expressions: "Detected ...", "Installed ...", "Fixed ...", "Impact assessed ...", "Characterized by regularities ...", etc. In an annotation, use an active rather than passive state.

Keywords: 4-6 words (or phrases).

"Introduction"

The introduction reflects the state of research and the relevance of the problem according to the world scientific literature (at least 15 references to English articles in international journals over the past 5 years). At the end of the entry, the purpose of the article is formulated (contains no more than 2-3 sentences, in which the problem or hypothesis is addressed, which is solved by the author).

"Materials and methods"

The section should allow other researchers to perform similar studies and check the results obtained by the author. If necessary, this section may be divided into subdivisions. Depending on the research objects, the ethical principles of the European Convention for the protection of vertebrate animals must be observed; Helsinki Declaration; informed consent of the surveyed, etc. (for more details, see "Public Ethics and its Conflict"). At the end of this section, a "statistical processing of results" section is required, which specifies the program and methods for processing the results obtained by the automobile.

"Results"

Requirements for writing this section are general, as well as for all international scientific publications. The data is presented clearly, in the form of short descriptions, and must be illustrated by color graphics (no more than 4) or drawings (no more than 8) and tables (no more than 4), the information is not duplicated.

"Discussion"

In the discussion, it is necessary to summarize and analyze the results, as possible, compare them with the data of other researchers. It is necessary to highlight the novelty and possible theoretical or practical significance of the results of the research. You should not repeat the information already listed in the "Introduction" section. At the end of the discussion, a separate paragraph should reflect the prospects for using the results obtained by the author.

"Conclusion"

5-10 sentences that summarize the work done (in the form of paragraphs or solid text).

"Acknowlegements"

Submitted after conclusion before bibliographic references.

"References"

References in the text are indicated by Arabic numerals in square brackets according to the numerology in the list of references. The list of references (made without abbreviations) sorted by alphabet, in accordance with the requirements of APA Style (American Psychological Association Style): with the obligatory referencing of all authors, work titles, journal names, or books (with obligatory publication by the publishing house, and editors when they are available), therefore, numbers or releases and pages. In the Cyrillic alphabets references, give the author's surnames and initials in English (Cyrillic alphabet in brackets), the title of the article or book, and the name of the magazine or the publisher first to be submitted in the original language of the article, and then in square brackets in English. If available, doi indexes must be provided on www.crossref.org (at least 80% of the bibliographic references must have their own doi indexes). Links to online publications, abstracts and dissertations are not welcome.

After the list of references, it is necessary to provide information about all authors (in English, Ukrainian and Russian): last name, first name and patronymic of the author, degree, place of work and position, **ORCID number** (each of the authors of the ORCID personal number if absence - free creation on the official website http://www.orcid.org) to facilitate the readers of this article to refer to your publications in other scientific publications.

The last page of the text should include the surname, name and patronymic of the author, degree, postal address, telephone number and e-mail of the author, with which the editors will maintain contact.

Concluding remarks

The manuscript should be executed in such a way that the number of refinements and revisions during the editorial of the article was minimal.

When submitting the article, please observe the following requirements. The volume of the article - not less than 15 and not more than 25 pages, Times New Roman, 14 pt, line spacing - one and a half, fields - 2 cm, sheet A4. Text materials should be prepared in the MS Word editor (* .docx), without indentations. Math formulas and equations to prepare in the embedded editor; graphics - in MS Excel. Use the units of the International Measurement System. Tables and drawings must contain the name, be numbered, and references to them in the text should be presented as follows: (fig. 1), or (table 1). The drawings should be in the format "jpg" or "tif"; when scanned, the resolution should be at least 800 dpi; when scanning half-tone and color images, the resolution should be at least 300 dpi. All figures must be represented in the CMYK palette. The statistical and other details are given below the table in the notes. Table materials and drawings place at the end of the text of the manuscript. All elements of the text in images (charts, diagrams, diagrams) must have the Times New Roman headset.

Articles are sent to the editorial board only in electronic form (one file) at the e-mail address nila@vnmu.edu.ua

Responsible editor - Gunas Igor Valeryovich (phone number: + 38-067-121-00-05; e-mail: igor.v.gunas@gmail.com).

Signed for print 23.12.2022
Format 60x84/8. Printing offset. Order № 3654. Circulation 100.
Vinnytsia. Printing house “TVORY”, Nemyrivske shose St., 62a,
Vinnytsya, 21034
Phone: 0 (800) 33-00-90, (096) 97-30-934, (093) 89-13-852,
(098) 46-98-043
e-mail: tvory2009@gmail.com
http://www.tvoru.com.ua